NONLINEAR INTERSUBBAND DYNAMICS IN SEMICONDUCTOR NANOSTRUCTURES

A Dissertation
Presented to
the Faculty of the Graduate School
University of Missouri – Columbia

In Partial Fulfillment
of the Requirements for the Degree

Doctor of Philosophy

By

HARSHANI OVAMINI WIJEWARDANE

Dr. Carsten A. Ullrich, Dissertation Supervisor

AUGUST 2007

The undersigned, appointed by the Dean of the Graduate School, have examined the dissertation entitled:

NONLINEAR INTERSUBBAND DYNAMICS IN SEMICONDUCTOR NANOSTRUCTURES

presented by Harshani Ovamini Wijewardane
a candidate for the degree of Doctor of Philosophy
and hereby certify that in their opinion it is worthy of acceptance.

Prof. C. A. Ullrich

Prof. G. Vignale

Prof. G. Triplett

Prof. S. Satpathy

Prof. W. Montfrooij

For my parents, Punchi my aunt, and Gune uncle.

ACKNOWLEDGMENTS

There are several people I'd like to thank for being helpful, and in some cases essential, to the completion of this thesis.

First to thank is my thesis advisor Dr. C. A. Ullrich, for taking me as a student, and for treating me so well. I greatly appreciate his support and guidance throughout my research, especially having the patience and willingness to answer my stupid and often repeated questions. Thanks and more thanks!

For all their support, I'm grateful to my committee members, Dr. G. Vignale, Dr. S. Satpathy, Dr. W. Montfrooij, and Dr. G. Triplett.

Much gratitude to the Department of Physics, University of Missouri-Rolla, for accepting me as a graduate student and allowing me to study physics!

Gratitude to the Department of Physcis, University of Missouri-Columbia, for allowing me to continue on with studies in physics!

Heartfelt thanks to all my teachers from the time that I started schooling.

Many many thanks to all my friends, who always inspire me and remind me how wonderful life is. The support they have given me on this never ending task is tremendous. I'm so grateful to them, especially for tolerating my nervous babblings!

Very many special thanks to my parents, sisters, Punchi and Gune uncle. Especially for my mother for listening to my grumblings, late night calls and encouraging not to quit! Sisters for making me laugh! They have encouraged and supported me for my entire life, and to them I owe everything. I love them dearly, and thank them.

Special thanks to Dr. Satpathy, for allowing me to use their cluster to do simulations.

For all their generous support, I thank the University of Missouri Research Board, the American Chemical Society's Petroleum Research Fund Grant No.

38982-G, Research Corporation, and the National Science Foundation Grant No. DMR-0553485.

I am so appreciative to everyone who teaches me to look past the world we can see with our eyes, in search of the things we can see with our hearts.....

Contents

List of Abbreviations

ALDA	Adiabatic Local Density Approximation
DFT	Density Functional Theory
GGA	Generalized-Gradient Approximation
GK	Gross-Kohn
HK	Hohenberg-Kohn
ISB	Intersubband
KLI	Krieger, Li and Iafrate
KS	Kohn-Sham
LDA	Local Density Approximation
OEP	Optimized Effective Potential
QV	Qian-Vignale
RWA	Rotating Wave Approximation
SIC	Self Interaction Correction
TDCDFT	Time-dependent Current Density Functional Theory
TDDFT	Time-dependent Density Functional Theory
TDKLI	Time-dependent Krieger, Li, and Iafrate method
TDKS	Time-dependent Kohn-Sham
THz	Terahertz

TDOEP	Time-dependent Optimized Effective Potential
xc	exchange-correlation

List of Figures

ABSTRACT

The intersubband (ISB) dynamics of conduction electrons in semiconductor quantum wells exhibits a variety of interesting and potentially useful nonlinear phenomena. At the same time, due to its simple (essentially one-dimensional) nature, ISB dynamics serves as an ideal test system to study collective electronic many-body dynamics. In this work we present three different formalisms which we use to describe ISB effects in the nonlinear regime. The time-dependent density functional theory (TDDFT) formalism contains many-body effects (exchange and correlation) in principle exactly, and hence is a suitable framework for studying ISB dynamics in quantum wells. We first develop a density-matrix approach based on TDDFT to describe nonlinear ISB conduction electron dynamics in the time domain. This formalism is capable of easily handling an arbitrary number of subband levels, and one can calculate non-adiabatic or transient effects associated with sudden switching or short pulses. We then focus on the fact that the exact time-dependent exchange-correlation (xc) potential contains information about the previous history of the system, including its initial state. However, almost all present applications of TDDFT employ the adiabatic approximation for the xc potential, ignoring all functional dependence on densities at previous times. We describe two different formalisms which go beyond the adiabatic approximation and apply them to collective charge-density oscillations in quantum wells. First, we develop a viscosity-based TDDFT in the time domain. A striking consequence of the memory and velocity dependence of the viscosity-based xc potential is that it introduces retardation, which in turn leads to decoherence and energy relaxation. From this formalism, we clarify the dissipation mechanism, and extract ISB relaxation rates. Also, for strong excitations we observe plasmon sidebands. The other formalism is an orbital-based approach, the time-dependent optimized effective potential method (TDOEP).

TDOEP has the advantage that it works for both finite and extended systems and yields the correct asymptotic behavior of the xc potential. We solve the full TDOEP integral equation with exact exchange for a quantum well with free and driven plasmon oscillations. We show how the memory arises from the exact exchange and results in retardation effects in the electron dynamics. This work represents the first successful implementation of exact exchange TDDFT in the time domain.

Chapter 1

Introduction and overview

Quantum wells are semiconductor nanostructures in which one can observe and control many quantum mechanical effects. These structures are grown using modern epitaxial growth techniques which allow one to control the composition of a heterostructure down to the level of a single atomic layer. The intersubband (ISB) dynamics of conduction electrons in semiconductor quantum wells exhibits a variety of interesting and potentially useful nonlinear phenomena. Many ISB effects of practical interest occur in the nonlinear regime, such as second and third harmonic generation [1], intensity dependent saturation photoabsorption [2, 3], directional control over photocurrents [4], generation of ultrashort THz pulses [5], plasma instability [6], or optical bistability [7–9]. Studying ISB dynamics is currently of great experimental and theoretical interest, since electronic ISB transitions are the basis of a variety of new devices operating in the THz frequency regime [10], for example detectors, modulators, quantum cascade lasers, etc.

Most previous theoretical studies of nonlinear ISB dynamics were based on the semiconductor Bloch equations in Hartree [11–13] or exchange-only [14, 15] approximations. The time-dependent density functional theory (TDDFT) [16] formalism contains many-body effects (exchange and correlation) from first principles. Hence it is an ideal framework for studying electron dynamics of finite systems such as individual atoms or molecules with fixed nuclei. In extended

systems such as bulk or heterostructured metals or semiconductors, additional intricacies in the electron dynamics arise due to dissipation effects. Intrinsic mechanisms (phonons, coulomb interactions) are present in any material or device. However, these effects are often overshadowed by strong extrinsic dissipation mechanisms caused by impurities or disorder.

This thesis presents the results of our various efforts aimed at a theoretical description of the collective electron dynamics in n-doped semiconductor quantum wells, with particular emphasis on electronic many-body effects and intrinsic and extrinsic dissipation. The work has been carried out in the formal frame of TDDFT; we have developed, explored, and numerically tested new methodologies to describe dynamical exchange and correlation in TDDFT. It turned out that quantum wells, due to their very simple geometry and simple electronic structure in effective-mass approximation are ideal systems in which to study novel TDDFT approaches. On the other hand, we have also focused on effects of practical interest, namely the coherent control of nonlinear ISB dynamics, which may lead to novel experimental realizations of electrooptical modulators in the THz regime.

Thus, the work presented here has a twofold character: (i) we use quantum wells as simple test systems to study fundamental aspects of dynamical many-body effects and dissipation, (ii) on the other hand, we use TDDFT in concrete, practical investigations of ultrafast nonlinear ISB dynamics in quantum wells, with an eye towards experiment and, of course, comparing to other theories in the literature.

Coming back to the problem of treating the collective electronic dynamics in the presence of dissipation: A generalization of TDDFT in the presence of dissipation was derived earlier in the linear response limit of weakly disordered systems [17]. This theory includes intrinsic damping due to electronic many-body effects via time-dependent current density functional theory [18], and extrinsic

damping due to impurities and disorder through the so called memory function formalism. This approach was used very successfully in $GaAs/Al_{0.3}Ga_{0.7}As$ quantum wells to calculate the linewidths of intersubband plasmons [19]. However, this theory, in particular the memory-functional formalism, is only available in linear response, and is formally and computationally expensive.

As an alternative, we have developed a density-matrix approach based on TDDFT beyond linear response to describe the ISB dynamics in the time domain in the presence of disorder [9, 20], which is treated phenomenologically. This formalism is capable of handling an arbitrary number of subband levels. Exchange and correlation can be included through local time-dependent potentials, and one can also calculate non-adiabatic or transient effects associated with sudden switching or short pulses. We have applied this density-matrix approach to coherent-control problems in quantum wells.

The exact time-dependent exchange-correlation (xc) potential contains information about the previous history of the system, including its initial state [21]. However, almost all present applications of TDDFT ignore all functional dependence on past densities at previous times by employing adiabatic approximations (i.e., no memory) for the xc potential. The most popular representative of this class of approximation is the adiabatic local density approximation (ALDA).

There have been several attempts to go beyond the ALDA [17, 18, 22, 23]. A non-adiabatic local approximation requires the time-dependent current as basic variable [22]. Non-adiabatic xc effects appear as viscoelastic stresses in the electron liquid, using the language of hydrodynamics [17, 18, 24, 25]. We present an analysis and applications of the current as basic variable in the time domain [26]. A striking consequence of this approach is that it introduces retardation into TDDFT, which in turn leads to decoherence and energy relaxation. We illustrated this for charge-density oscillations in quantum wells.

We have developed another attempt beyond ALDA to describe electron dy-

namics in quantum wells: the time-dependent optimized effective potential (OEP) method [27], which has the double advantage of working for both finite and extended systems and having a correct asymptotic behavior. Since the development of the static OEP method [28, 29], it has been recognized [30, 31] as the exact implementation of exchange-only DFT [32–34]. Due to the rather large computational effort involved, this scheme has not been used extensively in practice except for isolated atoms. However, there exists an approximate OEP scheme proposed by Krieger, Li and Iafrate (KLI) [36,37], which has been very successful in calculations of atomic and molecular properties in exchange-only approximation. We were successful in carrying out the full TDOEP scheme as well as the TDKLI for a quantum well. An interesting feature in this TDOEP method is that it has an infinite memory because of a time integral. We have explored the numerical and practical consequences of this infinite memory for the electron dynamics in quantum wells.

To summarize, this work comprises three different kinds of formalisms to describe the electron dynamics in quantum wells. In Chapter 2 of this work, we shall give a brief overview of TDDFT. The combination of TDDFT with density matrix formalism will be discussed in Chapter 3. Also, we will discuss optical bistability and nonlinear photoabsorption using the density matrix method. Chapter 4 is dedicated to an introduction of current density functional theory and to showing that one can describe interacting electrons as a viscous liquid with memory. We will clarify the dissipation mechanism, and also extract ISB relaxation rates. Our TDOEP scheme (in exchange-only) is presented in Chapter 5, showing how retardation in the electron dynamics arises from the time integral of TDOEP equation. Summary plus outlook are given in Chapter 6. Some technical details are given in the Appendices.

Chapter 2

Time-dependent density functional theory

2.1 Introduction

The basic idea of density functional theory (DFT) is to describe an interacting quantum many-particle system completely in terms of its particle density. There are two basic theorems associated with this formalism.

- Every observable quantity can be calculated, at least in principle, from the density alone. This means that each quantum mechanical observable can be written as a functional of the density.
- The density of the interacting system of interest can be obtained as the density of an auxiliary system of noninteracting particles moving in an effective local single particle potential.

The above theorems were proven in the work of Hohenberg and Kohn [32] and Kohn and Sham [33] for the ground-state density of static many-body systems. Based on this formal framework DFT has been successful in calculations of ground-state properties of atoms, molecules and solids over the past decades [34, 35].

The Hohenberg-Kohn theorem guarantees that the ground-state density uniquely determines the external potential up to an arbitrary constant. One may wonder if a similar statement can be made for time-dependent densities and potentials. 20 years after Hohenberg and Kohn, Runge and Gross [16] proved that a similar statement can indeed be made and hence provided the basis for the time-dependent density-functional theory (TDDFT). The proof of the Runge-Gross theorem is given in section 2.2. The essence of the theorem is that there is a unique correspondence, for $t \geq t_0$, where t_0 is some given initial time, between the time dependent density

$$n(\mathbf{r},t) = N \int ... \int dsdX_2...dX_N |\Psi(\mathbf{r},s,X_2,.....X_N,t)|^2 \tag{2.1}$$

and the time-dependent external potential $v_{ext}(\mathbf{r},t)$, where $X = (\mathbf{r},s)$ denotes the spatial and spin coordinates of an electron in an N-electron system described by the Hamiltonian

$$\hat{H}(t) = \sum_{i=1}^{N} \left(-\frac{\hbar^2 \nabla_i^2}{2m} + v_{\text{ext}}(\mathbf{r}_i,t) \right) + \frac{e^2}{2} \sum_{i \neq j}^{N} \frac{1}{|\mathbf{r}_i - \mathbf{r}_j|} \tag{2.2}$$

and evolving from an initial many-body state $\Psi_0 = \Psi(X_1,...X_N,t_0)$. This means that $n(\mathbf{r},t)$ uniquely determines $v_{\text{ext}}(\mathbf{r},t)$, and therefore the Hamiltonian and everything derivable from it. More details about TDDFT can be found in several reviews [38–41].

2.2 The Runge-Gross theorem

The Runge-Gross theorem states that two densities $n(\mathbf{r},t)$ and $n'(\mathbf{r},t)$ evolving from a common initial state $|\Psi_0\rangle = |\Psi(t_0)\rangle$ under the influence of two potentials $v(\mathbf{r},t)$ and $v'(\mathbf{r},t)$ (both expandable in Taylor series around the initial time $t = t_0$), cannot be the same, provided that the two potentials differ by more than a pure function of time,

$$v(\mathbf{r},t) \neq v'(\mathbf{r},t) + C(t). \tag{2.3}$$

To prove this theorem, we use the condition that the time-dependent potentials v and v' can be expanded in a Taylor series:

$$v(\mathbf{r},t) = \sum_{k=0}^{\infty} \frac{1}{k!} v_k(\mathbf{r})(t-t_0)^k \tag{2.4}$$

$$v'(\mathbf{r},t) = \sum_{k=0}^{\infty} \frac{1}{k!} v'_k(\mathbf{r})(t-t_0)^k. \tag{2.5}$$

From this we see that Eq. (2.3) is equivalent to the statement that for the expansion coefficients there exists a smallest integer $k \geq 0$ for which

$$v_k(\mathbf{r}) - v'_k(\mathbf{r}) = \frac{\partial^k}{\partial t^k}(v(\mathbf{r},t) - v'(\mathbf{r},t))\bigg|_{t=t_0} \neq const. \tag{2.6}$$

Using the quantum mechanical equation of motion for the expectation value of an operator $\hat{Q}(t)$,

$$\frac{\partial}{\partial t}\langle\Psi(t)|\,\hat{Q}(t)\,|\Psi(t)\rangle = \langle\Psi(t)|\left(\frac{\partial\hat{Q}}{\partial t} - i[\hat{Q}(t),\hat{H}(t)]\right)|\Psi(t)\rangle\,, \tag{2.7}$$

we obtain for the current densities:

$$\frac{\partial}{\partial t}\mathbf{j}(\mathbf{r},t) = \frac{\partial}{\partial t}\langle\Psi(t)|\,\hat{\mathbf{j}}_p(\mathbf{r})\,|\Psi(t)\rangle = -i\,\langle\Psi(t)|\,[\hat{\mathbf{j}}_p(\mathbf{r}),\hat{H}(t)]\,|\Psi(t)\rangle \tag{2.8}$$

$$\frac{\partial}{\partial t}\mathbf{j}'(\mathbf{r},t) = \frac{\partial}{\partial t}\langle\Psi'(t)|\,\hat{\mathbf{j}}_p(\mathbf{r})\,|\Psi'(t)\rangle = -i\,\langle\Psi'(t)|\,[\hat{\mathbf{j}}_p(\mathbf{r}),\hat{H}'(t)]\,|\Psi'(t)\rangle \tag{2.9}$$

where the paramagnetic current density operator is defined as

$$\hat{\mathbf{j}}_p = \frac{1}{2}\sum_j^N -i\{\nabla,\delta(r-r_j)\}. \tag{2.10}$$

In the above, $\{\hat{A},\hat{B}\} = (\hat{A}\hat{B}+\hat{B}\hat{A})$ denotes the anticommutator of two operators $\hat{A}$ and $\hat{B}$. Since the wave functions $|\Psi(t)\rangle$ and $|\Psi'(t)\rangle$ evolve from the same initial state we can write

$$\frac{\partial}{\partial t}(\mathbf{j}(\mathbf{r},t) - \mathbf{j}'(\mathbf{r},t))|_{t=t_0} = -i\,\langle\Psi_0|\,[\hat{\mathbf{j}}_p(r),\hat{H}(t_0) - \hat{H}'(t_0)]\,|\Psi_0\rangle \tag{2.11}$$

since $|\Psi(t_0)\rangle = |\Psi'(t_0)\rangle = |\Psi_0\rangle$. Since the two Hamiltonians are the same except for the potentials, we can simplify Eq. (2.11) as

$$\frac{\partial}{\partial t}(\mathbf{j}(\mathbf{r},t) - \mathbf{j}'(\mathbf{r},t))\Big|_{t=t_0} = -n_0(\mathbf{r})\nabla(v(\mathbf{r},t_0) - v'(\mathbf{r},t_0)), \tag{2.12}$$

where $n_0(\mathbf{r}) = n(\mathbf{r},t_0)$ is the initial density. If condition (2.6) is satisfied for $k=0$ then the right hand side of Eq. (2.11) cannot vanish and the current densities $\mathbf{j}$ and $\mathbf{j}'$ will become different infinitesimally later than t_0. If condition (2.6) is not satisfied for $k=0$ then one can always find a smallest $k>0$ for which it is satisfied. One can repeatedly use the Eq. (2.7) to arrive at

$$\frac{\partial^{k+1}}{\partial t^{k+1}}(\mathbf{j}(\mathbf{r},t) - \mathbf{j}'(\mathbf{r},t))\Big|_{t=t_0} = -n_0(\mathbf{r})\nabla\omega_k(\mathbf{r}) \neq 0 \tag{2.13}$$

where

$$\omega_k(\mathbf{r}) = \frac{\partial^k}{\partial t^k}(v(\mathbf{r},t) - v'(\mathbf{r},t))\Big|_{t=t_0} . \tag{2.14}$$

Therefore we can conclude that the two current densities will differ infinitesimally later than t_0. To prove an analogous statement for the corresponding densities we make use of the continuity equation,

$$\frac{\partial}{\partial t}(n(\mathbf{r},t) - n'(\mathbf{r},t)) = -\nabla\cdot(\mathbf{j}(\mathbf{r},t) - \mathbf{j}'(\mathbf{r},t)) \tag{2.15}$$

which, after differentiating $k+1$ times, gives for the density difference at t_0

$$\frac{\partial^{k+2}}{\partial t^{k+2}}(n(\mathbf{r},t) - n'(\mathbf{r},t))\Big|_{t=t_0} = \nabla\cdot(n_0(\mathbf{r})\nabla\omega_k(\mathbf{r})). \tag{2.16}$$

To prove that the densities $n(\mathbf{r},t)$ and $n'(\mathbf{r},t)$ will become different infinitesimally later than t_0, we have to demonstrate that the right hand side of Eq. (2.16) cannot vanish. This can be shown using the following arguments. Applying the Green's theorem, consider the integral

$$\begin{aligned}\int d\mathbf{r} n(\mathbf{r})(\nabla\omega_k(\mathbf{r}))^2 &= -\int d\mathbf{r}\omega_k(\mathbf{r})\nabla\cdot(n_0(\mathbf{r}\nabla\omega_k(\mathbf{r})) \\ &\quad + \oint d\mathbf{S}\cdot(n_0(\mathbf{r})\omega_k(\mathbf{r})\nabla\omega_k(\mathbf{r})).\end{aligned} \tag{2.17}$$

For finite systems the surface integral will vanish, since any realistic potential (i.e. potentials due to normalizable external charge densities) falls off at least as $1/r$ at $r \to \infty$, while the density will decay exponentially. This immediately leads to the conclusion that $\nabla \cdot (n_0(\mathbf{r})\nabla\omega_k(\mathbf{r})) \neq 0$ because if it were equal to zero, it would imply that $(\nabla\omega_k)^2 = 0$, which is a contradiction to the assumption $\omega_k(\mathbf{r})$ is not constant [Eqs. (2.6), (2.14)]. An important observation is that the density difference in Eq. (2.16) is linear in the $\omega_k(\mathbf{r})$. Hence, this difference is already nonvanishing to first order in $v(\mathbf{r},t) - v'(\mathbf{r},t)$. In particular this implies that the linear density response function is invertible.

From the previous discussion we can thus say that there is a 1-1 correspondence between time-dependent densities and time dependent potentials. This can be established for any given interaction and also for non-interacting particles. Therefore the external potential of a non-interacting system reproducing a given density is uniquely determined.

2.3 The time-dependent Kohn-Sham equation

The goal of this section is to generalize the Kohn-Sham equations of stationary DFT to generate time-dependent densities at all times. In the following we consider systems that are everywhere nonmagnetic, and thus ignore spin whenever appropriate. The most convenient method for obtaining the density $n(\mathbf{r},t)$ is by considering an auxiliary system of noninteracting electrons moving in an effective one-body potential

$$v(\mathbf{r},t) = v_{\text{ext}}(\mathbf{r},t) + v_{\text{H}}(\mathbf{r},t) + v_{\text{xc}}(\mathbf{r},t), \tag{2.18}$$

where

$$v_{\text{H}}(\mathbf{r},t) = e^2 \int d^3r \frac{n(\mathbf{r}',t)}{|\mathbf{r}-\mathbf{r}'|} \tag{2.19}$$

is the time-dependent Hartree potential, and $v_{\text{xc}}(\mathbf{r},t)$ is the time-dependent exchange-correlation (xc) potential. Similar to static DFT [34,42,43], one arrives

at a time-dependent Kohn-Sham (TDKS) equation:

$$i\hbar\frac{\partial\varphi_j(\mathbf{r},t)}{\partial t} = \left[-\frac{\hbar^2\nabla^2}{2m} + v(\mathbf{r},t)\right]\varphi_j(\mathbf{r},t), \tag{2.20}$$

which yields the density via

$$n(\mathbf{r},t) = \sum_{j=1}^{N} |\varphi_j(\mathbf{r},t)|^2. \tag{2.21}$$

Eq. (2.20) thus has the form of a single-particle time-dependent Schrödinger equation, featuring an effective potential. Formally, the TDKS equation represents an initial-value problem. The summation in Eq. (2.21) is over all the orbitals j that are occupied at the initial time.

Like in static DFT, the effective potential (2.18) is a functional of the density, which means that the TDKS scheme requires a self-consistent solution of Eqs. (2.18), (2.20) and (2.21). The time-dependent xc potential is an unknown functional of the density and needs to be approximated. In stationary DFT, approximations for the xc potential can be obtained from the knowledge that it is the functional derivative of the xc energy with respect to the density. There exists a huge body of literature on approximate xc functionals. Most prominent among these are the local-density approximation (LDA) and the generalized-gradient approximation (GGA).

Unfortunately, in TDDFT it is not possible to write $v_{\mathrm{xc}}(\mathbf{r},t)$ as the functional derivative with respect to the density of any functional; in particular, v_{xc} is not the functional derivative of the standard quantum mechanical action, although it can be defined as functional derivative of a Keldysh action functional [44]. This new kind of action functional is defined on the Keldysh contour [45], in which the physical time is parametrized by an underlying pseudotime parameter. In this case the TDKS equations do not require the variational principle for their derivation, but a functional derivative of the Keldysh action functional. However, it is also possible to derive the TDKS equation without involving a variational principle at all [41].

2.4 The adiabatic local density approximation

The diabatic approximation, which is the most straightforward method to derive time-dependent xc functionals, uses any one of the available xc potentials from static DFT and evaluates them at the time-dependent density. The most popular method is the adiabatic local-density approximation (ALDA), which is defined as

$$v_{\rm xc}^{\rm ALDA}(\mathbf{r},t) = \left.\frac{d\epsilon_{\rm xc}(\bar{n})}{d\bar{n}}\right|_{\bar{n}=n(\mathbf{r},t)}, \tag{2.22}$$

where $\epsilon_{\rm xc}(\bar{n})$ is the xc energy density of a homogeneous electron gas of density $\bar{n}$, which is known from quantum Monte Carlo calculations. Note that $v_{\rm xc}^{\rm ALDA}(\mathbf{r},t)$ is equal to the functional form of $v_{\rm xc}^{\rm LDA}(\mathbf{r})$ evaluated at the instantaneous time-dependent density $n(\mathbf{r},t)$. Therefore, $v_{\rm xc}^{\rm ALDA}(\mathbf{r},t)$ is both local in space and local in time. This means that it neglects memory effects arising from the dependence of the exchange-correlation potential at a time t on the density at earlier times $t' < t$.

The ALDA too will suffer from the shortcomings of LDA, for example the incorrect long range behavior. However there are many successful applications using ALDA even for systems that are not slowly varying in space and time [39]. In the next chapter we will discuss such an application using TDDFT with the density matrix formalism. In later chapters we shall discuss xc functionals beyond the adiabatic approximation.

2.5 Applications of TDDFT

This section highlights some of the practical successes of TDDFT calculations, which are discussed in recent reviews and recent literature [46–49]. Applications of TDDFT have enjoyed exponential growth in the last few years and this scheme yields predictions for a huge variety of phenomena.

The majority of successful applications have so far been in the linear response regime. Most of the applications in Chemistry use TDDFT to calculate electronic excitation energies [50, 51]. In this area, TDDFT is rapidly becoming a standard tool, compared to the traditional wave-function band techniques of quantum chemistry [52]. This allows to study larger systems, due to the advantage in computational efficiency. A survey given in Refs. [48, 52] shows that typical results for molecular electronic transition frequencies fall within 0.4eV of experimental data. Structural properties of excited states are almost as good as those of ground state calculations with bond lengths to within 1%, dipole moments to within 5%, and vibrational frequencies to within 5%.

In organic chemistry [48], TDDFT has been applied to study the response of molecules such as thiouracil and s-tetrazine, and annulated porphyrins. Particularly impressive applications were for the photochemistry of biological molecules such as chlorophyll [53]. In inorganic chemistry, the optical response of transition metal complexes and some X-ray absorption were calculated. Linear response TDDFT can also be used to calculate both electronic and magnetic circular dichroism [54, 55]. There are also many successful applications in nanocrystals [56] and quantum dots within and beyond the linear regime, such as second- and third-order response ([48] and references within).

In the fully nonlinear regime, where the time-dependent field cannot be treated perturbatively and where electron-electron interaction is important, TDDFT is essentially the only practical scheme. Due to advances in laser technology, many experiments are now possible in regimes where the laser field is stronger than the nuclear attraction. In this regime, many interesting nonlinear phenomena take place, for example, high harmonic generation, multi-photon ionization, above-threshold ionization, and (for molecules) above threshold dissociation or (for clusters) coulomb explosion.

TDDFT has been successful in describing high-harmonic generation in atoms

and molecules [57, 58]. Furthermore, the electronic kinetic-energy spectra from above-threshold ionization have been calculated [59, 60]. A tough problem remains to calculate the relative proportion of double to single ionization for He in strong laser pulses. Here, TDDFT has failed to describe the direct double ionization processes leading to famous "knee" structure seen in experiments [61,62].

Some of the other applications of TDDFT are to van der Waals forces and bond-breaking with symmetry problems [63]. Quantum control and quantum nuclear motion beyond the Born-Oppenheimer approximation are other recent areas of increasing interest [49].

Chapter 3

Time-dependent density functional theory in a density-matrix framework

3.1 Density-matrix TDDFT formalism

The TDKS scheme is capable of describing, in principle exactly, the electron dynamics of finite systems such as individual atoms or molecules with fixed nuclei, since it includes dynamical many-body effects through the time-dependent xc potential. In extended systems such as bulk or heterostructured metals or semiconductors, dissipation effects play an important role in addition to the dynamical many-body effects. Intrinsic dissipation mechanisms are present even in ideal materials or devices, and arise from electron-electron and electron-phonon interaction. In reality, these effects are often overshadowed by strong extrinsic dissipation mechanisms, such as impurities or disorder.

First steps towards a generalization of TDDFT in the presence of dissipation were recently taken for the linear response of weakely disordered systems [19]. In Ref. [19], disorder was treated microscopically using the so-called memory-function formalism. This approach, however, is difficult to generalize to the time domain. In this section, we formulate a computationally efficient TDDFT

approach beyond linear response in the presence of disorder. We shall treat intrinsic and extrinsic scattering mechanisms phenomenologically, and show that this approach is very useful for many practical applications.

In the following, we describe a density-matrix TDDFT formalism. We begin by expanding the occupied TDKS orbitals in terms of the ground state KS orbitals:

$$\varphi_j(\mathbf{r},t) = \sum_k c_{jk}(t)\varphi_k^0(\mathbf{r}),\ j = 1..N, \tag{3.1}$$

and we define the associated KS density matrix $\underline{\rho}_j$ as

$$\rho_{jkl}(t) = c_{jk}^*(t)c_{jl}(t). \tag{3.2}$$

Then the TDKS Eq. (2.20) for the orbital $\varphi_j(\mathbf{r},t)$ can rewritten as a Liouville-von Neumann equation for ρ_j:

$$\frac{\partial \underline{\rho}_j}{\partial t} = -\frac{i}{\hbar}[\underline{h}(t), \underline{\rho}_j(t)], \tag{3.3}$$

where the TDKS Hamiltonian matrix is

$$h_{kl} = \int d^3r \varphi_k^0(\mathbf{r}) \left[-\frac{\hbar^2\nabla^2}{2m} + v(\mathbf{r},t)\right] \varphi_l^0(\mathbf{r}). \tag{3.4}$$

The time-dependent density is given by

$$n(\mathbf{r},t) = \sum_{j=1}^{N}\sum_{kl} \rho_{jkl}(t)\varphi_k^0(\mathbf{r})\varphi_l^0(\mathbf{r}). \tag{3.5}$$

To include intrinsic and extrinsic scattering mechanisms on a phenomenological level, we use a standard approach [11, 12] and introduce a relaxation term [9, 20] $\underline{R}$ so that Eq. (3.3) becomes

$$\frac{\partial \underline{\rho}_j}{\partial t} = -\frac{i}{\hbar}[\underline{h}(t), \underline{\rho}_j(t)] - \underline{R}_j, \tag{3.6}$$

where

$$R_{jkl} = \Gamma_{jkl}(\rho_{jkl}(t) - \rho_{jkl}^0). \tag{3.7}$$

The elements of $\underline{\Gamma}_j$, $\Gamma_{jkl} = \Gamma_{jlk}$, are phenomenological scattering rates, and $\underline{\rho}_j^0 = \underline{\rho}_j(t_0)$. For a two-level system, the relaxation matrix is

$$R = \begin{pmatrix} \Gamma_1(\rho_{11} - \rho_{11}^0) & \Gamma_2(\rho_{12} - \rho_{12}^0) \\ \Gamma_2(\rho_{21} - \rho_{21}^0) & \Gamma_1(\rho_{12} - \rho_{12}^0) \end{pmatrix}, \tag{3.8}$$

where $\Gamma_1 = \hbar/T_1$ and $\Gamma_2 = \hbar/T_2$ introduce the usual relaxation and decoherence times T_1 and T_2.

3.2 Intersubband dynamics in quantum wells

We apply our density-matrix TDDFT formalism to describe ISB conduction electron dynamics in strongly driven modulation doped GaAs/$Al_{0.3}Ga_{0.7}$As quantum wells [9, 20]. For simplicity, we treat the conduction electrons in the effective-mass approximation, where $m^* = 0.067m$ and $e^* = e/\sqrt{\epsilon}$, $\epsilon = 13$, are the effective mass and charge for GaAs. The difference of the conduction band edges is 257.6 meV for GaAs/$Al_{0.3}Ga_{0.7}$As. The conduction electrons therefore live in a square potential well, where we assume the z-axis to be in the direction of quantum confinement (i.e., the direction of growth of the heterostructure). The electrons are not confined along the x and y directions and form essentially a two-dimensional electron gas.

The electronic ground state in a quantum well is then characterized by single-particle states of the form $\Psi^0_{j\mathbf{q}_{||}}(\mathbf{r}) = A^{-1/2} e^{i\mathbf{q}_{||}\mathbf{r}_{||}} \psi_j^0(z)$, with $\mathbf{r}_{||}$ and $\mathbf{q}_{||}$ in the $x-y$ plane. The envelope function for the jth subband $\psi_j^0(z)$ follows self-consistently from a one-dimensional Kohn-Sham (KS) equation [65]:

$$\left(-\frac{\hbar^2}{2m*}\frac{d^2}{dz^2} + v_{\rm conf}(z) + v_{\rm H}(z) + v_{\rm xc}(z) - \varepsilon_j \right) \psi_j^0(z) = 0. \tag{3.9}$$

Here, $v_{\rm conf}(z)$ is the confining potential (here, a square well), and the Hartree potential $v_{\rm H}(z)$ follows from Poisson's equation, $d^2 v_{\rm H}(z)/dz^2 = -4\pi e^{*2} n(z)$. The

ground-state density is given by

$$n(z) = 2\sum_{j,q_{||}} |\psi_j^0(z)|^2 \, \theta(\varepsilon_F - E_{jq_{||}}) \,, \tag{3.10}$$

assuming a parabolic energy dispersion, $E_{jq_{||}} = \varepsilon_j + \hbar^2 q_{||}^2/2m^*$, and ε_j are the subband energy levels. The subband states are occupied up to the conduction band Fermi level

$$\varepsilon_F = \frac{\pi\hbar^2}{m^*}\frac{N_s}{N_{\rm occ}} + \frac{1}{N_{\rm occ}}\sum_{j=1}^{N_{\rm occ}} \varepsilon_j, \tag{3.11}$$

where N_s is the electronic sheet density, and $N_{\rm occ}$ is the number of occupied subbands. This is illustrated in Fig. 3.1, where only the lowest subband is occupied up to the conduction band Fermi level.

We consider the ISB dynamics under the influence of linearly polarized electromagnetic fields, with associated one-dimensional external potential

$$v_{\rm ext}(z,t) = v_{\rm dr}(z,t) + v_{\rm conf}(z). \tag{3.12}$$

Here, $v_{\rm dr}(z,t) = e\mathcal{E}zf(t)\sin(\omega t)$ describes the driving field in dipole approximation, with electric field amplitude $\mathcal{E}$, frequency ω, and envelope $f(t)$. $v_{\rm conf}(z)$ is the confining square-well potential. The time-dependent states have the form $\Psi_{\mathbf{q}||}(\mathbf{r},t) = \frac{1}{\sqrt{A}} e^{i\mathbf{q}_{||}\mathbf{r}_{||}}\psi_j(z,t)$, since $v_{\rm ext}(z,t)$ depends only on z. Therefore we only have to deal with the time evolution of the envelope function $\psi_j(z,t)$. In the absence of scattering this follows from a TDKS equation:

$$\left(-\frac{\hbar^2}{2m^*}\frac{d^2}{dz^2} + v(z,t)\right)\psi_j(z,t) = i\hbar\frac{\partial}{\partial t}\psi_j(z,t), \tag{3.13}$$

where, as before,

$$v(z,t) = v_{\rm ext}(z,t) + v_{\rm H}(z,t) + v_{\rm xc}(z,t), \tag{3.14}$$

and $\psi_j(z,t_0) = \psi_j^0(z)$. We use the ALDA, Eq. (2.22), to get $v_{\rm xc}(z,t)$. The time-dependent density directly follows from Eq. (3.10):

$$n(z,t) = \frac{m^*}{\pi\hbar^2}\sum_{j=1}^{N_{\rm occ}} |\psi_j(z,t)|^2(\varepsilon_F - \varepsilon_j), \tag{3.15}$$

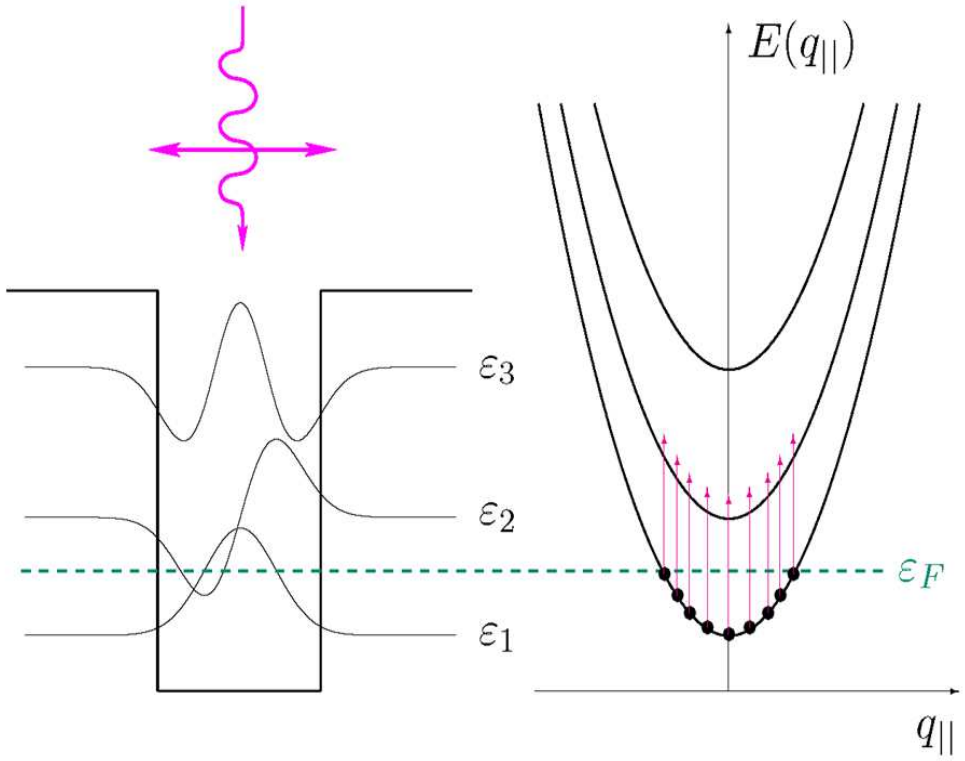

Figure 3.1: Quantum well subbands. Right: Only the lowest level is occupied up to the Fermi level. Left: Electronic envlope functions for three levels. We consider far-infrared light polarized along the growth direction of the quantum well, which excites electrons from first level to second level collectively.

since we propagate those states that were initially occupied, i.e. $E_j(q_{||}) \leq \varepsilon_F$.

We will consider the density-matrix equation (3.6) for quantum well ISB dynamics in the presence of phenomenological relaxation and decoherence. The density matrix $\rho_{jkl} = c^*_{jk}(t)c_{jl}(t)$ is constructed from the envelope functions as

$$\psi_j(z,t) = \sum_k c_{jk}(t)\psi^0_k(z), \tag{3.16}$$

and the TDKS Hamiltonian matrix elements are

$$h_{kl}(t) = \int dz \psi^0_k(z) \left[-\frac{\hbar^2}{2m^*}\frac{d^2}{dz^2} + v(z,t) \right] \psi^0_l(z). \tag{3.17}$$

We limit the size of the density matrix by including only the lowest N_b bound subband levels in the expansion (3.16), which is a good approximation as long as the intensity of the driving field is too weak to cause substantial ionization. Details about how to solve the density matrix Eq. (3.6) numerically given in Appendix A.

3.3 Iterative solution of the density matrix equation of motion

Before going on and presenting results, let us say a few words on analytical solutions of the density-matrix equation of motion. A special role is played here by two-level systems, which have been extensively treated in the literature [64]. In particular, the ISB dynamics in quantum wells has been treated using 2-level systems in the popular so-called rotating wave approximation (RWA) [11] or other averaging methods [13]. In the following, we will show how the RWA can be viewed as the lowest order contribution in an iterative solution of the density-matrix equation of motion. This will be useful later on when we discuss how the RWA breaks down for the nonlinear dynamics in asymmetric wells.

We consider a non-interacting two-level system driven by a sinusoidal electromagnetic field. The density matrix equation of motion (3.6) can be written as [11]

$$\dot{\rho}_{12} = [i\omega_{21} - \Gamma_2 - i(H_{11} - H_{22})]\rho_{12} + iH_{12}\Delta \tag{3.18}$$

$$\dot{\Delta} = 2iH_{12}(\rho_{12} - \rho_{12}^*) - \Gamma_1(\Delta - \Delta^{(0)}), \tag{3.19}$$

where $\hbar\omega_{21} = \varepsilon_2 - \varepsilon_1$ is the bare subband spacing, and $\Delta = \rho_{11} - \rho_{22}$ is the population difference between the first and the second subband level. It measures, basically, how many electrons are excited. In turn, Γ_1 is the relaxation rate which measures deexcitation back into the first level. ρ_{12} is the polarization of the first and second subband level, and Γ_2 is the decoherence rate. Initially

$\Delta^{(0)} = 1$, and $\rho_{12}^{(0)} = 0$. We write the Hamiltonian matrix elements as

$$H_{kl} = H_{kl}^{\text{ext}} + H_{kl}^{\text{H+xc}}, \tag{3.20}$$

where

$$H_{kl}^{\text{ext}} = \mathcal{E} e \sin(\omega t) \int dz \psi_k^0(z) z \psi_l^0(z) \tag{3.21}$$

is the dipole matrix element, and

$$H_{kl}^{\text{H+xc}} = \int dz \psi_k^0(z) (v_{\text{H}}(z,t) + v_{\text{xc}}(z,t) - v_{\text{H}}(z,0) - v_{\text{xc}}(z,0)) \psi_l^0(z) \tag{3.22}$$

are the dynamical Hartree+xc matrix elements. General solutions for (3.18) and (3.19) can be expressed through the following ansatz:

$$\rho_{12}(t) = \sum_n \rho_{12}(n\omega) e^{-in\omega t} \tag{3.23}$$

$$\Delta(t) = \sum_n \Delta(n\omega) e^{-in\omega t}. \tag{3.24}$$

A detailed description of obtaining the above expressions is given in Appendix B. For a symmetric quantum well, $H_{11}^{\text{ext}} = H_{22}^{\text{ext}} = 0$. Therefore one can find closed solutions for ρ_{12} and Δ within the rotating-wave approximation (RWA) [12, 68],

$$\rho_{12}^{\text{RWA}}(t) = \rho_{12}^{\text{RWA}}(-\omega) e^{i\omega t} + \rho_{12}^{\text{RWA}}(\omega) e^{-i\omega t} \tag{3.25}$$

and similar for Δ^{RWA}. This type of solution has been used by Załużny [11] to analyze nonlinear ISB photoabsorption. In the following, we examine these solutions more closely, comparing with our fully numerical results. It will turn out that the RWA becomes unreliable for asymmetric systems.

3.4 ISB dynamics within and beyond RWA

In this section, we calculate photoabsorption spectra for GaAs/AlGaAs symmetric and asymmetric single wells and compare the results with a simplified two-level model within RWA.

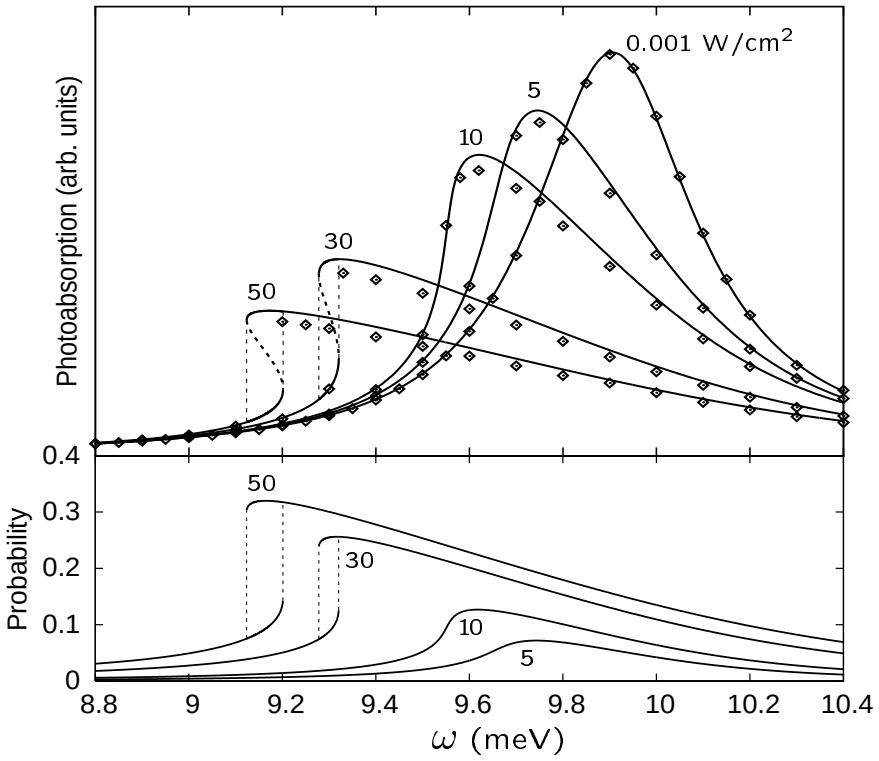

Figure 3.2: ISB photoabsorption and second-level occupation probability p_2 for a 40 nm GaAs/AlGaAs quantum well with electron density $6.4 \times 10^{10}\mathrm{cm}^{-2}$, driven by THz fields with intensities as indicated (lines: 2-level rotating-wave approximation [11]; points: 6-level TDDFT density-matrix calculation).

3.4.1 Photoabsorption in a symmetric single well

We consider a 40 nm $\mathrm{GaAs/Al_{0.3}Ga_{0.7}As}$ square quantum well with $N_s = 6.4 \times 10^{10}\mathrm{cm}^{-2}$, following Craig *et al.* [3]. The lowest subband spacing is $\varepsilon_2 - \varepsilon_1 = 8.72$ meV, and the ISB plasmon frequency is found from linear-response theory [65] as $\hbar\omega_{\mathrm{ISB}} = 9.91$ meV. The system has 9 bound levels, and we take the lowest six to construct the density matrix ($N_b = 6$). We use the ISB scattering times $T_1 = 40$ ps and $T_2 = 3.1$ ps, consistent with recent measurements of T_1 and T_2 for similar systems [66,67]. To describe ISB photoabsorption, we propagate Eq. (3.6) in the presence of THz driving fields, switched on at t_0 over a 5-cycle linear ramp and

then kept at constant intensity for several hundred ps. From the dipole moment

$$d(t) = N_s \sum_{kl}^{N_b} \rho_{kl}(t) \int dz\, \psi_k^0(z) z \psi_l^0(z), \tag{3.26}$$

we obtain the photoabsorption cross section (the dissipated power)

$$\sigma(\omega) \sim \omega \int_t^{t+T} \cos(\omega t') d(t')\, dt', \tag{3.27}$$

where T is one cycle of the driving field $v_{\rm dr}$. Following the switching on of the THz field, $\sigma(\omega)$ fluctuates considerably from one cycle to the next, but eventually approaches a stable value as the transients settle down.

Fig. 3.2 shows $\sigma(\omega)$ calculated with our 6-level density-matrix formalism, in close agreement with the two-level rotating-wave approximation [11] including xc. For low intensities, $\sigma(\omega)$ is a Lorentzian with maximum at $\omega_{\rm ISB}$ and width $2\hbar/T_2$. Approaching the saturation intensity

$$I_0 = c\epsilon^{1/2}\hbar^2/8\pi T_1 T_2 e^2 |\langle\psi_2^0|z|\psi_1^0\rangle|^2, \tag{3.28}$$

the photoabsorption peak shifts to lower energies and changes shape (here, $I_0 = 26.8\,\mathrm{W/cm^2}$). The physical reason for this effect is that the depolarization shift $\hbar\omega_{\rm ISB} - (\varepsilon_2 - \varepsilon_1)$ is proportional to the population difference $p_1 - p_2$. Initially, $p_1 = 1$ and $p_2 = 0$. Strong driving fields lead to a decrease of $p_1 - p_2$ because of transitions into the second and, eventually, higher levels, see the lower panel of Fig. 3.2. Since this population transfer is most efficient around the ISB resonance, the peak of $\sigma(\omega)$ shifts more than the tails, leading to an asymmetric line shape. For intensities over $16\,\mathrm{W/cm^2}$ we discover regions of optical bistability in $\sigma(\omega)$: the system responds in two different ways to one and the same driving field (the middle branch is unstable). We will say more about this bistability in section 3.5.

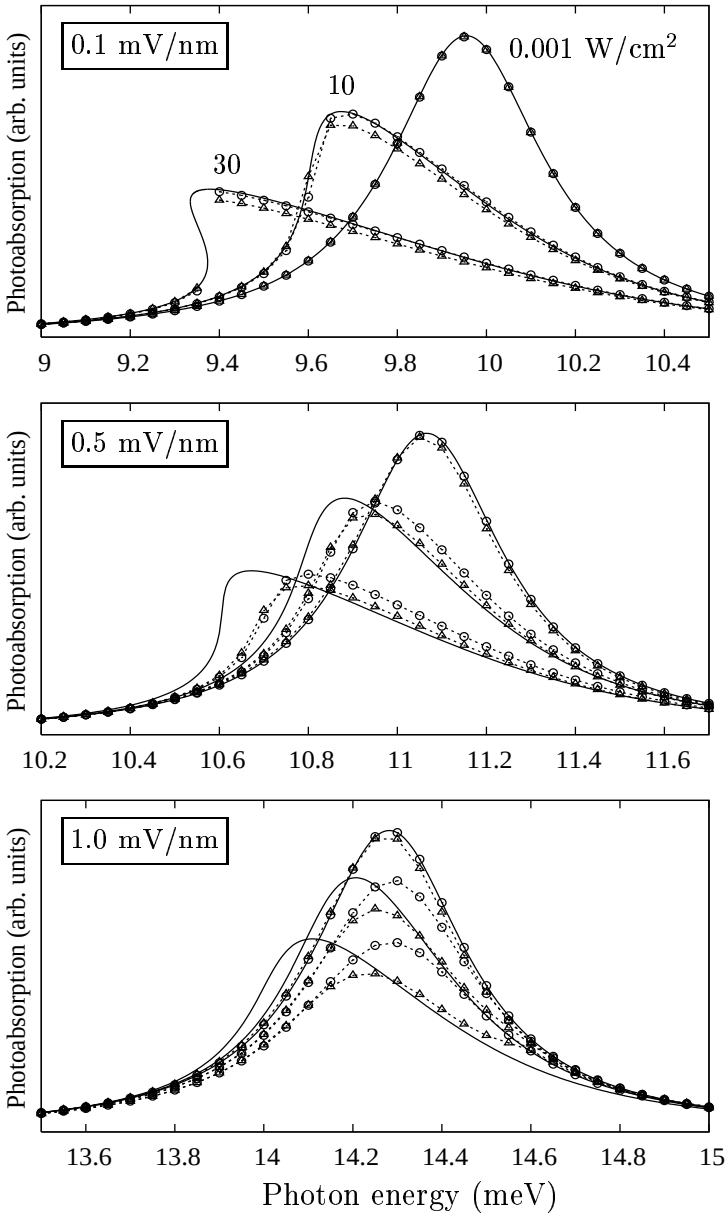

Figure 3.3: ISB photoabsorption for a 40 nm GaAs/AlGaAs quantum well with electron density 6.4×10^{10} cm^{-2} and DC bias 0.1, 0.5, and 1.0 mV/nm, driven by THz fields with intensities as indicated. Lines: 2-level RWA [11]. Symbols: full 2-level (circles) and 6-level (triangles) density-matrix propagation.

3.4.2 Photoabsorption in an asymmetric single well

Using our TDDFT density-matrix formalism, we have demonstrated numerically that the 2-level RWA [11] works well for symmetric quantum wells, yet it breaks down when the system becomes asymmetric under the influence of DC electric fields [20]. We consider the same type of well described in section 3.4.1 and apply DC electric fields 0.1, 0.5, and 1.0 mV/nm, and perform 2-level and 6-level density matrix calculations. Fig. 3.3 shows the results for the photoabsorption.

At low intensities the photoabsorption has a Lorentzian shape, and the RWA and full calculations agree very well for all cases of DC bias. The Lorentzian lineshape was changed at higher intensities of the driving field, since population transfer into higher levels reduces the depolarization shift. The 2-level RWA and the full density-matrix calculations remain close for small asymmetries (less than 0.1mV/nm).

With increasing DC bias (0.5mV/nm and higher) and at high intensities, we find strong discrepancies between the 2-level RWA and the more rigorous calculations. Overall, the RWA tends to strongly exaggerate the redshift and asymmetry of the absorption peaks. The reason for this discrepency is twofold. First of all, at higher intensities, more than the lowest 2 levels play a role in the electron dynamics. Indeed, we find that there is a sizable difference between out 2-level and 6-level exact numerical results.

However, even more dramatic is the failure of the RWA itself, compared with the exact 2-level results. Our analytical investigations in Appendix B show clearly which contributions are neglected in the RWA: namely, higher harmonics of the driving frequency ω, and the coupling to the diagonal matrix elements of the total time-dependent potential, which become finite for asymmetric wells.

Thus, the bottom line is clearly that the RWA provides a quick and easy method to obtain the linear and nonlinear ISB dynamics in quantum wells, as

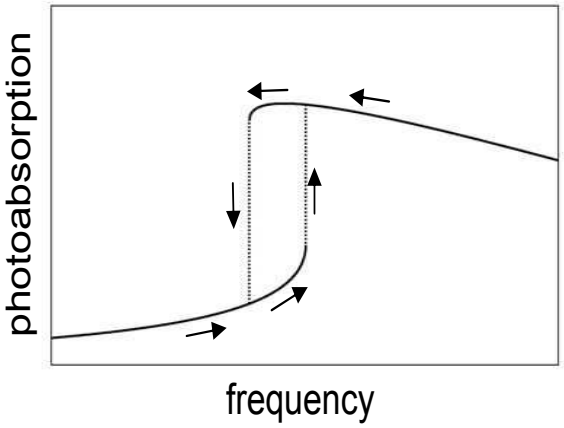

Figure 3.4: Illustration of hysteresis-like behavior in optical bistability

shown by Załużny. [11], but it breaks down for asymmetric wells and strong driving fields. The density-matrix equation must then be solved fully numerically.

3.5 Coherent control of optical bistability

In section 3.4.1 we discussed the appearance of optical bistability. The two states are characterized by density oscillations with different amplitudes and phases (upper branch: close to $\pi/2$; lower branch: around $\pi/4$), and different level populations.

Whether the system will be in the upper or lower bistable state depends on its history. A hysteresis-like behavior (see Fig. (3.4)) is observed at fixed intensity and under adiabatically slow frequency changes of the driving field [13]: Entering the bistability region from the low-frequency side, the system continues on the *lower* branch and then jumps up at the end of the bistability region. Entering from the other side, the system follows the *upper* branch. The required continuous, adiabatic frequency tuning of THz driving fields is difficult to realize in experiment, and of little practical use in exploring ISB optical bistability for

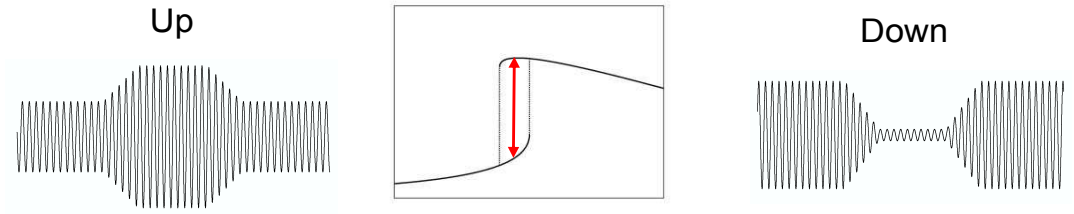

Figure 3.5: Illustration of control pulses used for switching between bistable states.

potential applications. Instead, it would be desirable to switch rapidly between the two bistable states.

In the following, we demonstrate coherent control of ISB optical bistability by short THz control pulses. This method is both rapid and robust, and lends itself for experimental implementation. Fig. 3.2 suggests that a switch from the lower to the upper bistable state requires a transfer of population into the second level. The necessary energy can be rapidly injected into the system by a short THz pulse. On the other hand, we expect switching down from the upper to the lower state to be inherently slower, since upper-level population needs time to relax.

We consider a driving field with $I = 30\ \mathrm{W/cm^2}$ and $\hbar\omega = 9.3$ meV (0.445 ps per cycle) in the middle of the bistable region, such that the system is in the lower bistable state. At t_1, we apply a short pulse with the same frequency and *in phase* with the driving field, and with a trapezoidal pulse envelope (left panel of Fig. 3.5): linearly turned on and off over 5 cycles, constant in between over N_c cycles (the precise pulse shape is not essential). We calculate $d(t)$ and $\sigma(\omega)$ as above, using our density-matrix formalism. After transients and other disturbances induced by the pulse have subsided, the system either slowly returns to the lower state, or converges towards the upper bistable state, in which case we define a "switching time" as that time after t_1 when $\sigma(\omega)$ is converged to

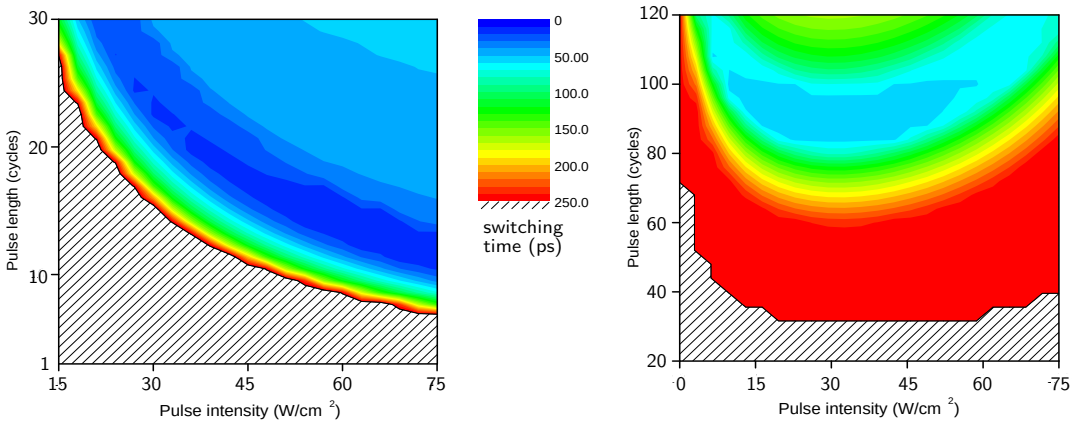

Figure 3.6: Intensity and length of THz control pulses for ultrafast switching (left/right panel: up/down) between the lower and upper ISB bistable states at $I = 30\,\mathrm{W/cm^2}$ and $\omega = 9.3$ meV driving field. Contour labels indicate the switching times in ps. No switching occurs in the hatched regions.

within 5% of its final value. To study the reverse process, we prepare the system in the upper bistable state and then apply similar control pulses, *phase shifted by* π with respect to the driving field (right panel of Fig. 3.5). After the transients have settled, the system either remains in the upper state, or goes down to the lower state.

Control pulses as shown in Fig. 3.5 of various intensity and length N_c were tested to determine the conditions for successful up- or down-switching, and to find those pulses that induce the fastest switching. The results are summarized in Fig. 3.6. The hatched areas indicate the unsuccessful pulses: in the case of up-switching, they do not have sufficient energy to promote enough electrons to the upper level, and in the case of down-switching, they are too short to allow enough electrons to relax down.

The limiting curve in Fig. 3.6 (left) separating the successful from the unsuccessful pulses corresponds to pulses of energy $1.87 \times 10^{-10}\,\mathrm{J/cm^2}$. The shortest switching times of 15–20 ps are achieved for somewhat higher pulse energy,

around 3.3×10^{-10} J/cm^2. No systematic effort was made to further optimize the control pulses. A physical limit for switching speed is set by the decoherence time T_2 (here 3.1 ps), which governs the decay of transients.

Down-switch from the upper to the lower ISB bistable state requires longer control pulses, at least 30 cycles. The associated switching times are limited by the ISB relaxation time T_1 (here 40 ps). We find that the shortest down-switching times of 50–60 ps are achieved by control pulses with intensity not far from the driving field, 30 W/cm^2. Due to the phase difference π, these control pulses effectively suppress the driving field, giving electrons time to relax from the upper level.

In summary, we have simulated coherent control of ISB optical bistability in quantum wells, using THz control pulses to switch rapidly between the bistable states. Switching times are in principle limited only by the intrinsic relaxation and decoherence times. Interestingly, a shorter relaxation time T_1 (i.e., more scattering) implies faster switching.

More realistic simulations would replace T_1 and T_2 with microscopic, intensity-dependent scattering theories, including finite temperatures, and detailed modeling of the absorption profile and waveguide geometry of the choice. This may open up opportunities for new experimental and theoritical studies of optical bistability, which in the long run may lead to THz application such as high-speed all-optical modulators and switches.

Chapter 4

Time-dependent current density functional theory in the nonlinear regime

In this chapter, we turn to a different method of introducing dissipation. In Chapter 3, we treated dissipation through phenomenological scattering times T_1 and T_2, which account for both intrinsic and extrinsic scattering mechanisms. Now we focus exclusively on intrinsic scattering caused by electron-electron interactions due to Coulomb forces. We will treat this scattering mechanism microscopically using the idea of viscoelastic forces in the electron liquid.

4.1 Introduction to TDCDFT

The central idea of time-dependent current density functional theory (TDCDFT) is that one uses the current density as the basic variable. This idea was first introduced by Ghosh and Dhara [71,72], in order to include time-dependent magnetic fields in the TDDFT framework. They provided a generalization of the Runge-Gross theorem for arbitrary fields, that is, they showed that the single particle current density uniquely determines, up to an arbitrary gauge transformation, the time-dependent scalar and vector potentials. Compared to the

1987 Ghosh and Dhara formulation, Vignale [74] has given an easier and more complete formulation of the TDCDFT, which can be viewed as a generalized van Leeuwen theorem [44] to include general time dependent fields. Vignale's theorem will be summarized in the following.

Let $n(\mathbf{r},t)$ and $\mathbf{j}(\mathbf{r},t)$ be the density and current density of a many-particle system that evolves from an initial state $|\Psi(t_0)\rangle$. The motion of the system is governed by the following Hamiltonian:

$$\hat{H}(t) = \sum_j \left(\frac{1}{2}[-i\nabla_j + \frac{1}{c}\mathbf{A}(\mathbf{r}_j,t)]^2 + v(\mathbf{r}_j,t)\right) + \hat{V}_{ee}, \tag{4.1}$$

where $v(\mathbf{r},\mathbf{t})$ and $\mathbf{A}(\mathbf{r},t)$ are scalar and vector potentials, which are analytic functions of time around t_0. $\hat{V}_{ee}$ represents the electron-electron interaction. The current density operator is given in term of the velocity operator

$$\hat{v}_j = (-i\nabla_j + \frac{1}{c}\mathbf{A}(\mathbf{r}_j,t)) \tag{4.2}$$

as,

$$\hat{\mathbf{j}}(\mathbf{r},t) = \frac{1}{2}\sum_j [\hat{v}_j(t), \delta(\mathbf{r}-\mathbf{r}_j)]. \tag{4.3}$$

Following [74], one can prove that the same density and current density can be reproduced by another many-particle system evolving under a different Hamiltonian $H'(t)$. This Hamiltonian will have the form,

$$\hat{H}'(t) = \sum_j \left(\frac{1}{2}[-i\nabla_j + \frac{1}{c}\mathbf{A}'(\mathbf{r}_j,t)]^2 + v'(\mathbf{r}_j,t)\right) + \hat{V}'_{ee}. \tag{4.4}$$

This Hamiltonian propagates a different initial state Ψ'_0, which produces the same density and current density as Ψ_0 at $t = t_0$ in the unprimed system. The potentials $v'(\mathbf{r},t)$ and $\mathbf{A}'(\mathbf{r},t)$ are uniquely determined up to gauge transformations of the form

$$\begin{aligned} v'(\mathbf{r},t) &\rightarrow v'(\mathbf{r},t) + \frac{\partial\Lambda(\mathbf{r},t)}{\partial t} \\ \mathbf{A}'(\mathbf{r},t) &\rightarrow \mathbf{A}'(\mathbf{r},t) + \nabla\Lambda(\mathbf{r},t). \end{aligned} \tag{4.5}$$

Here $\Lambda(\mathbf{r},t)$ is a regular function of $\mathbf{r}$ and t. One can choose $\Lambda(\mathbf{r},t)$ such that the scalar potential is always zero in both primed and unprimed systems. One can then solve the equation of motion, such that the vector potential $\mathbf{A}'(\mathbf{r},t)$ produces the same current density as the vector potential $\mathbf{A}(\mathbf{r},t)$ in the unprimed system. In the case in which the primed and unprimed systems are such that $\hat{V}'_{ee} = \hat{V}_{ee}$ and $\Psi'(t_0) = \Psi(t_0)$ one can show that $\mathbf{A}'(\mathbf{r},t) = \mathbf{A}(\mathbf{r},t)$ at all times. This result is the analogue of the Runge-Gross theorem for the TDCDFT. That is, two vector potentials that produce the same current-density in two systems evolving from the same initial state must be the same up to a gauge transformation. In other words, there exits a one-to-one mapping between vector potentials and current densities.

The current density produced in an interacting system under a vector potential $\mathbf{A}(\mathbf{r},t)$ can thus always be reproduced in a system with a different type of interaction evolving under a suitable vector potential $\mathbf{A}'(\mathbf{r},t)$, even in the case in which the primed system is noninteracting, i.e., $\hat{V}'_{ee} = 0$. In this case we have a solid basis to use the TDKS formalism. Keeping in mind that the current couples to a vector potential, the ordinary xc potential can be replaced by an xc vector potential [22, 73, 74]; in the next section we will discuss the TDKS formalism with TDCDFT in the time domain.

4.2 TDKS with TCDFT in the time domain

In the presence of external scalar and vector potentials, $v(\mathbf{r},t)$ and $\mathbf{A}(\mathbf{r},t)$, the TDKS equation is

$$\begin{aligned} i\hbar\dot{\varphi}_j(\mathbf{r},t) &= \left[\frac{1}{2}\left(\frac{\nabla}{i} + \frac{1}{c}\,\mathbf{A}(\mathbf{r},t) + \frac{1}{c}\,\mathbf{A}_{\rm xc}(\mathbf{r},t)\right)^2 \right. \\ &\quad \left. + v(\mathbf{r},t) + v_{\rm H}(\mathbf{r},t)\right]\varphi_j(\mathbf{r},t)\,, \end{aligned} \tag{4.6}$$

where $v_{\rm H}$ is the Hartree potential and $\mathbf{A}_{\rm xc}(\mathbf{r},t)$ is the xc vector potential. A non-adiabatic, nonlinear xc vector potential has been given by [18]

$$\frac{e}{c}\,\dot{\mathbf{A}}_{{\rm xc},i}(\mathbf{r},t) = -\nabla_i v_{\rm xc}^{\rm ALDA}(\mathbf{r},t) + \sum_j \frac{\nabla_j \sigma_{{\rm xc},ij}(\mathbf{r},t)}{n(\mathbf{r},t)}\,, \tag{4.7}$$

where the viscoelastic stress tensor $\underline{\sigma}_{\rm xc}$ of the electron liquid is defined in terms of the velocity field $\mathbf{u}(\mathbf{r},t) = \mathbf{j}(\mathbf{r},t)/n(\mathbf{r},t)$:

$$\begin{aligned}\sigma_{{\rm xc},ij}(\mathbf{r},t) &= \int_{-\infty}^{t} dt' \Big\{ \eta(\mathbf{r},t,t') \Big[\nabla_j u_i(\mathbf{r},t') + \nabla_i u_j(\mathbf{r},t') \\ &\quad - \frac{2}{3}\,\nabla\cdot\mathbf{u}(\mathbf{r},t')\delta_{ij} \Big] + \zeta(\mathbf{r},t,t')\nabla\cdot\mathbf{u}(\mathbf{r},t')\delta_{ij} \Big\}. \end{aligned} \tag{4.8}$$

The viscosity coefficients in Eq.(4.8) are defined as

$$\eta(\mathbf{r},t,t') = \int \frac{d\omega}{2\pi}\,\tilde{\eta}(\bar{n},\omega) e^{-i\omega(t-t')}\Big|_{\bar{n}=n(\mathbf{r},t)}\,, \tag{4.9}$$

and similar for ζ, where

$$\tilde{\eta}(n,\omega) = -\frac{n^2}{i\omega}\, f_{\rm xc}^T \tag{4.10}$$

$$\tilde{\zeta}(n,\omega) = -\frac{n^2}{i\omega}\left[f_{\rm xc}^L - \frac{4}{3}\, f_{\rm xc}^T - \frac{d^2\epsilon_{\rm xc}}{dn^2} \right], \tag{4.11}$$

and $f_{\rm xc}^L$ and $f_{\rm xc}^T$ are the longitudinal and transverse frequency-dependent xc kernels of a homogeneous electron gas of density n [75,76]. For quantum wells, since all spatial dependence is along the z direction, the xc vector potential (4.7) can be transformed into a scalar potential by integrating Eq. (4.7). One can write it as $v_{\rm xc}(z,t) = v_{\rm xc}^{\rm ALDA}(z,t) + v_{\rm xc}^{\rm M}(z,t)$ (ALDA+M), with the memory part given by

$$v_{\rm xc}^{\rm M}(z,t) = -\int_{-\infty}^{z} \frac{dz'}{n(z',t)}\,\nabla_{z'}\,\sigma_{{\rm xc},zz}(z',t). \tag{4.12}$$

The zz component of the xc stress tensor is given below. The density entering the viscosity coefficients can be evaluated at t or at the earlier time t'. Without loss

of generality, we use t, since the difference is only of higher order in gradients. Notice that the lower limit of time integration can be replaced by 0 if the system has been in a steady state with zero velocity field for $t \leq 0$,

$$\sigma_{\mathrm{xc},zz}(z',t) = \int_0^t Y(n(z',t),t-t')\nabla_{z'}u_{z'}(z',t')dt' \ , \tag{4.13}$$

where the memory kernel Y is defined as

$$Y(n,t-t') = \frac{4}{3}\eta(n,t-t') + \zeta(n,t-t') \ . \tag{4.14}$$

This quantity is of central importance, since it determines the retardation effects in the xc potential.

4.3 Gross-Kohn and Qian-Vignale memory kernels

With the help of the Kramers-Kronig relations for f_{xc}^L, one can express the memory kernel given by the Eq.(4.14) as:

$$Y(n,t-t') = \frac{4}{3}\mu_{\mathrm{xc}} - \frac{n^2}{\pi}\int \frac{d\omega}{\omega}\,\Im f_{\mathrm{xc}}^L(\omega)\cos\omega(t-t'), \tag{4.15}$$

with the static xc shear modulus of the electron liquid [76],

$$\mu_{\mathrm{xc}} = \frac{3n^2}{4}\left(\Re f_{\mathrm{xc}}^L(0) - \frac{d^2\epsilon_{\mathrm{xc}}}{dn^2}\right). \tag{4.16}$$

The short-time behavior of $Y(n,t-t')$ is of particular interest, since it governs the high-frequency dynamics. $Y(n,0)$ can be expressed analytically using the Kramers-Kronig relation,

$$\frac{1}{\pi}\int_{-\infty}^{\infty}\frac{d\omega}{\omega}\,\Im f_{\mathrm{xc}}^L(\omega) = \Re f_{\mathrm{xc}}^L(0) - f_{\infty}^L, \tag{4.17}$$

where the high-frequency limit f_{∞}^L is known via the third moment sum rule [76]. The result is [77]

$$Y(n,0) = -\frac{20}{3}\epsilon_{\mathrm{xc}} + \frac{26n}{5}\frac{d\epsilon_{\mathrm{xc}}}{dn} - \frac{d^2\epsilon_{\mathrm{xc}}}{dn^2}. \tag{4.18}$$

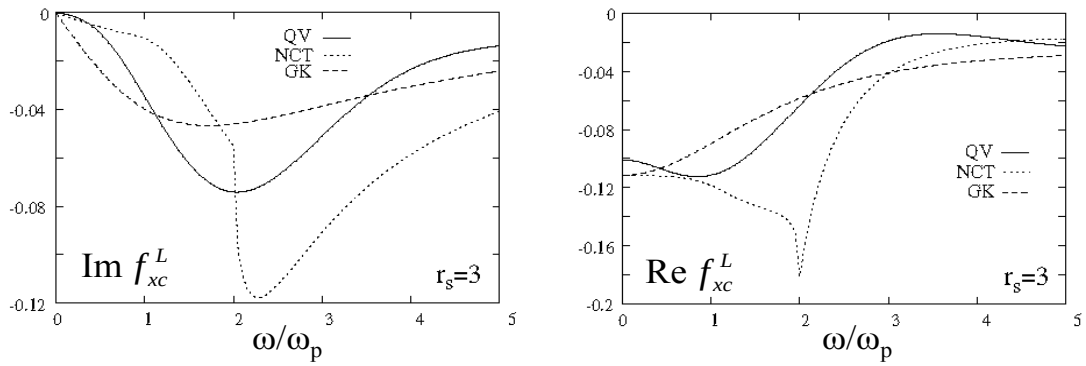

Figure 4.1: Imaginary and real part of $f_{\rm xc}^L(\omega)$ within the GK and QV parametrization for an electron gas at Wigner-Seitz radius r_s=3.

It is also straightforward to see that $\frac{dY}{dt}(n,0) = 0$, i.e., the memory kernel starts with zero slope.

We compared the behavior of the memory kernel Y evaluated with two different parametrizations for $f_{\rm xc}^L(\omega)$, Gross-Kohn (GK) [75] and Qian-Vignale(QV) [76] (see Fig (4.1) for the behavior of the real and imaginary part of $f_{\rm xc}^L(\omega)$). Fig. 4.2 shows the memory kernel for a homogeneous electron gas of Wigner-Seitz radius $r_s = 3$, evaluated with GK and QV. Overall, the behavior of $Y^{\rm GK}$ and $Y^{\rm QV}$ looks similar, although $Y^{\rm GK}$ decreases monotonically, rapidly approaching its asymptotic exponential falloff. Physically, it means that the electron liquid rapidly forgets, on a timescale of less than one plasma cycle. On the other hand, $Y^{\rm QV}$ goes through a minimum and then approaches its asymptotic value. As shown in the inset, it appears that the memory of the electron gas becomes more and more long ranged for lower densities. In other words, the short-term dynamics of the system is governed by the high-density regions, whereas the long-term memory resides in the low-density regions.

To get a first impression of the behavior of the xc memory potential $v_{\rm xc}^{\rm M}(z,t)$,

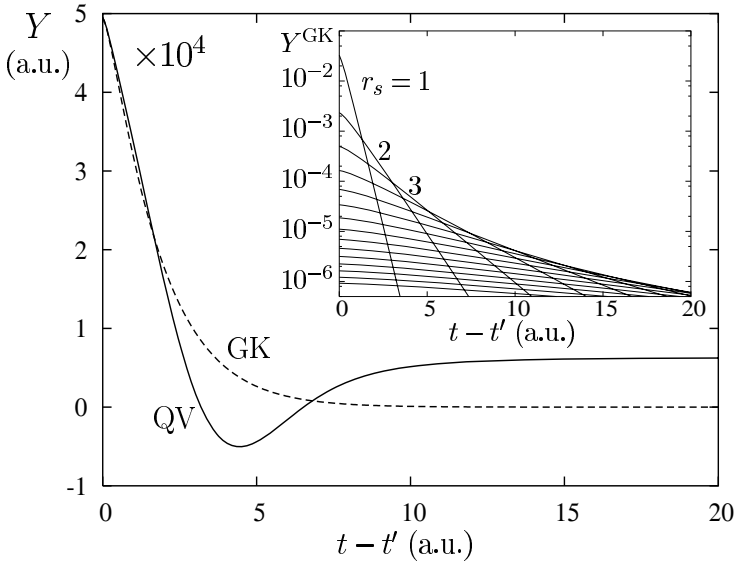

Figure 4.2: Memory kernel $Y(n, t-t')$ for $r_s = 3$, using the QV and GK parametrizations [75, 76] for $f_{\rm xc}^L(\omega)$. Inset: $Y^{\rm GK}$ for r_s between 1 and 15, indicating exponential memory loss, with a longer-ranged memory for lower densities.

we evaluate it using a simple analytical model density [26] :

$$n(z,t) = \frac{2N_s}{L}\,\cos^2\left(\frac{\pi z}{L}\right)\left[1 + A\sin\omega t\,\sin\left(\frac{\pi z}{L}\right)\right], \tag{4.19}$$

which mimics the non-interacting density in a hard wall quantum well, driven by an AC field of frequency ω. We take A=0.01, $N_s = 1{a_0}^{-2}$ and $L = 10a_0$, such that $r_s \sim 1$ in the center and the system is in a weakly driven case.

Fig. 4.3 shows a stroboscopic plot of $v_{\rm xc}^{\rm M}(z,t)$ during the 4^{th} cycle after switch-on of the time dependent model density. It can be seen from the four highlighted snapshots that, when the density passes through equilibrium, turns around at the right wall, sloshes back and hits the left wall, $v_{\rm xc}^{\rm M}$ opposes the instantaneous current flow by building up a S-like potential barrier in the central part of the wall, trying to slow down the sloshing motion of density. There is little overall impact from the large-amplitude fluctuations of $v_{\rm xc}^{\rm M}$ close to edges since they occur

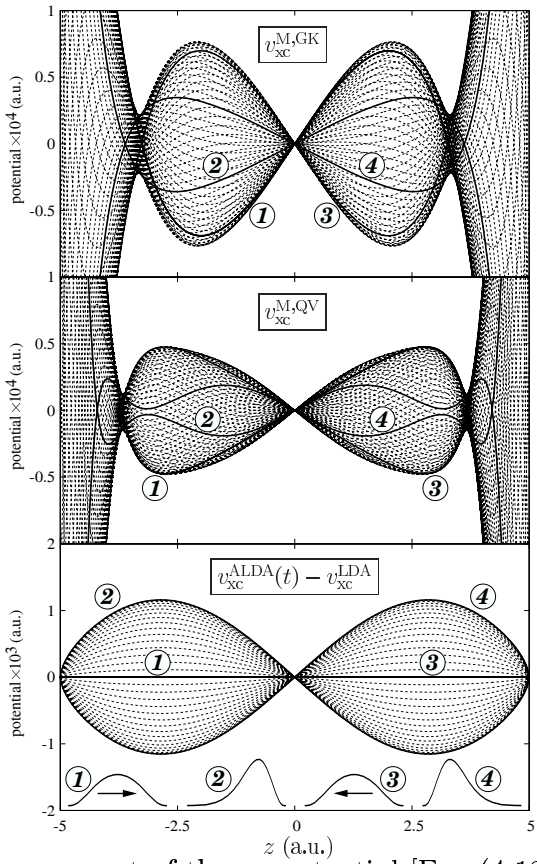

Figure 4.3: Memory part of the xc potential [Eq. (4.12)], evaluated for $n(z,t)$ of Eq. (4.19) in GK and QV parametrization, shown in a stroboscopic plot during the 4th cycle after switch-on. The heavy lines indicate equidistant snapshots. Compared to the ALDA fluctuations (bottom panel), $v_{\rm xc}^{\rm M,QV}$ and $v_{\rm xc}^{\rm M,GK}$ have a phase lag a little over $\pi/2$. The density oscillation in the inset is drawn with enhanced amplitude for clarity.

in low-density regions. Both the GK and QV potential have similar magnitude and shape, but lag behind the fluctuations of ALDA. For a purely dissipative, quarter-cycle ($\pi/2$) phase lag, the opposing potential barriers would be largest at the instants of maximal current flow, and flat when the density hits the wall and turns. The QV causes stronger damping than GK, since its phase lag is a bit closer to $\pi/2$, which is most efficient for retardation. The observation of a phase lag slightly higher than $\pi/2$ for both QV and GK is due to the presence

of dissipative as well as elastic contributions.

4.4 Dipole moment, energy dissipation and sideband generation

We now turn to a more realistic case and solve the TDKS equation with memory for a 40nm GaAs/$Al_{0.3}Ga_{0.7}As$ quantum well as in Chapter 3, but with electron density $1 \times 10^{11}\text{cm}^{-2}$ and without periodic driving field. Initially, the ground state was calculated in the presence of an electric field. Then the electric field is abruptly switched off. This leaves the quantum well electrons in an excited state and triggers collective charge-density oscillations. We calculate the dipole moment for weak excitation and strong excitation. Fig. 4.4 shows the dipole moment $d(t) = \int z\, n(z,t) dz$ versus time (1 a.u. = 61 fs in GaAs) for two initial electric fields, $\mathcal{E}_1 = 0.01$ and $\mathcal{E}_2 = 0.5$ mV/nm, comparing ALDA with ALDA+M. For weak excitation, we see regular oscillations associated with ISB plasmon. In ALDA, there is no damping, but with memory we find an exponential damping with characteristic decay time [26] and a small blueshift of the ISB plasmon frequency, very similar to the pump-probe experiments done by Heyman *et al.* [5]. With stronger excitation, the plasmon oscillation picks up higher harmonics and thus becomes more irregular.

The decoherence of the dipole oscillations is accompanied by energy dissipation. Fig. 4.5 shows the excitation energy per unit area, $E(t)$, scaled by the square of the initial electric field $\mathcal{E}$ [26, 78]. As a consequence of the quadratic Stark effect, $E(t)/\mathcal{E}^2$ is independent of $\mathcal{E}$ for small fields < 0.01 mV/nm, i.e., all curves lie on top of one another. For larger $\mathcal{E}$, higher-order deviations from the quadratic Stark effect emerge, and the curves start to move down.

For small $\mathcal{E}$, the excitation energy decreases as $E(t) = E(0)e^{-2\Gamma t}$, where $\Gamma = (48\text{ ps})^{-1}$. For larger $\mathcal{E}$, there is a more rapid initial decay. Also, note the appearance of a larger step structure. As long as these steps are not too

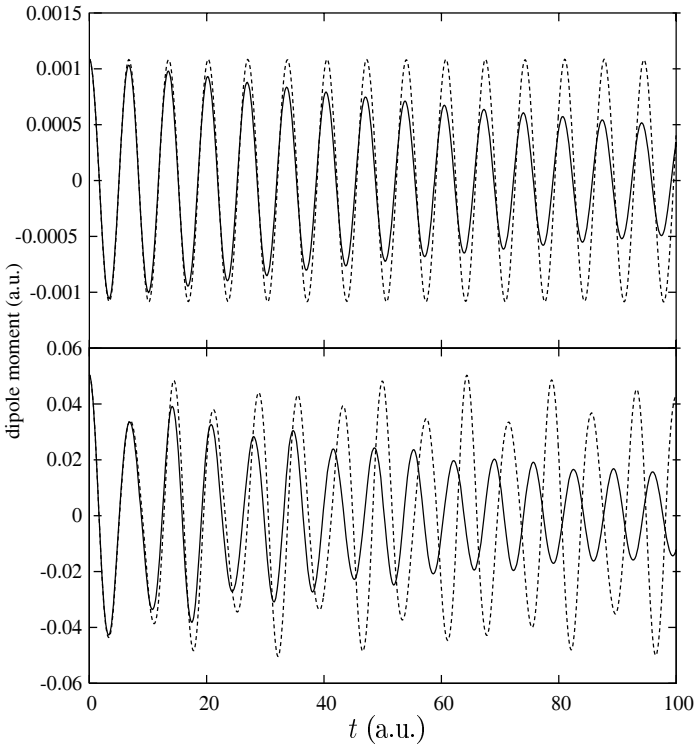

Figure 4.4: Dipole moment $d(t)$ of a 40-nm GaAs/$Al_{0.3}Ga_{0.7}As$ quantum well with electron density 1×10^{11} cm^{-2}, initially in a uniform electric field $\mathcal{E}_1 = 0.01$ mV/nm (top) and $\mathcal{E}_2 = 0.5$ mV/nm (bottom), which is abruptly switched off at $t = 0$. Dashed lines: ALDA. Full lines: ALDA+M (using QV).

pronounced, $E(t)$ is well described by a biexponential model, with an additional fast channel accounting for the hot-electron relaxation from higher subbands [26, 78]. The associated relaxation rate varies between 0.017 and 0.021 a. u. for $\mathcal{E}$ between 0.1 and 0.3 mV/nm.

The steps in $E(t)$ arise from a nonlinear coupling between the lowest (1-2, odd-parity) and next higher (1-3, even-parity) ISB plasmon modes, mediated through modulations in the TDKS effective potential. The crosstalk of these modes generates sidebands around ω_{12}, as shown in the right panel of Fig. 4.5, which depicts the dipole power spectrum for weak and strong excitations. The

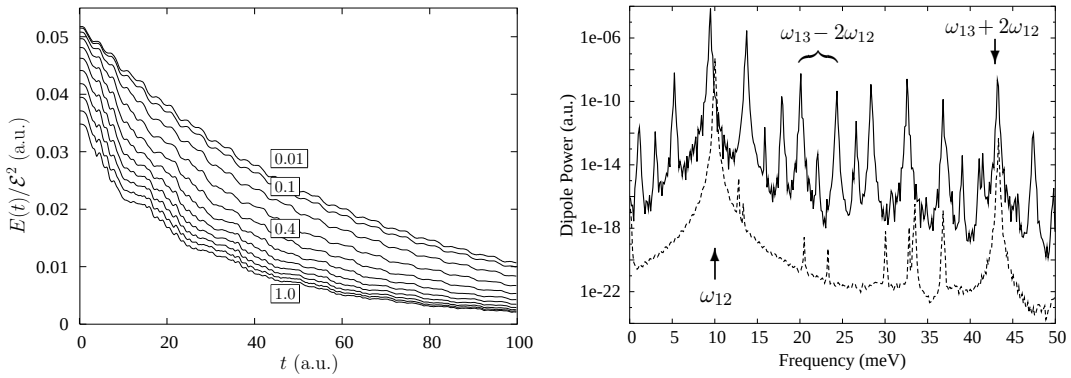

Figure 4.5: Left: dissipation of excitation energy $E(t)$ for a 40 nm GaAs/AlGaAs quantum well after sudden switch-off of initial fields $\mathcal{E}$ between 0.01 and 1 mV/nm. Right: dipole power spectrum of the associated charge-density oscillations for $\mathcal{E} = 0.01$ and 0.5 mV/nm (dashed and full lines), the latter showing sideband generation.

frequency spacing $\omega_{13} - 2\omega_{12}$ increases with $\mathcal{E}$ (0.27, 0.39, and 0.52 a.u. for 0.1, 0.5, and 1 mV/nm). We emphasize that the sidebands observed here arise purely from ISB collective electron dynamics, mediated through modulation of the time-dependent KS potential.

Finally, we comment on the physical mechanism for energy dissipation. In the linear regime, the Vignale-Kohn theory locally assumes a homogeneous electron gas subject to small periodic modulations. The frequency-dependent xc kernels then cause the decay of collective modes into multiple particle-hole excitations, even if Landau damping is forbidden [17, 18, 22]. In the time domain, one can view the dynamics of an inhomogeneous electron distribution as a superposition of local plasmon modes, each subject to decay into multiple particle-hole excitations.

In conclusion, we have given an explicit demonstration how memory effects introduce the element of intrinsic decoherence and energy relaxation into TDKS theory. We have explicitely solved, for the first time, a TDKS equation where

the xc potential is retarted, i.e., depends on previous densities.

This represents an alternative viewpoint to the density-matrix approach of Chapter 3, which, in its simplest form, describes dissipation through phenomenological decoherence and relaxation times (known as T_1 and T_2 for 2-level systems). A combination of the two approaches suggests itself as a powerful TDDFT tool to describe nonlinear electron dynamics in the presence of intrinsic and extrinsic (impurities and disorder) dissipation mechanisms.

Chapter 5

Time-dependent optimized effective potential method

In this chapter we will present another TDDFT approach to go beyond the adiabatic approximation to describe the electron dynamics in quantum wells: the time-dependent optimized effective potential (TDOEP) method. It is the time dependent version of the well-known OEP [28, 29], as introduced by [27] for atoms in strong laser pulses. In the following, we will consider mainly the exchange-only limit of the TDOEP approach. It will turn out that this leads again to a theory which features retardation. However, as we will discuss in detail, there will be no dissipation on the exchange-only level of the theory. We will use atomic units ($\hbar = m = e = 1$ where m and e refer to effective masses and charges whenever appropriate) in this chapter.

5.1 OEP and TDOEP basics: three generations of functionals

Modern DFT is based on the Hohenberg-Kohn (HK) theorem [32]. This theorem can be viewed as an exact reformulation of the quantum many body problem, only using the one-particle electronic density instead of the much more complicated many-body wave function. We will now briefly discuss how, over the

successful history of DFT, the constructions of functionals has proceeded over three generations.

In the first generation of DFT, explicitly density-dependent functionals were used to approximate both the kinetic energy of noninteracting particles, i.e., $T_s[n]$, and the xc energy $E_{\rm xc}$; both are not known exactly as a functional of the density n. The simplest and oldest approximation is the Thomas-Fermi model, where

$$T_s[n] = \frac{3}{10}(3\pi^2)^{2/3} \int d^3r\, n(\mathbf{r})^{5/3}. \tag{5.1}$$

In this model $E_{\rm xc}$ is completely neglected. For functionals of this type, one can easily use the HK variational principle which implies a differentiation of the total energy with respect to the density. This leads to equations of the Thomas-Fermi type. These equations can be easily solved numerically, since they contain only one basic variable, namely the density. Results obtained in this method are moderately accurate; in particular, they fail to give a realistic account of chemical binding.

The major advance of the second generation of DFT was introduced by Kohn and Sham [33]. The essential idea was to introduce the exact functional for the kinetic energy of non-interacting particles. This can be written as

$$T_s[n] = \sum_i^N \int d^3r \varphi_i^*[n](\mathbf{r}) \left(-\frac{1}{2}\nabla^2\right) \varphi_i[n](\mathbf{r}), \tag{5.2}$$

where φ_i are single particle orbitals. According to the HK theorem, any functional depending explicitly on the set of single-particle orbitals, like the above expression for kinetic energy is an implicit functional of the density. In this case, the orbitals should come from a local potential. In the second generation of DFT, since we are treating the kinetic energy functional exactly, only the xc energy has to be approximated. In practice, the KS equations have to be solved self-consistently employing approximate but explicitly density-dependent functionals for $E_{\rm xc}[n]$. The most commonly use approximation is the LDA, where one uses

the xc energy per particle of the homogeneous electron gas of constant density n. More recently, the so called generalized gradient approximations (GGAs) have shown excellent results for a wide range of atomic, molecular and solid state systems [79–82].

In the third generation of DFT, one opts to use explicitly orbital dependent functionals for $E_{\rm xc}$, thus providing more freedom in the construction of xc functionals. This approach has a much better chance for successful calculations where GGAs are failing. For example, GGA does not predict the existence of negative ions, fails to produce dispersion forces, and has some difficulties with the treatment of higher angular momentum [83, 84]. In this generation, not only the exact expression for kinetic energy, but also the exact expression for the exchange energy is employed. The exchange energy is given by the Fock expression,

$$E_{\rm x}[n] = -\frac{1}{2}\sum_{\sigma}\sum_{j,k}^{N_\sigma}\int d^3r\int d^3r'\frac{\varphi^*_{j\sigma}(\mathbf{r})\varphi^*_{k\sigma}(\mathbf{r}')\varphi_{k\sigma}(\mathbf{r})\varphi_{j\sigma}(\mathbf{r}')}{|r-r'|}. \tag{5.3}$$

Therefore, only the correlation energy needs to be approximated in this approach. The level of approximation to the xc energy makes the difference between the second and third generation.

However, the calculation of xc potentials needs a differentiation with respect to the density and is not straightforward, since now $E_{\rm xc}$ explicitly depends on the orbitals. The corresponding indirect scheme to obtain this is known as the OEP method [28, 29]. In this method, the minimization of the orbital functional with respect to the density is achieved by repeated application of the chain rule for functional differentiation,

$$v_{\rm xc}[n](\mathbf{r}) = \frac{\delta E_{\rm xc}[\{\varphi_i\}]}{\delta n(\mathbf{r})} = \int d^3r'\int d^3r''\sum_i\left[\frac{\delta E_{\rm xc}[\{\varphi_i\}]}{\delta\varphi_i(\mathbf{r}')}\frac{\delta\varphi_i(\mathbf{r}')}{\delta v_s(\mathbf{r}'')}\frac{\delta v_s(\mathbf{r}'')}{\delta n(\mathbf{r})} + c.c.\right]. \tag{5.4}$$

Further evaluation of Eq. (5.4) gives rise to the OEP integral equation which we will discuss below in detail. As an alternative to solving the full OEP equation, Krieger, Li, and Iafrate (KLI) have proposed a simple but surprisingly accurate

approximation instead of the full OEP [36, 37]. The high accuracy attained in applications of OEP for example in spherical atoms [36,37,85] and for solids [86], and the fact that it is easier to devise orbital functionals than explicit density functionals, makes the OEP concept attractive. Yet, due to the rather large computational effort involved in this scheme, it has not been used extensively. Most of the OEP methodology carried out using exchange energy only, neglecting the correlation energy, thus known as exact-exchange method.

There are interesting properties associated with the OEP and KLI methods.

- No spurious self-interactions

  Both OEP and KLI methods are constructed to deal with orbital dependent functionals. Therefore, one can employ functionals, which exactly cancel the spurious self interaction contained in the Hartree term. Such functionals are the exact-exchange, or the Perdew-Zunger self-interaction corrected functionals (see below).

- Asymptotics

  Both the OEP and the KLI potential fall of correctly as $-1/r$ as $r \to \infty$ [36, 88] if the exact exchange is used. This holds for all orbitals, unlike in Hartree-Fock where this happens only for the occupied orbitals. This is because the KS potential is the same for all orbitals.

- Derivative discontinuities

  The exact xc potential exhibits discontinuities at integer values of N [87], if we consider it to be a function of the particle number N. The OEP and the KLI potential can reproduce this important feature. Neither LDA nor the GGAs can produce these discontinuities.

The time-dependent generalization of the OEP method was first introduced by Ullrich *et al.* and has been successfully applied to non-perturbative descriptions of atoms and clusters [27]. Like in the stationary case, the TDOEP method

offers a valuable route to go beyond the local density approximations. In the coming sections of this chapter, we will show the full, real-time TDOEP scheme for electronic dynamics in a quantum well. This approach genaralizes the work done by Hirata *et al.* [89] who used the exact-exchange frequency-dependent kernel in linear response, and the work by Mundt and Kümmel [90] who made first (but ultimately unsuccessful) attempts at the time-dependent formalism. We will start by introducing the OEP for stationary (static) quantum wells.

5.2 OEP for quantum wells

We take as starting point a given expression for the total energy $E[\{\varphi_{j\sigma}\}]$ of an N-electron system as a functional of a set of spin orbitals $\{\varphi_{j\sigma}(\mathbf{r})\}$,

$$\begin{aligned} E[\{\varphi_{j\sigma}\}] &= \sum_{\sigma}\sum_{j}^{N_\sigma}\int d^3r\varphi^*_{j\sigma}(\mathbf{r})(-\nabla^2/2)\varphi_{j\sigma}(\mathbf{r}) + \sum_{\sigma}\int d^3n_\sigma(\mathbf{r})v_{\rm ext}(\mathbf{r}) \\ &\quad + \frac{1}{2}\int d^3r\int d^3r'\frac{n(\mathbf{r})n(\mathbf{r}')}{|\mathbf{r}-\mathbf{r}'|} + E_{\rm x}[\{\varphi_{j\sigma}\}]. \end{aligned} \tag{5.5}$$

A detailed description of obtaining the OEP integral equation is given in Appendix C. We have just summarize the essentials here. The Fock exchange term $E_{\rm x}$ for a quantum well reads [91]:

$$E_{\rm x} = -\sum_{i,j,\sigma} k_F^{i\sigma}k_F^{j\sigma}\int dz\int dz'\varphi^*_{i\sigma}(z)\varphi_{i\sigma}(z')\varphi^*_{j\sigma}(z')\varphi_{j\sigma}(z)F^{11}_{ij}(z,z'), \tag{5.6}$$

where

$$F^{11}_{ij}(z,z') = \frac{A}{4\pi}\int_0^\infty \frac{d\rho J_1(k_F^{i\sigma}\rho)J_1(k_F^{j\sigma}\rho)}{\rho\sqrt{\rho^2+(z-z')^2}}. \tag{5.7}$$

Here, J_1(x) stands for the cylindrical Bessel function of order 1, A represents the area, and $(k_F^{i\sigma})^2 = 2(\epsilon_F - \epsilon_i)$. The exact exchange potential is defined as

$$V_{XX\sigma}(z) = \frac{\delta E_{\rm x}}{\delta n_\sigma(z)}, \tag{5.8}$$

which cannot be immediately evaluated, since $E_{\rm x}$ is a functional of the orbitals, not of the density. However, using the chain rule for functional differentiation twice, we find

$$V_{XX\sigma}(z) = A\sum_i \int dz' \frac{\delta V_{KS\sigma}(z')}{\delta n_\sigma(z)} \int dz'' \left[\frac{\delta E_{\rm x}}{\varphi_i^\sigma(z'')} \frac{\delta \varphi_i^\sigma(z'')}{\delta V_{KS\sigma}(z')} + c.c. \right]. \tag{5.9}$$

$\delta V_{KS\sigma}(z')/\delta n_\sigma(z) = \chi_\sigma^{-1}(z,z')$ is the inverse of the KS noninteracting response function $\chi_\sigma(z,z') = \delta n_\sigma(z)/\delta V_{KS\sigma}(z')$, given by

$$\chi_\sigma(z,z') = \sum_i \left\{ \frac{(k_F^{i\sigma})^2}{4\pi A} [\varphi_i^\sigma(z)\varphi_i^\sigma(z') G_{i\sigma}(z,z') + c.c.] \right\}. \tag{5.10}$$

The static Green's function $G_{i\sigma}$ is given by

$$G_{i\sigma}(z',z) = \sum_{i\neq j} \frac{\varphi_{j\sigma}^*(z')\phi_{j\sigma}(z)}{\epsilon_{j\sigma} - \epsilon_{i\sigma}}. \tag{5.11}$$

From Eq. (5.9), the OEP equation for N occupied subbands follows as [91]:

$$\boxed{\sum_{i=1}(k_F^{i\sigma})^2 \int dz' \{[V_{XX\sigma}(z') - u_{X\sigma i}(z')] G_{i\sigma}(z',z)\varphi_{i\sigma}^*(z')\varphi_{i\sigma}(z) + c.c\} = 0,} \tag{5.12}$$

where

$$u_{X\sigma i}(z') = \frac{4\pi}{(k_F^{i\sigma})^2 \varphi_{i\sigma}^*(z')} \frac{\delta E_X}{\delta \varphi_i(z')}. \tag{5.13}$$

The OEP integral equation (5.12) needs to be solved numerically for $V_{XX\sigma}$, which relatively is straightforward, since it needs the solution of system of linear equations. In this section, I will not give the numerical details of solving this equation. However, in later section I will give numerical details of solving the TDOEP scheme, which is more complicated than the OEP equation.

5.2.1 Slater, KLI, OEP

Solving the full OEP integral equation is computationally more demanding mainly due to the presence of the Green's function (5.11). This Green's function depends on the complete KS spectrum, not just the occupied states. The full solution of (5.12) thus requires the evaluation, as well as the storage of all occupied and unoccupied KS states. There is a simplified procedure to avoid this: the KLI method. The idea is to use a closure approximation for the Green's function. By approximating the eigenvalue difference, $\epsilon_{j\sigma} - \epsilon_{i\sigma} \approx \Delta E$ in the denominator of Eq. (5.11) and substituting that into Eq. (5.12), one arrives at the KLI equation [36, 37] as shown below:

$$\sum_{j\neq i}\sum_{i=1}(k_F^{i\sigma})^2 \int dz'[V_{XX\sigma}(z') - u_{X\sigma i}(z')]\varphi_{j\sigma}(z')\varphi^*_{j\sigma}(z)\varphi^*_{i\sigma}(z')\varphi_{i\sigma}(z) + c.c = 0. \tag{5.14}$$

We can rewrite Eq. (5.14) as

$$\begin{aligned}&\sum_{j=1}\sum_{i=1}(k_F^{i\sigma})^2 \int dz'[V_{XX\sigma}(z') - u_{X\sigma i}(z')]\varphi_{j\sigma}(z')\varphi^*_{j\sigma}(z)\varphi^*_{i\sigma}(z')\varphi_{i\sigma}(z)\\ &-\sum_{i=1}(k_F^{i\sigma})^2 \int dz'[V_{XX\sigma}(z') - u_{X\sigma i}(z')]\varphi_{i\sigma}(z')\varphi^*_{i\sigma}(z)\varphi^*_{i\sigma}(z')\varphi_{i\sigma}(z)\\ &+c.c = 0.\end{aligned} \tag{5.15}$$

Using completeness $\sum_j \varphi_{j\sigma}(z')\varphi^*_{j\sigma}(z) = \delta(z-z')$, and defining $(k_F^{i\sigma})^2\varphi^*_{i\sigma}(z)\varphi_{i\sigma}(z) = n_{i\sigma}(z)$, we can write Eq. (5.15) as

$$\begin{aligned}V_{XX\sigma}(z) &= \frac{1}{n_\sigma(z)}\sum_i n_{i\sigma}(z)u_{X\sigma i}(z) + \frac{1}{n_\sigma(z)}\sum_i n_{i\sigma}(z)\\ &\quad\times\int dz'\varphi^*_{i\sigma}(z')\varphi_{i\sigma}(z')[V_{XX\sigma}(z') - u_{X\sigma i}(z')],\end{aligned} \tag{5.16}$$

where $n_\sigma(z) = \sum_j (k_F^{j\sigma})^2\varphi^*_{j\sigma}(z)\varphi_{j\sigma}(z)$. This equation can now be solved explicitly for $V_{XX\sigma}$, as follows. The so called Slater potential [92] is given by the first term in Eq. (5.16),

$$V_X^S = \frac{1}{n_\sigma(z)}\sum_i n_{i\sigma}(z)u_{X,i}(z,\sigma). \tag{5.17}$$

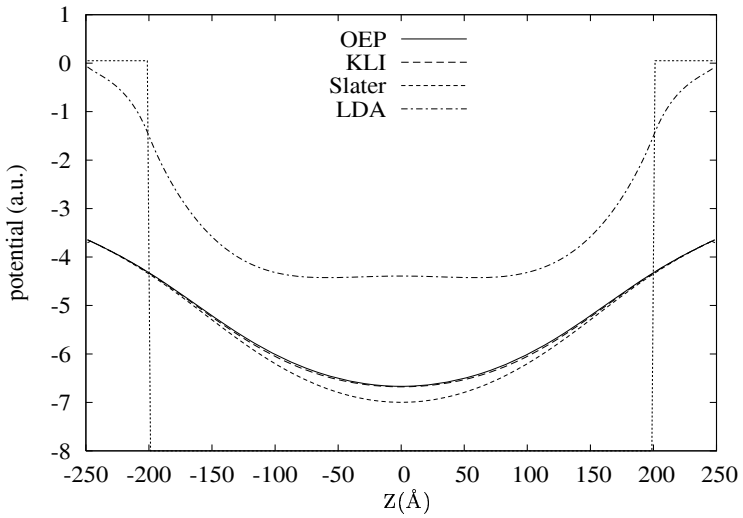

Figure 5.1: Exchange potential of a 40-nm GaAs/$Al_{0.3}Ga_{0.7}As$ quantum well with two occupied subbands calculated with different approximations. The edges of the quantum well are also indicated.

Therefore, letting $\int dz' \varphi^*_{i\sigma}(z')\varphi_{i\sigma}(z')V_{XX}(z',\sigma) = \overline{V}_{XXi}$, and operating on Eq. (5.16) with $\int dz \varphi^*_{k\sigma}(z)\varphi_{k\sigma}(z)$ on both sides, we get

$$\overline{V}_{XXk} = \overline{V}^S_{Xk} + \int dz \varphi^*_{k\sigma}(z)\varphi_{k\sigma}(z)\frac{1}{n_\sigma(z)}\sum_i n_{i\sigma}(z)[\overline{V}_{XXi} - \overline{u}_{xi}]. \tag{5.18}$$

Letting $M_{ki} = \int dz \varphi^*_{k\sigma}(z)\varphi_{k\sigma}(z)n_{i\sigma}(z)/n_\sigma(z)$ one can write Eq. (5.18) as

$$\overline{V}_{XXi} = (\mathbf{1} - \underline{\underline{M}})^{-1}(\overline{V}^S_{Xk} - \sum_i M_{ki}\overline{u}_{xi}). \tag{5.19}$$

In the following, we consider only two occupied subbands. Then Eq. (5.19) can be solved analytically for $V_{XX\sigma}$ without matrix inversion. We solved the full OEP equation, together with the KLI and Slater approximations for a 40-nm GaAs/$Al_{0.3}Ga_{0.7}As$ quantum well as described in Chapter 3, with a sheet density of $N_s = 2.2 \times 10^{11}$ cm^{-2}, i.e. the two lowest subbands are occupied. Agreeing with the features describe at the beginning of this chapter, we found the following (see Fig. 5.1):

- LDA differs significantly from the other potentials and does not have the

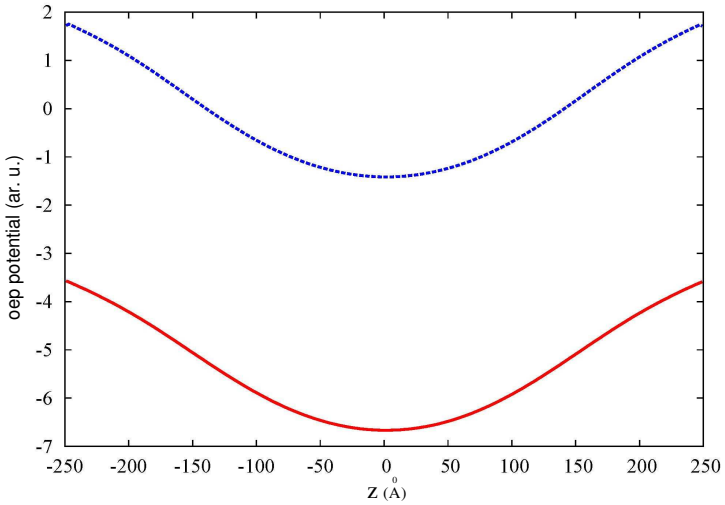

Figure 5.2: Exchange potential of a 40-nm GaAs/$Al_{0.3}Ga_{0.7}As$ quantum well with slightly different sheet densities. Solid line: Potential only with the first subband occupied. Dotted line: Potential when the second subband is occupied infinitesimally.

correct asymptotic behavior: it drops exponentially to zero outside the well. By contrast, Slater, KLI and OEP potentials all go to zero as $-1/z$.

- There is only a marginal difference between the KLI exchange potential and the OEP exact-exchange potential. The Slater potential is a bit deeper than KLI and OEP. This is well known for atoms [37].

- The KLI as well as OEP exchange potentials reproduce an important property of the exact xc potential: they jump discontinuously when a new level is filled [37, 94]. We observe this discontinuity when we start occupying the second subband (Fig. 5.2). This effect is absent in LDA.

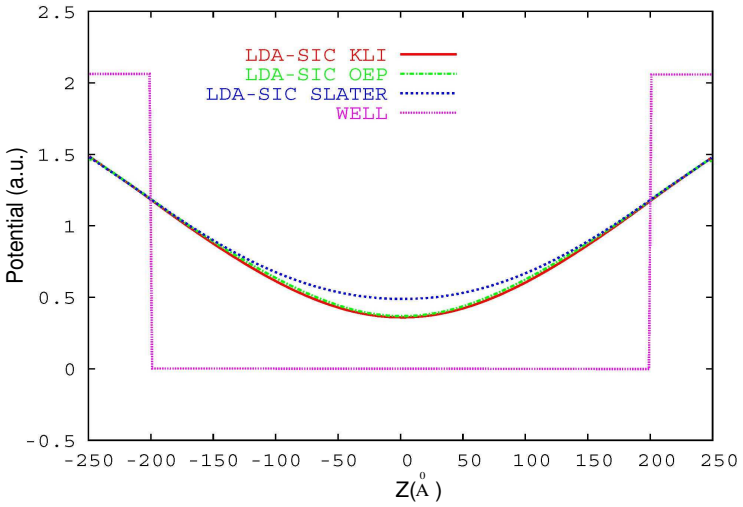

Figure 5.3: LDA-SIC OEP potential of a 40-nm GaAs/$Al_{0.3}Ga_{0.7}As$ quantum well with two occupied subbands calculated with different approximations. The edges of the quantum well are also indicated.

5.2.2 LDA-SIC OEP potential

A major drawback of the LDA is that it has the wrong asymptotic behavior. As a consequence, the energy eigenvalue of the highest occupied KS orbital deviates considerably from the exact ionization energy of the system (the two should be equal if the exact $v_{\rm xc}$ were used). Thus, for example, in atoms, this violates Koopmans' theorem which states that the ionization energy is identical with the single-particle energy of the last bound electron [95]. In metal clusters, because of the inappropriate ionization potential, features of electron emission are spoiled. This is because LDA includes an interaction of localized electrons with themselves. Various efforts have been made to eliminate the self interaction error in LDA [96]. The most widely used scheme is the self-interaction correction (SIC) by Perdew and Zunger [97]. It turns out that SIC leads to improvements in total energies of atoms, and also improves the band gap of solids. The LDA-SIC has been used successfully to describe electron affinities, static

and dynamical properties, as well as transition metal oxides [98–102]. In the LDA-SIC one eliminates the self-interaction component by explicitly subtracting the erroneous terms for the each orbital, which results in an orbital-dependent xc functional [97]. Therefore it is a suitable candidate for the OEP scheme.

We calculated the LDA-SIC potential for quantum well, closely following the implementation suggested by Ullrich *et al.* [103]. In this case the LDA-SIC exchange potential for a spin-up particle in state j for a quantum well is given by

$$u_{Xj\uparrow}(z') = v_{X\uparrow}^{LDA}[n_\uparrow, n_\downarrow](z') - v_{\mathrm{H}}[n_{j\uparrow}](z') - v_{X\uparrow}^{LDA}[n_{j\uparrow}, 0](z'). \tag{5.20}$$

One can easily prove, using the exchange energy functionals with spin polarization, that

$$v_{X\uparrow}^{LDA}[n_\uparrow, n_\downarrow](z') = -\left(\frac{3n}{\pi}\right)^{1/3}, \tag{5.21}$$

and

$$v_{X\uparrow}^{LDA}[n_{j\uparrow}, 0](z') = -\left(\frac{6n_{j\uparrow}}{\pi}\right)^{1/3}. \tag{5.22}$$

In the LDA-SIC OEP scheme, one can use (5.20) instead of Eq. (5.13). Therefore, numerically solving the full OEP equation with LDA-SIC is much simpler, especially in the time-dependent case, since one doesn't need to deal with orbitals and the Bessel function integrations.

We compared the validity of this scheme with the full OEP exact-exchange scheme. In the static case, results were similar to that of OEP exact-exchange case, in particular, the LDA-SIC gives the correct asymptotic behavior (see Fig. (5.3)). The time-dependent results are given in further below. Our main purpose of solving LDA-SIC OEP was to see whether we can get a stable solution in the time-dependent scheme, since at first we encountered a numerical problem with full TDOEP exact exchange. In a later section we will show that we overcame this problem and were able to solve for the first time the TDOEP equation with exact exchange.

5.3 TDOEP for quantum wells

5.3.1 Formalism

The full, exchange-only TDOEP equation for a quantum well for N occupied subbands is given by

$$i\sum_{j=1}^{N\sigma}(k_F^{j\sigma})^2\int_{-\infty}^{t}dt'\int dz'[V_{XX\sigma}(z',t')-u_{Xj\sigma}(z',t')]K_{j\sigma}(z',t',z,t) \times \phi^*_{j\sigma}(z',t')\phi_{j\sigma}(z,t)+c.c=0, \qquad (5.23)$$

where

$$K_{j\sigma}(z',t',z,t)=\sum_{k\neq j}^{\infty}\phi_{k\sigma}(z',t')\phi^*_{k\sigma}(z,t), \qquad (5.24)$$

and $u_{Xj\sigma}(z',t')$ is obtained from the time dependent version of Eq. (5.13). The detailed derivation of above (5.23) is not given here, one can easily obtain it by closely looking at the derivation given by Ullrich *et al.* for atoms and molecules [27], but here for a quantum well.

There are several interesting features in this optimized potential method. Eq. (5.23) reduces to the static case, and since it contains a time integral (not like TDKLI [93]), it has an infinite memory. Also, it was shown that in Eq. (5.23), one has to take -∞ as the lower limit of the time integral in order to recover the static limit from the time-dependent formalism, otherwise with a finite lower time boundary this results in an unphysical time dependence even in the static case. This is due to the fact that a finite limit does not correctly account for the full memory in V_{XX}. The information that the system has been in the ground state for all times up until $t=t_0$ must be built into the formalism [93]. We can rewrite Eq. (5.23) as follows:

$$i\sum_{j=1}^{N\sigma}(k_F^{j\sigma})^2\left[\int_{-\infty}^{t_0}dt'+\int_{t_0}^{t}dt'\right]\int dz'[V_{XX\sigma}(z',t')-u_{Xj\sigma}(z',t')] \times K_{j\sigma}(z',t',z,t)\phi^*_{j\sigma}(z',t')\phi_{j\sigma}(z,t)+c.c=0. \qquad (5.25)$$

The system is assumed to be in its ground state for -$\infty < t < t_0$. We can write the time-dependent orbitals as $\phi_{j\sigma}(z,t) = \varphi_{j\sigma}(z)e^{-i\epsilon_{j\sigma}t}$ for $t < t_0$. Then Eq. (5.25) becomes

$$
\begin{aligned}
i\sum_{j=1}^{N\sigma}\sum_{k\neq j}(k_F^{j\sigma})^2\int_{-\infty}^{t_0}dt'\int dz'[V_{XX\sigma}(z')-u_{Xj\sigma}(z')]\phi_{j\sigma}(z,t)\phi^*_{k\sigma}(z,t) \\
\times\,\varphi^*_{j\sigma}(z')\varphi_{k\sigma}(z')e^{-i(\epsilon_{k\sigma}-\epsilon_{j\sigma})(t'-t_0)}+c.c. \\
+i\sum_{j=1}^{N\sigma}\sum_{k\neq j}(k_F^{j\sigma})^2\int_{t_0}^{t}dt'\int dz'[V_{XX\sigma}(z',t')-u_{Xj\sigma}(z',t')]\phi^*_{j\sigma}(z',t') \\
\times\,\phi_{j\sigma}(z,t)\phi^*_{k\sigma}(z,t)\phi_{k\sigma}(z',t')+c.c.=0. \qquad (5.26)
\end{aligned}
$$

In the first part of Eq. (5.26), the integral over t' can be carried out. Thus, we get the TDOEP equation with the initial condition explicitly built in [41, 104]:

$$
\begin{aligned}
&\sum_{j=1}^{N\sigma}\sum_{k\neq j}(k_F^{j\sigma})^2\int dz'[V_{XX\sigma}(z')-u_{Xj\sigma}(z')]\phi_{j\sigma}(z,t) \\
&\qquad\times\,\phi^*_{k\sigma}(z,t)\frac{\varphi^*_{j\sigma}(z')\varphi_{k\sigma}(z')}{\epsilon_{j\sigma}-\epsilon_{k\sigma}}+c.c. \\
&+i\sum_{j=1}^{N\sigma}\sum_{k\neq j}(k_F^{j\sigma})^2\int_{t_0}^{t}dt'\int dz'[V_{XX\sigma}(z',t')-u_{Xj\sigma}(z',t')] \\
&\qquad\times\,\phi^*_{j\sigma}(z',t')\phi_{j\sigma}(z,t)\phi^*_{k\sigma}(z,t)\phi_{k\sigma}(z',t')+c.c=0
\end{aligned} \qquad (5.27)
$$

Letting $R(z,t)$ and $M(z,t,z',t')$ be

$$
\begin{aligned}
R(z,t) \;=\; & i\sum_{j=1}^{N\sigma}(k_F^{j\sigma})^2\int_{t_0}^{t}dt'\int dz'[u_{Xj\sigma}(z',t')]\phi^*_{j\sigma}(z',t')\phi_{j\sigma}(z,t) \\
&\times\sum_{k\neq j}\phi^*_{k\sigma}(z,t)\phi_{k\sigma}(z',t')+c.c. \\
&-\sum_{j=1}^{N\sigma}\sum_{k\neq j}(k_F^{j\sigma})^2\int dz'[V_{XX\sigma}(z')-u_{Xj\sigma}(z')]\phi_{j\sigma}(z,t) \\
&\times\,\phi^*_{k\sigma}(z,t)\frac{\phi^*_{j\sigma}(z')\phi_{k\sigma}(z')}{\epsilon_{j\sigma}-\epsilon_{k\sigma}}+c.c. \qquad (5.28)
\end{aligned}
$$

$$M(z,t,z',t') = i\sum_{j=1}^{N\sigma}(k_F^{j\sigma})^2 V_{XX\sigma}(z',t')\phi^*_{j\sigma}(z',t')\phi_{j\sigma}(z,t) \times \sum_{k\neq j}\phi^*_{k\sigma}(z,t)\phi_{k\sigma}(z',t') + c.c., \quad (5.29)$$

we can rewrite Eq.(5.27) in a more compact form

$$\boxed{\int_{t_0}^{t} dt' \int dz' V_{XX\sigma}(z',t')M(z,t,z',t') = R(z,t).} \quad (5.30)$$

Solving Eq. (5.30) for $V_{XX\sigma}$, we will be able to calculate the exact exchange potential in the TDOEP scheme. Solving the full TDOEP equation has always been computationally and numerically a challenging task. For the first time, we have shouldered this task and were able to solve the full TDOEP equation for a quantum well. Unlike the instabilities suggested by Mundt and Kümmel [94] from a different method, we were able to get stable solutions for the quantum well.

5.3.2 Numerical Solution

Solving the TDOEP equation

Our task is to solve (5.30) for $V_{XX\sigma}$ for a quantum well. To do this we discretize the time variable in uniform time steps Δt. (The spatial variable is discretized in a similar way, which is more straightforward and does not need to be discussed here.)

From Eq. (5.29), we see that $M(z,t,z',t') = 0$ for $t = t'$. Therefore, in order to solve for $V_{XX\sigma}$ we need to consider the $t + 2\Delta t$ region, given that we use a time step of Δt for our time propagation. Eq. (5.30) yields

$$\int_0^{t+2\Delta t} dt' \int dz' V_{XX\sigma}(z',t')M(z,t+2\Delta t,z',t') = R(z,t+2\Delta t). \quad (5.31)$$

We have

$$\int_t^{t+2\Delta t} dt' \int dz' V_{XX\sigma}(z',t') M(z,t+2\Delta t,z',t')$$
$$= R(z,t+2\Delta t) - \int_0^t dt' \int dz' V_{XX\sigma}(z',t') M(z,t+2\Delta t,z',t'). \quad (5.32)$$

We use the simple trapezoidal rule [105] to evaluate the t' integrals. Eq. (5.32) becomes

$$\Delta t \int dz' V_{XX\sigma}(z',t+\Delta t) M(z,t+2\Delta t,z',t+\Delta t)$$
$$= R(z,t+2\Delta t) - \Delta t/2 \int dz' V_{XX\sigma}(z',0) M(z,t+2\Delta t,z',0)$$
$$-\Delta t \int dz' V_{XX\sigma}(z',t) M(z,t+2\Delta t,z',t)$$
$$- \sum_{j=2}^{N_t-2} \int dz' V_{XX\sigma}(z',t_j) M(z,t+2\Delta t,z',t_j), \quad (5.33)$$

where we use the notation $t_j = (j-1)\Delta t$, and $t = (N_t - 1)\Delta t$. Since we have placed the static and time dependent orbitals on a uniform one-dimensional spatial grid with typically $N_{grid} \sim 250$ points, we can use the same trapezoidal rule to do the z' and z integration. The value of $V_{XX\sigma}(z',0)$ was obtained from solving the static OEP equation. We then solved Eq. (5.33) by matrix inversion using the singular value decomposition method [105]. The important trick at this moment to remember is that you need to evaluate (5.7) only once. Then we used a look-up table procedure, whenever we need it in evaluating $R(z,t+2\Delta t)$. In practice, we were able to carry out time propagation over approximately $N_t = 600$ time steps, limited by CPU time and single-processor RAM.

Self-consistent iterative scheme

A potential pitfall of the TDOEP scheme is the fact that $V_{XX\sigma}$ depends on the time-dependent orbitals, which, in turn, are determined by $V_{XX\sigma}$. In other words, the TDOEP scheme requires self-consistency over the entire interval [0,T] of time propagation. Mundt and Kümmel [94] have claimed that the TDOEP

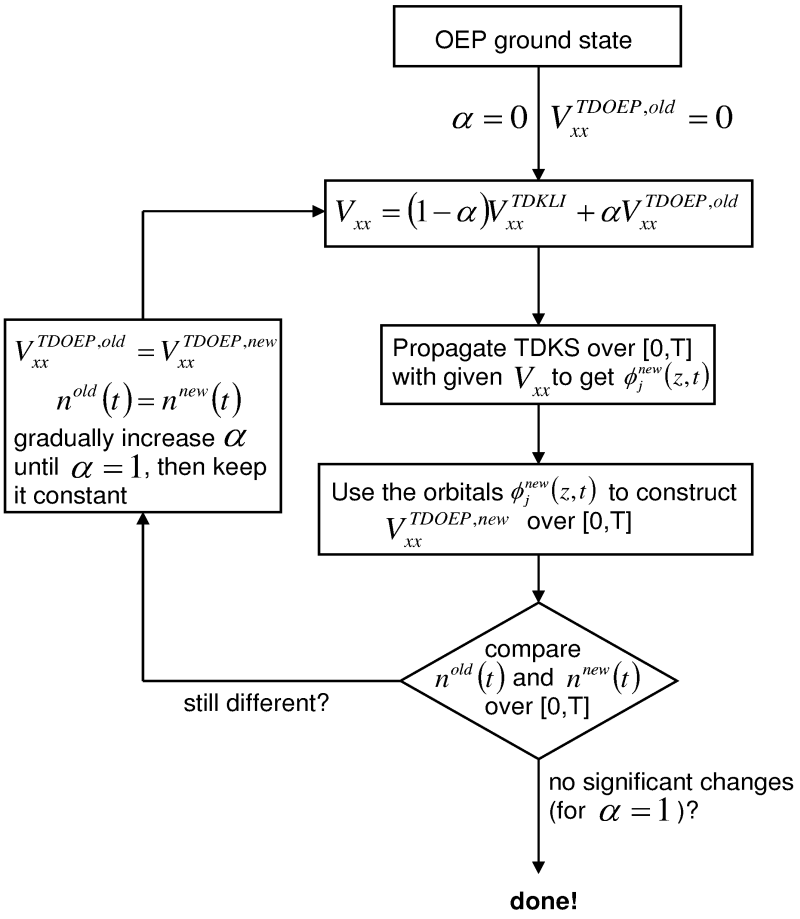

Figure 5.4: Self-consistence numerical procedure

scheme is inherently unstable. We have, however, developed a stable iterative scheme with which we have successfully reached self-consistency.

Our scheme is summarized in the flow chart of Fig. (5.4). The procedure consists of the following steps.

Step 1: start with the full OEP ground state.

Step 2: solve the TDKS equation using the TDKLI functional over the interval [0,T]. This yields approximate TDKS orbitals $\phi_j^{\rm new}(z,t)$.

Step 3: use the so obtained TDKS orbitals as input in Eq. (5.33) to construct

the approximate TDOEP potential, $V_{XX}^{\mathrm{TDOEP,\,new}}$ in [0,T].

Step 4: solve the TDKS equation in [0,T] again with the total potential

$$V_{XX}(t) = (1-\alpha)V_{XX}^{\mathrm{TDKLI}}(t) + \alpha V_{XX}^{\mathrm{TDOEP}}(t) \tag{5.34}$$

where $\alpha \in [0,1]$.

Step 5: solve the TDKS equation using V_{XX}, which gives new approximate orbitals.

Step 6: repeat steps 3, 4 and 5, while gradually increasing α from 0 to 1, in steps of 0.1 or 0.2. Once we have $\alpha = 1$, it means that we feed in the full TDOEP potential of the previous iteration. This is then repeated until convergence is achieved (typically about 10-20 times).

In this way, we have found that we were able to solve the TDOEP scheme without any instabilities. It is essential for convergence to start with KLI and only gradually mix in TDOEP with the help of the α-parameter.

5.4 Adiabatic TDOEP

The adiabatic approximation for v_{xc} is one in which we ignore all dependence on the past, and allow only dependence on the instantaneous density. That is, in the approximations it uses the same functional as for the ground state, but this functional is evaluated using a time-dependent input. This operational definition can be written as

$$v_{\mathrm{xc}}^{adia}[n](\mathbf{r},t) = v_{\mathrm{xc}}^{static}[n(t)](\mathbf{r}). \tag{5.35}$$

The most commonly used one is the ALDA, which is an explicit functional of n, and one just needs to plug in the time-dependent density $n(\mathbf{r},t)$. Now the question is how does it work for orbital functionals? The TDKLI and time-dependent Slater functionals are in a sense already adiabatic approximations, since they are explicit functionals of the occupied orbitals φ_j and one simply needs to plug in the time-dependent ϕ's. Now for full TDOEP, it is not that

easy, since it is an explicit functional of all orbitals and all the eigenenergies. Since one cannot exactly say what the $\epsilon_j(t)$ are, the TDOEP scheme cannot be made adiabatic in a straightforward way. Since we don't know the phases $e^{i\epsilon_j t}$, one cannot exactly say how TDOEP in the adiabatic approximations, will reduce to static OEP. So the normal operational definition for ALDA, KLI is no good for OEP, and we need to look at it from a different perspective.

The adiabatic approximation means that one pretends that the system evolves so slowly in $v_{\rm ext}(t)$, that it always remains in the ground state which belongs to the instantaneous $v_{\rm ext}$. So, in TDOEP, we therefore need to find that static OEP potential which produces $n(t)$ as a ground state. That is, take the density at some time t_0, and ask: what is the static OEP potential which leads to $n(\mathbf{r}, t_0)$ as its ground state? We proceed in two steps:

(1) Inversion of the KS equation

Closely following the iterative scheme given by van Leeuwen [106], one can calculate the KS potential corresponding to a density n. Suppose at some time during the iteration, we have calculated orbitals φ_j^{old} with eigenvalues ϵ_j^{old} and corresponding density n^{old} and potential v^{old}. Then in the next step one can define the new potential v^{new} to be

$$v^{new}(\mathbf{r}) = \frac{n^{old}(\mathbf{r})}{n(\mathbf{r})} v^{old}(\mathbf{r}), \tag{5.36}$$

following the KS equation. Then using this potential one can calculate new orbitals and a new density and find the same way a new potential. This procedure is continued until the density calculated from the orbitals is the same as the given density. In the first step, we therefore use the van-Leeuwen procedure to construct that single-particle potential $v^{static}(z,t)$ which produces $n(t)$ as its ground state. From the static KS equation featuring $v^{static}(z,t)$, we then get a complete spectrum of eigenvalues $\epsilon_j^{static}(t)$ and eigenfunctions $\phi_j^{static}(z,t)$.

(2) Constructing the adiabatic TDOEP potential

We next take the eigenvalues $\epsilon_j^{static}(t)$ and eigenfunctions $\phi_j^{static}(z,t)$ which we obtained in our inversion procedure and plug them into the static OEP integral equation (5.12). This yields $V_{XX}^{adia}(z,t)$.

5.5 Results and Discussion

This section is dedicated to a discussion of the results we have obtained solving the full TDOEP equation with the numerical methods described earlier. All our simulations were performed for a 40nm GaAs/$Al_{0.3}Ga_{0.7}As$ quantum well as described in Chapter 3 with $N_s = 2.2\times10^{11}\text{cm}^{-2}$, i.e. the lowest two subband levels are occupied. We have performed our calculations for two different types of plasmon oscillations: free and driven oscillations.

5.5.1 Free oscillations

Initially, the ground state was calculated in the presence of an electric field ("tilted" quantum well). At $t = 0$, the electric field is abruptly switched off, which leaves the quantum well electrons in an excited state and triggers collective charge-density oscillations. We use an electric field of 0.01mV/nm, so that the oscillations mainly probe the lowest ISB plasmon, since it is a rather weak excitation.

We calculate the time-dependent dipole moment $d(t) = \int zn(z,t)dz$ versus time from the full TDOEP method and compare it with the TDKLI method which has no memory. We follow the numerical procedure given earlier in this Chapter to solve the TDOEP equation (see Fig. (5.4)). The convergence is checked as follows: Suppose at one iteration, we have calculated the dipole moment $d_{new}(t)$ and we have the dipole moment of previous iteration d_{old}(t). Then

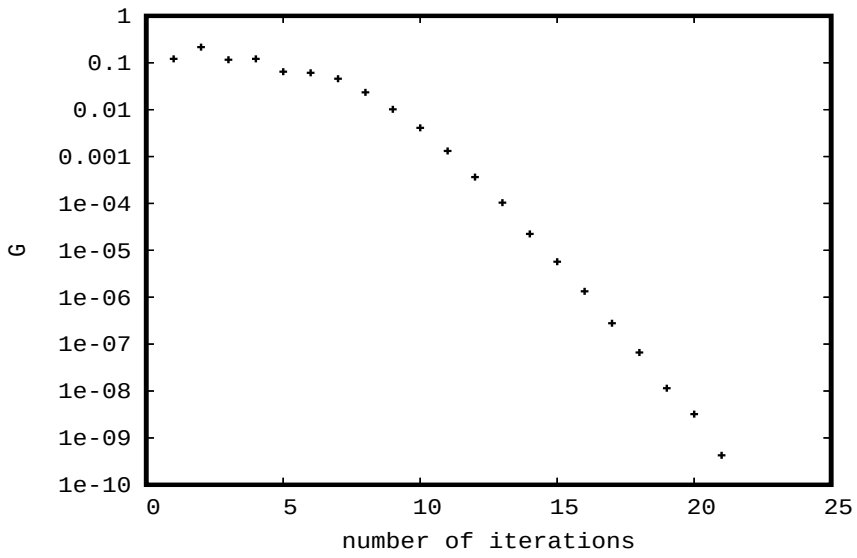

Figure 5.5: G [Eq. (5.37)] versus number of iterations until convergence is achieved for exact-exchange free oscillations.

we calculated a quantity G as given below for total time of propagation T:

$$G = \frac{\int_0^T dt |d_{old}(t) - d_{new}(t)|}{\int_0^T dt |d_{new}(t)|}. \tag{5.37}$$

We say that convergence has occurred when G $\leq 10^{-8}$. Fig. 5.5 shows the convergence for exact-exchange calculations for free oscillations. Similar checks have been done throughout all our calculations described in this section.

Fig. 5.6 shows the dipole moment, calculated by our numerical procedure using TDOEP and TDKLI. We can clearly see the retardation effect associated with exact exchange. The full TDOEP oscillates a bit faster than the TDKLI, as one would expect from the elastic behavior of exact exchange [25]. This may at first appear a bit paradoxical, but is explained in the subsequent paragraphs. The power spectrum shows that the TDOEP peak is blueshifted in relation to the TDKLI peak, and the appearance of a higher plasmon mode (ω_{23}), which is responsible for the somewhat irregular dipole oscillations.

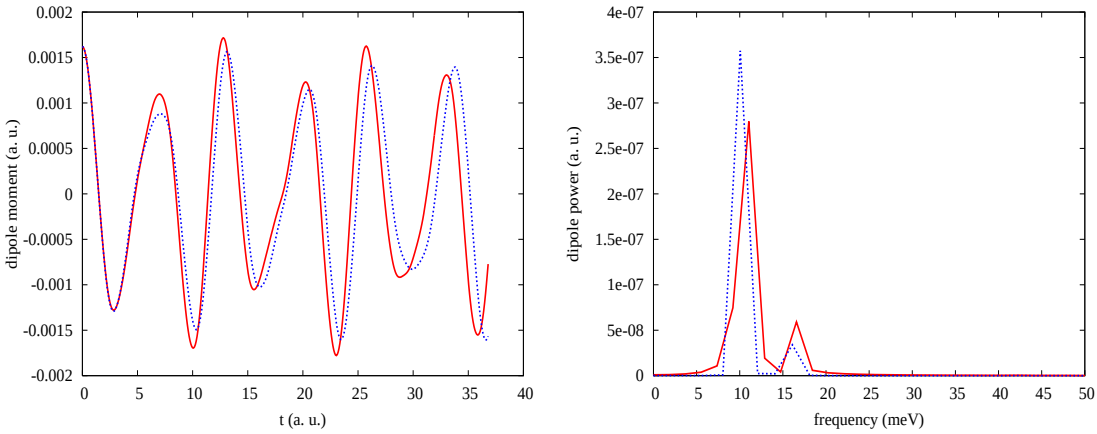

Figure 5.6: Left: time-dependent dipole moment for free oscillations in exact exchange. Right: dipole power for free oscillations in exact exchange. (blue dotted line: TDKLI, red solid line: TDOEP)

We had discussed in the previous chapter that the electron liquid can be viewed as a medium with viscoelastic propeties, which stand in a direct relationship with dynamical xc effects. In general, these effects cause both dissipation and frequency renormalization of collective charge-density oscillations. It was shown recently [107] that dissipation is a result of the decay of a collective mode into incoherent multiple particle-hole excitations. In the exchange-only limit, this mechanism is not possible, since this limit represents the lowest order in a diagrammatic expansion in the Coulomb interaction, and thus does not couple to multiple excitations. What remains, instead, is a renormalization of the plasmon frequency. This can be viewed as a purely elastic effect.

In Ref. [77], it was shown that elastic effects can become dominant at high frequencies in the nonlinear regime. The elasticity of the electron liquid tends to oppose attempts to subject the system to strong and rapid deformations. This general tendency explains, for example, why the Vignale-Kohn theory has been successful for molecular polarizabilities, which are greatly overestimated in ALDA [108]. Dynamic polarization of the system corresponds to a redistribution

of the charge density, i.e. to the deformation of an electron subsystem, which causes a counteracting xc force. This force is an intrinsically nonadiabatic effect that is completely missing in approximations such as ALDA or TDKLI. Put in different words, the retardation of TDOEP causes a "stiffening" of the "spring constant" associated with the collective ISB plasmon oscillations, which causes the blueshift observed in Fig. 5.6.

Let us now investigate whether these effects are also captured with the exchange-only LDA-SIC method (see section 5.2.2), when combined with the TDOEP scheme. Fig. 5.7 shows dipole moment and dipole power spectrum from the LDA-SIC using the TDOEP and TDKLI methods. Unlike in exact-exchange (Fig. 5.6), here the higher plasmon peak is less pronounced, which is due to the fact that the second subband level is not as populated for the same set of parameters. We clearly see that SIC fails to capture the retardation: on the contrary, when used in conjunction with the TDOEP, the plasmon oscillations slightly slow down! This unphysical behavior indicates that the SIC, although it has many nice features such as correct asymptotics, fails to produce the essential signature of non-adiabaticity in exchange-only TDDFT.

5.5.2 Driven oscillations

So far we have shown that one can solve the full TDOEP equation in exact exchange, the infinite memory due to the time integral causing retardation. We suspect that memory will play an even more dramatic role if the system undergoes sudden changes or moves with high frequencies. To illustrate and analyze the retardation effects we use a similar quantum well as described above in the presence of a laser driven field.

To observe the retardation effects, we use different frequencies to drive the system. We solve the full TDOEP equation with TDKS propagation in the presence of THz laser fields, switched on at initial time t_0 over a 1-cycle linear

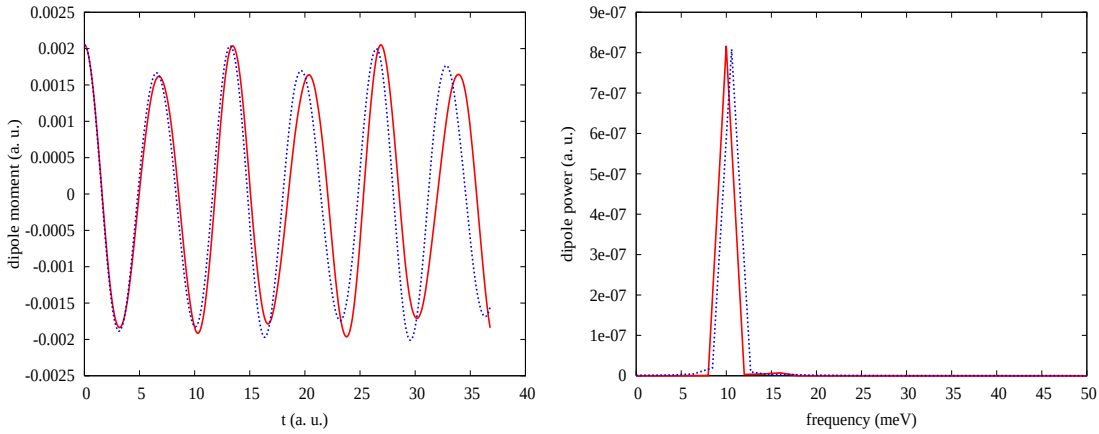

Figure 5.7: Left: time-dependent dipole moment for free oscillations in LDA-SIC approximations. Right: dipole power for free oscillations in LDA-SIC approximations. (blue dotted line: LDA-SIC TDKLI, red solid line: LDA-SIC TDOEP)

ramp and then kept constant throughout the propagation. We calculate the dipole moment for TDOEP exact-exchange, TDKLI, and also from the adiabatic TDOEP discussed in section 5.4, for laser frequencies of 5 meV, 11.2 meV (close to the lowest ISB plasmon resonance), 20 meV and 40 meV. Fig. 5.8 shows dipole moment calculations for different frequencies of the driving field. The intensities of the driving fields are 20, 10, 20 and 40 W/cm^2 respectively. Since 11.2 meV is close to resonance, the dipole amplitude is largest. Overall, we find that the three methods give comparable results. The adiabatic TDOEP falls somewhere in between full TDOEP and TDKLI. The discrepancy between full TDOEP and the other schemes is most pronounced at the 40 meV laser field.

In the driven oscillations, unlike in free oscillations, one cannot say much about the phase lag (retardation effect) just looking at the dipole moments of these methods. Besides one gets messy irregular dipole moments when driving with higher frequencies, since we are hitting the higher excitations. Therefore, for more qualitative analysis, it is useful to consider the xc power associated with the charge-density oscillations, since it is directly associated with the xc potential.

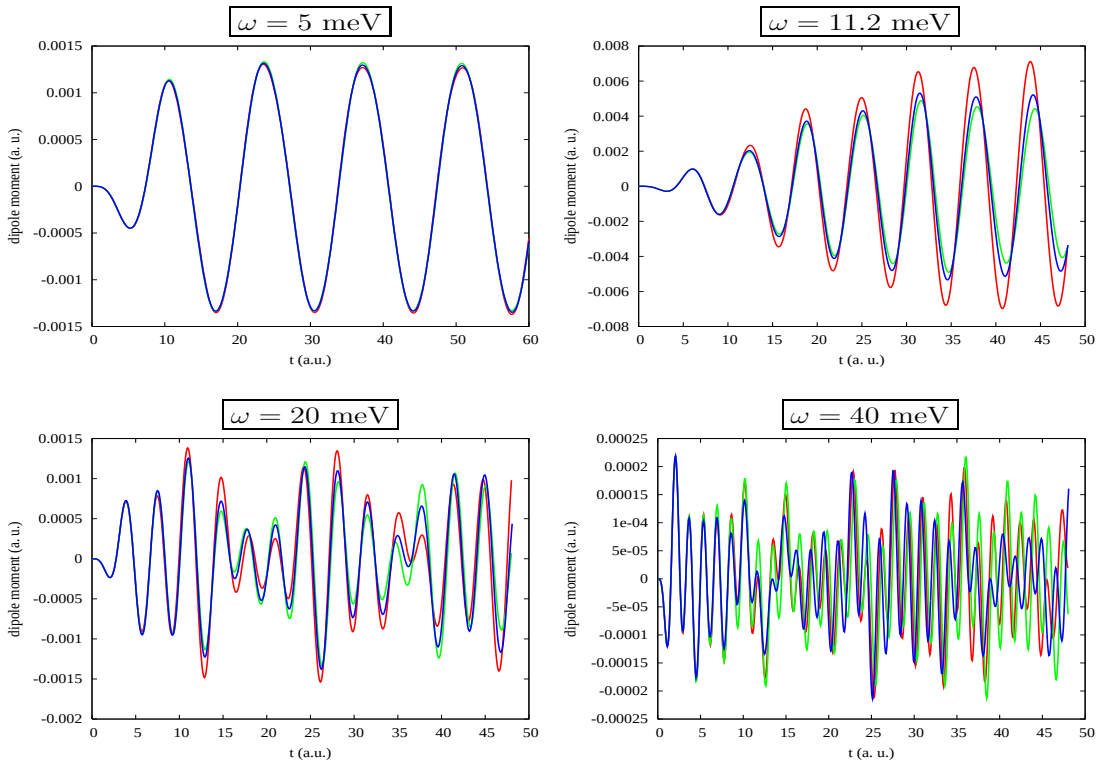

Figure 5.8: Time-dependent dipole moment for laser driven oscillations in TDOEP exact exchange (red), TDKLI (green), and adiabatic TDOEP (blue). Top left: ω=5 meV, Top right: ω=11.2 meV, Bottom left: ω=20 meV, Bottom right: ω=40 meV.

We define the power in the usual way as xc force density times velocity:

$$P_{\mathrm{x}}(t) = \int dz v(z,t) n(z,t) \frac{\partial}{\partial z}(V_{XX}(z,t) - V_{XX}(z,0)). \tag{5.38}$$

Since one can write the velocity field in terms of the current density $j(z,t)$, Eq. (5.38) can be written as

$$P_{\mathrm{x}}(t) = \int dz j(z,t) \frac{\partial}{\partial z}(V_{XX}(z,t) - V_{XX}(z,0)). \tag{5.39}$$

One can obtain the current density as follows:

$$j(z,t) = -\frac{i}{2\pi} \sum_{k=1}^{OCC} (\phi_k^*(z,t)\nabla\phi_k(z,t) - \nabla\phi_k^*(z,t)\phi_k(z,t))(\epsilon_F - \epsilon_k). \tag{5.40}$$

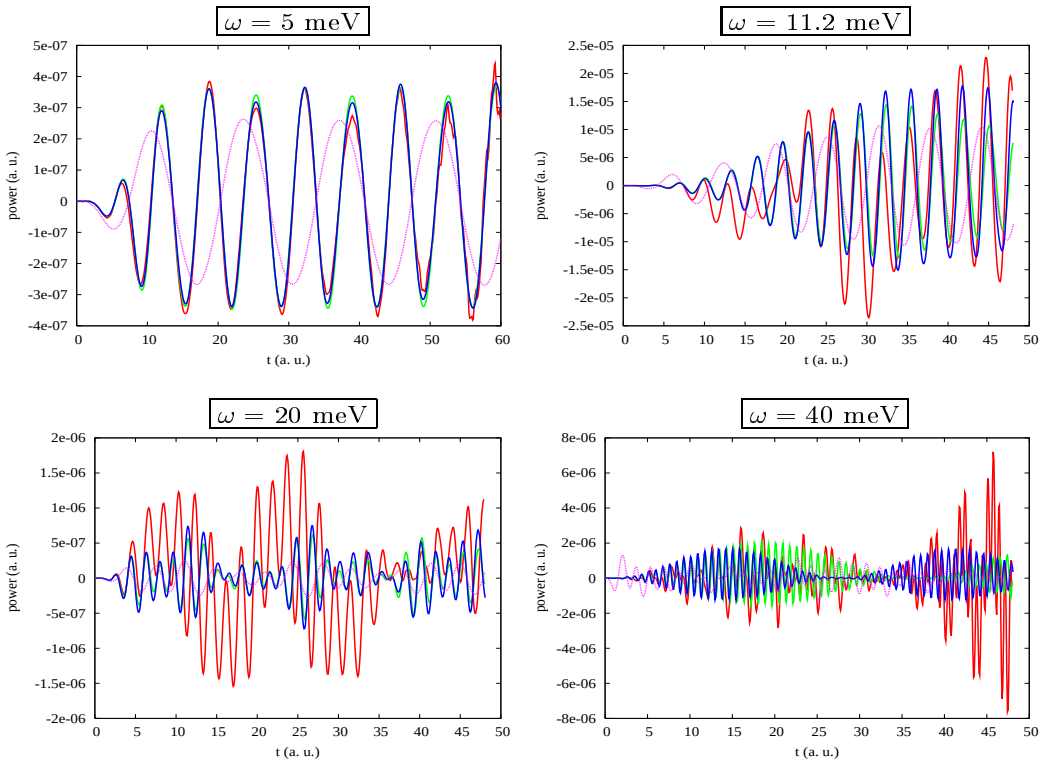

Figure 5.9: Time-dependent xc power for laser driven oscillations in TDOEP exact exchange (red), TDKLI (green), and adiabatic TDOEP (blue). Dotted line: adiabatic dipole moment scaled to fit power. Top left: ω=5 meV, Top right: ω=11.2 meV, Bottom left: ω=20 meV, Bottom right: ω=40 meV.

Fig. 5.9 shows the power P_{x} calculated with laser frequencies of 5 meV, 11.2 meV, 20 meV and 40 meV for TDOEP, TDKLI and adiabatic TDOEP. We have plotted adiabatic dipole oscillations in the same graph, scaled to fit the power, as a point of reference to understand the behavior of the TDOEP exact-exchange. One can clearly observe the retardation associated with the exact exchange with increasing frequency of the driving field: for 11.2 meV, 20 meV it is slightly going ahead of TDKLI and adiabatic TDOEP. For 40 meV, similar to dipole oscillations we observe irregular oscillations and we can see clearly TDOEP deviates from its adiabatic approximations. Since the power is the product of current and

gradient of potential, we can see that power oscillates twice as fast as the dipole oscillations.

We also mention that we carried out numerical checks of the zero-force theorem in TDDFT,

$$\int dz n(z,t) \frac{d}{dz} v_{\rm xc}(z,t) = 0, \tag{5.41}$$

i.e. the system cannot exert a Coulomb force on itself. We found this to be satisfied in our qunatum wells to within our numerical limits, for all time-dependent functionals, even TDKLI. This sheds new light on the recent work by Mundt *et al.* [109], who have found a violation of the zero-force theorem by TDKLI, leading to spurious self-excitation. We find that this violation does not play a role in our systems, probably due to the strong confinement of the quantum well. TDKLI is therefore safe to use.

We thus see from our results of driven oscillations in a quantum well that retardation has a significant impact on the electron dynamics, producing a change in the time-dependent dipole amplitude of order $\sim$ 10-20% for oscillations not far above the resonance. The effects thus seems to be clearly nonnegligible, and certainly warrants more exploration in other systems such as atoms and molecules.

We also mention the work by Hirata *et al.* [89], who applied frequency-dependent (i.e., retarded) excat-exchange kernels in linear response, and found only small effects in dynamical polarizabilities. This is in hindsight not very surprising, since these applications were performed at relatively low frequencies where retardation can be expected play only a minor role. In our case, the frequencies were higher (around or above the ISB plasmon), and we found significant effects.

Chapter 6

Summary and Outlook

Semiconductor devices are used for generating electromagnetic radiation in many everyday applications. Radiation in the low frequency region is produced by oscillating circuits based on transistors. On the other hand, semiconductor lasers produce light in the visible region. The terahertz region (1-10THz) between these high and low frequency ranges has been identified as suitable for various possible applications. Chemical detection, astronomy and medical imaging are some of them [110–113]. However, THz technology is still underdeveloped despite much research activity [114, 115]. Semiconductor heterostructures are natural candidates for THz sources since the intersubband transitions lie in the THz region. To interpret experimental results and guide further research, one should have a clear understanding of the physical mechanisms governing THz dynamics in quantum wells, especially in the nonlinear regime.

To describe electron dynamics, many different theoretical tools are available. Mostly used ones are density-matrix techniques such as the semiconductor Bloch equations [116]. The solution of these equations can be difficult, and one often negelects Coulomb interactions [117], or uses simplifications such as the RWA [11]. However, for an accurate description of electron dynamics, non-adiabatic and many-body effects play a major role.

In this thesis, we presented three different formalisms based on TDDFT to

describe electron dynamics beyond the adiabatic approximation, including many-body effects. First we treated decoherence and relaxation by intrinsic and extrinsic mechanisms, by combining TDDFT with a density matrix formalism. We applied this formalism to study coherent control of optical bistability. It turns out that one can achieve theoretical switching times in picoseconds range, which in principle is limited only by the relaxation and decoherence time T_1 and T_2. More realistic simulations would replace T_1 and T_2 with microscopic, intensity-dependent scattering theories, including finite temperatures and a detailed modeling of the absorption profile and waveguide geometry of the device. In the search for THz devices and applications, nonliner ISB effects such as bistability merit further exploration. We also observed discrepancies between the 2-level RWA to our method in the photoabsorption for a quantum well with increasing DC bias. The RWA breaks down for asymmetric systems, and thus has to be used with caution.

Next we presented a formalism based on current-TDDFT, which described dynamic exchange and correlation beyond the adiabatic approximation to study retardation and memory effects. We showed that one can describe interacting electrons as a viscous liquid with memory, and how memory effects introduced the element of intrinsic decoherence and energy relaxation to TDKS theory. This is an alternate method to the density matrix formalism described before in which we described dissipation through phenomenological decoherence and relaxation times.

The next formalism, TDOEP, is yet another method to describe the electron dynamics in quantum wells beyond the adiabatic approximation. The advantage of orbital-based TDOEP is that it works for both finite and extended systems. A discontinuity is built up in the exact exchange potential when a new subband is filled. The major difference between the TDOEP and TDKLI is that it contains a time integral and therefore it has an infinite memory.

A major breakthrough reported in this thesis is that we have succeeded to solve the full exact-exchange TDOEP equation for a quantum well for the first time. We have seen under free oscillations, that memory causes retardation in exact exchange. Since exact exchange is purely elastic, we have seen a phase difference in the calculations of exact power under driven oscillations. We have also seen that adiabatic TDOEP changes drastically with higher frequencies of the driving fields with respect to TDKLI. Therefore one should pay close attention if a system undergoes sudden changes or oscillates with high frequencies.

The calculations presented here were carried out for simple quantum wells in effective-mass approximation. These systems are ideal to test the complex nonadiabatic approaches that we considered here, and have shown that it is feasible to carry out TDKS calculations where the xc potential includes a memory. The nonadiabatic behavior of the electron liquid, in the form of elastic and dissipative effects, can be expected to play a role in a multitude of applications, from atoms and molecules and polymers to solids and nanostrutures. The present work thus constitutes a first step towards many new and exciting applications in TDDFT.

Appendix A

Numerical details for solving the density-matrix equation of motion

The numerical solution of TDKS equations is a well-documented subject [118]. A multitude of propagation algorithms and several well-established computer codes are available [119]. In the following, we give some details on the numerical procedure used in our home-made density-matrix code for quantum wells. We discretize the static and time-dependent wave functions $\psi_j^0(z)$ and $\psi_j(z,t)$ on a uniform one-dimensional spatial grid with typically about $N_{grid} \sim 400$ points. We use a standard eigenvalue solver to get the self-consistent solution of the static KS equation (3.9). The ground state subband envelope functions are the initial state, to be propagated in time.

We need an algorithm to propagate the KS wave function from time t to $t + \Delta t$ in the TDKS Eq. (3.13). We use the Crank-Nicholson algorithm [120],

$$U(t + \Delta t, t) \approx (I - \frac{i}{2} H_{\rm KS} \Delta t)(I + \frac{i}{2} H_{\rm KS} \Delta t)^{-1} \tag{A.1}$$

to carry out the step

$$\psi_j(z, t + \Delta t) = U(t + \Delta t, t) \psi_j(z, t), \tag{A.2}$$

where U is the time evolution operator, which transforms state $|\psi(0)\rangle$ into state $|\psi(t)\rangle$:

$$|\psi(t)\rangle = U(t,0)\,|\psi(0)\rangle\,. \tag{A.3}$$

In order to ensure that the system is in the state $|\psi(0)\rangle$ at time $t = 0$ it is necessary to have the initial condition $U(0,0) = \mathbf{1}$. To conserve the norm, the time evolution operator must be unitary, i.e., $U^\dagger = U^{-1}$. If $H_{\rm KS}$ is time independent, by formally integrating time-dependent Schrödinger equation, we get

$$U(t,0) = e^{(-i/\hbar)H_{\rm KS}t} \tag{A.4}$$

which yields Eq. (A.1). In general, the Hamiltonian is of course time dependent $H_{\rm KS}$(t), and the expression (A.4) becomes more complicated. However, for propagation from t to $t + \Delta t$, we can write

$$U(t+\Delta t, t) = e^{(-\frac{i}{\hbar})H_{\rm KS}(t+\frac{\Delta t}{2})t}. \tag{A.5}$$

The Crank-Nicholson algorithm is unitary and of second order accuracy in Δt. In the above, U, I and $H_{\rm KS}$ are all matrices of dimension $N_{grid}\times N_{grid}$. I is a unit matrix, and H_{KS} is a tridiagonal matrix following from a finite-difference discretization of the TDKS Hamiltonian,

$$H_{\rm KS}(t+\frac{\Delta t}{2}) = -\frac{\hbar^2}{2m^*}\frac{d^2}{dz^2} + v(z, t+\Delta t/2). \tag{A.6}$$

The time-dependent potential in Eq. (A.6) is evaluated midway along the time step between t and $t + \Delta t$. Both $v_{\rm H}$ and $v_{\rm xc}$ require $n(z, t+\Delta t/2)$ as input, but at this point we know the density only up until the time t. Therefore we use a predictor corrector approach to get the potential at $t + \Delta t/2$. This means that we use $v(z,t)$ in $H_{\rm KS}$ to predict a solution $\psi_j^{(p)}(z, t+\Delta t)$, and use the resulting $n^{(p)}(z, t+\Delta t)$ to construct $v^{(p)}(z, t+\Delta t)$. Next, we use a corrected potential, $v^{(c)}(z, t+\Delta t/2) = [v(z,t) + v^{(p)}(z, t+\Delta t)]/2$ in $H_{\rm KS}$ and propagate again to get a corrected solution $\psi_j^{(c)}(z, t+\Delta t)$. It may be necessary to perform several

corrector steps to get the desired accuracy in the time propagation of $\psi_j(z,t)$. If $\psi_j(z,t)$ does not significantly change anymore within a given tolerance over the total time propagation interval including another corrector step, then self-consistency has been achieved. In practice, we found 2-3 corrector steps to be sufficient.

The numerical solution of the density-matrix equation of motion (3.6) starts from discretization $\dot{\rho}_j = [\rho(t+\Delta t) - \rho(t)]/\Delta t$, leading to

$$\rho_j(t+\Delta t) = \tilde{U}(t+\Delta t, t)\rho_j(t)\tilde{U}^{\dagger}(t+\Delta t, t) - \Delta t R_j(t). \tag{A.7}$$

For the time-evolution operator we again use the Crank-Nicholson form:

$$\tilde{U}(t+\Delta t, t) \approx (I - \frac{i}{2}h\Delta t)(i + \frac{i}{2}h\Delta t)^{-1}, \tag{A.8}$$

where h is the TDKS Hamiltonian matrix (3.17) evaluated at $t + \Delta t/2$. We include only the lowest N_b bound quantum well states. Therefore, together with the predictor-corrector scheme and inversion of $N_b \times N_b$ matrices, the TDDFT density-matrix equation (3.6) can be solved solved numerically in a rather straightforward manner.

Appendix B

Order by order expansion of the density matrix

The task is to get an analytical scheme for solving the density-matrix equation of motion for a two-level system. We start with Eqs. (3.18) and (3.19):

$$\dot{\rho}_{12} = [i\omega_{21} - \Gamma_2 - i(H_{11} - H_{22})]\rho_{12} + iH_{12}\Delta \tag{B.1}$$

$$\dot{\Delta} = 2iH_{12}(\rho_{12} - \rho_{12}^*) - \Gamma_1(\Delta - \Delta^{(0)}). \tag{B.2}$$

Since we start from the ground state, the initial value of the population difference Δ is $\Delta^{(0)} = 1$, and the initial ISB polarization is $\rho_{12}^{(0)} = 0$.

In the following, our goal is an iterative solution of Eqs. (B.1)+(B.2) in orders of the external electric field strength $\mathcal{E}$, which is taken as our small parameter. Clearly, the external-field matrix element H_{kl}^{ext} is of first order in $\mathcal{E}$. We assume that the Hartree and xc matrix elements $H_{kl}^{\mathrm{H+xc}}$ can be formally represented in a suitable expansion in orders of $\mathcal{E}$. Clearly, $H_{kl}^{\mathrm{H+xc}}$ will also contain higher orders of $\mathcal{E}$, due to the nonlinear dependence on the density. Therefore, we have

$$H_{kl} = \sum_{n=1}^{\infty} H_{kl}^{(n)}, \tag{B.3}$$

where

$$H_{kl}^{(n)} = \mathcal{E}^n \sum_{q=-n}^{n} \mathcal{H}^{(n)}(q\omega)e^{qi\omega t}. \tag{B.4}$$

1. First order

We notice that the term $2iH_{12}(\rho_{12}-\rho_{12}^*)$ starts out with second order in $\mathcal{E}$ (since the lowest order of ρ_{12} is the first). So to lowest order (linear in $\mathcal{E}$), Eq. (B.2) is $\Delta = \Delta^{(0)}$, and the lowest order approximation for ρ_{12} follows from (B.1) as

$$\dot{\rho}_{12}^{(1)} = (i\omega_{21} - \Gamma_2)\rho_{12}^{(1)} + iH_{12}^{(1)}\Delta^{(0)}. \tag{B.5}$$

We use the ansatz

$$\rho_{12}^{(1)}(t) = \tilde{\rho}_{12}^{(1)}(\omega)e^{-i\omega t} + \tilde{\rho}_{12}^{(1)}(-\omega)e^{i\omega t}. \tag{B.6}$$

This gives:

$$\begin{aligned} -i\omega\tilde{\rho}_{12}^{(1)}(\omega)e^{-i\omega t} + i\omega\tilde{\rho}_{12}^{(1)}(-\omega)e^{i\omega t} &= (i\omega_{12} - \Gamma_2)[\tilde{\rho}_{12}^{(1)}(\omega)e^{-i\omega t} + \tilde{\rho}_{12}^{(1)}(-\omega)e^{i\omega t} \\ &\quad +\tilde{\rho}_{12}^{(1)}(0)] + i[\tilde{H}_{12}^{(1)}(-\omega)e^{i\omega t} \\ &\quad +\tilde{H}_{12}^{(1)}(\omega)e^{-i\omega t}]\Delta^{(0)}. \end{aligned} \tag{B.7}$$

Comparing $e^{-i\omega t}$ and $e^{i\omega t}$ terms, we get

$$\tilde{\rho}_{12}^{(1)}(\omega) = \frac{i\tilde{H}_{12}^{(1)}(\omega)\Delta^{(0)}}{-i\omega - i\omega_{12} + \Gamma_2} \tag{B.8}$$

$$\tilde{\rho}_{12}^{(1)}(-\omega) = \frac{i\tilde{H}_{12}^{(1)}(-\omega)\Delta^{(0)}}{i\omega - i\omega_{12} + \Gamma_2}. \tag{B.9}$$

If we assume $\tilde{H}_{12}$ to be constant then above Eqs. (B.8), (B.9) are identical to the solutions given in [11].

2. Second order

Now let's look at the second order,

$$\dot{\rho}_{12}^{(2)} = (i\omega_{21} - \Gamma_2)\rho_{12}^{(2)} - iR^{(1)}\rho_{12}^{(1)} + iH_{12}^{(2)}\Delta^{(0)}, \tag{B.10}$$

where $R^{(1)} = H_{11}^{(1)} - H_{22}^{(1)}$. Using the ansatz

$$\begin{aligned}\rho_{12}^{(2)}(t) &= \tilde{\rho}_{12}^{(2)}(0) + \tilde{\rho}_{12}^{(2)}(\omega)e^{-i\omega t} + \tilde{\rho}_{12}^{(2)}(-\omega)e^{i\omega t} \\ &\quad + \tilde{\rho}_{12}^{(2)}(2\omega)e^{-2i\omega t} + \tilde{\rho}_{12}^{(2)}(-2\omega)e^{2i\omega t}, \end{aligned} \tag{B.11}$$

which accounts for second-harmonic generation as well as rectification, we get

$$\begin{aligned} & -i\omega\tilde{\rho}_{12}^{(2)}(\omega)e^{-i\omega t} + i\omega\tilde{\rho}_{12}^{(2)}(-\omega)e^{i\omega t} - 2i\omega\tilde{\rho}_{12}^{(2)}(2\omega)e^{-2i\omega t} + 2i\omega\tilde{\rho}_{12}^{(2)}(-2\omega)e^{2i\omega t} \\ = \; & (i\omega_{21} - \Gamma_2)[\tilde{\rho}_{12}^{(2)}(0) + \tilde{\rho}_{12}^{(2)}(\omega)e^{-i\omega t} + \tilde{\rho}_{12}^{(2)}(-\omega)e^{i\omega t} + \tilde{\rho}_{12}^{(2)}(2\omega)e^{-2i\omega t} \\ & + \tilde{\rho}_{12}^{(2)}(-2\omega)e^{2i\omega t}] - i[\tilde{R}^{(1)}(\omega)e^{-i\omega t} + \tilde{R}^{(1)}(-\omega)e^{i\omega t}][\tilde{\rho}_{12}^{(2)}(\omega)e^{-i\omega t} \\ & + \tilde{\rho}_{12}^{(2)}(-\omega)e^{i\omega t}] + i[\tilde{H}_{12}^{(2)}(0) + \tilde{H}_{12}^{(2)}(\omega)e^{-i\omega t} + \tilde{H}_{12}^{(2)}(-\omega)e^{i\omega t} \\ & + \tilde{H}_{12}^{(2)}(2\omega)e^{-2i\omega t} + \tilde{H}_{12}^{(2)}(-2\omega)e^{2i\omega t}]\Delta^{(0)}. \end{aligned} \tag{B.12}$$

Comparing $e^{-2i\omega t}$and $e^{2i\omega t}$ terms, we get

$$\tilde{\rho}_{12}^{(2)}(2\omega) = \frac{i\tilde{H}_{12}^{(2)}(2\omega)\Delta^{(0)} - i\tilde{R}^{(1)}(\omega)\tilde{\rho}_{12}^{(1)}(\omega)}{-2i\omega - i\omega_{12} + \Gamma_2} \tag{B.13}$$

$$\tilde{\rho}_{12}^{(2)}(-2\omega) = \frac{i\tilde{H}_{12}^{(2)}(-2\omega)\Delta^{(0)} - i\tilde{R}_{(1)}(-\omega)\tilde{\rho}_{12}^{(1)}(-\omega)}{2i\omega - i\omega_{12} + \Gamma_2}. \tag{B.14}$$

Next comparing $e^{-i\omega t}$ and $e^{i\omega t}$ terms, we have

$$\tilde{\rho}_{12}^{(2)}(\omega) = \frac{i\tilde{H}_{12}^{(1)}(\omega)\Delta^{(0)}}{-i\omega - i\omega_{12} + \Gamma_2} \tag{B.15}$$

$$\tilde{\rho}_{12}^{(2)}(-\omega) = \frac{i\tilde{H}_{12}^{(1)}(-\omega)\Delta^{(0)}}{i\omega - i\omega_{12} + \Gamma_2}, \tag{B.16}$$

which is similar to first order term. Now we compare the $e^{0\omega t}$ term. Then we have

$$\tilde{\rho}_{12}^{(2)}(0) = \frac{i\tilde{H}_{12}^{(2)}(0)\Delta^{(0)} - i[\tilde{R}^{(1)}(\omega)\tilde{\rho}_{12}^{(1)}(-\omega) + \tilde{R}^{(1)}(-\omega)\tilde{\rho}_{12}^{(1)}(\omega)]}{-i\omega - i\omega_{12} + \Gamma_2} \tag{B.17}$$

Now we are ready to get the third-order solution. Important at this moment is to note that the terms $\tilde{\rho}_{12}^{(2)}(\pm 2\omega)$ and $\tilde{\rho}_{12}^{(2)}(0)$ will contribute to the solution,

which is ignored in the RWA. Before going into the third order of ρ_{12}, let's look at the second order of Δ. This can be written as

$$\dot{\Delta}^{(2)} = 2i[H_{21}^{(1)}\rho_{12}^{(1)} - H_{12}^{(1)}\rho_{21}^{(1)}] - \Gamma_1(\Delta^{(2)} - 1), \tag{B.18}$$

where we have used $\Delta^{(0)} = 1$. We make the ansatz

$$\Delta^{(2)}(t) = \tilde{\Delta}^{(2)}(0) + \tilde{\Delta}^{(2)}(2\omega)e^{-2i\omega t} + \tilde{\Delta}^{(2)}(-2\omega)e^{2i\omega t}. \tag{B.19}$$

This gives

$$\begin{aligned}
&-2i\omega\tilde{\Delta}^{(2)}(2\omega)e^{-2i\omega t} + 2i\omega\tilde{\Delta}^{(2)}(-2\omega)e^{2i\omega t} \\
&= 2i[(\tilde{H}_{21}^{(1)}(\omega)e^{-i\omega t} + \tilde{H}_{21}^{(1)}(-\omega)e^{i\omega t})(\tilde{\rho}_{12}^{(1)}(\omega)e^{-i\omega t} + \tilde{\rho}_{12}^{(1)}(-\omega)e^{i\omega t} \\
&-(\tilde{H}_{12}^{(1)}(\omega)e^{-i\omega t} + \tilde{H}_{12}^{(1)}(-\omega)e^{i\omega t})(\tilde{\rho}_{21}^{(1)}(\omega)e^{-i\omega t} + \tilde{\rho}_{21}^{(1)}(-\omega)e^{i\omega t}] \\
&-\Gamma_1[\tilde{\Delta}^{(2)}(0) + \tilde{\Delta}^{(2)}(2\omega)e^{-2i\omega t} + \tilde{\Delta}^{(2)}(-2\omega)e^{-2i\omega t} - 1].
\end{aligned} \tag{B.20}$$

Comparing $e^{2i\omega t}$ and $e^{-2i\omega t}$, we get

$$\tilde{\Delta}^{(2)}(-2\omega) = \frac{2i}{2i\omega + \Gamma_1}\left[\frac{\tilde{H}_{21}^{(1)}(-\omega)\tilde{H}_{12}^{(1)}(-\omega)}{(\omega - \omega_{21} - i\Gamma_2)} + \frac{\tilde{H}_{12}^{(1)}(-\omega)\tilde{H}_{12}^{(1)*}(\omega)}{(\omega + \omega_{21} - i\Gamma_2)}\right] \tag{B.21}$$

$$\tilde{\Delta}^{(2)}(2\omega) = \frac{2i}{-2i\omega + \Gamma_1}\left[\frac{\tilde{H}_{21}^{(1)}(\omega)\tilde{H}_{12}^{(1)}(\omega)}{(-\omega - \omega_{21} - i\Gamma_2)} + \frac{\tilde{H}_{12}^{(1)}(\omega)\tilde{H}_{12}^{(1)*}(-\omega)}{(-\omega + \omega_{21} - i\Gamma_2)}\right] \tag{B.22}$$

Comparing constant terms, we get

$$\begin{aligned}
\tilde{\Delta}^{(2)}(0) = 1 &+ \frac{2i}{\Gamma_1}\left[\frac{\tilde{H}_{21}^{(1)}(\omega)\tilde{H}_{12}^{(1)}(-\omega)}{(\omega - \omega_{21} - i\Gamma_2)} + \frac{\tilde{H}_{21}^{(1)}(-\omega)\tilde{H}_{12}^{(1)}(\omega)}{(-\omega - \omega_{21} - i\Gamma_2)}\right] \\
&+ \frac{2i}{\Gamma_1}\left[\frac{\tilde{H}_{12}^{(1)}(\omega)\tilde{H}_{12}^{(1)*}(\omega)}{(\omega + \omega_{21} - i\Gamma_2)} + \frac{\tilde{H}_{12}^{(1)}(-\omega)\tilde{H}_{12}^{(1)*}(\omega)}{(-\omega + \omega_{21} - i\Gamma_2)}\right].
\end{aligned} \tag{B.23}$$

3. Third order

The next task is to look at the third order of ρ_{12}. The 3^{rd} order equation is

$$\dot{\rho}_{12}^{(3)} = (i\omega_{21} - \Gamma_2)\rho_{12}^{(3)} - iR^{(1)}\rho_{12}^{(2)} - iR^{(2)}\rho_{12}^{(1)} + iH_{12}^{(1)}\Delta^{(2)} + iH_{12}^{(3)}\Delta^{(0)}. \tag{B.24}$$

We make the ansatz

$$\begin{aligned}\rho_{12}^{(3)}(t) &= \tilde{\rho}_{12}^{(3)}(0)+\tilde{\rho}_{12}^{(3)}(\omega)e^{-i\omega t}+\tilde{\rho}_{12}^{(3)}(-\omega)e^{i\omega t}+\tilde{\rho}_{12}^{(3)}(2\omega)e^{-2i\omega t}\\ &+ \tilde{\rho}_{12}^{(3)}(-2\omega)e^{2i\omega t}+\tilde{\rho}_{12}^{(3)}(3\omega)e^{-3i\omega t}+\tilde{\rho}_{12}^{(3)}(-3\omega)e^{3i\omega t}. \qquad \text{(B.25)}\end{aligned}$$

This gives

$$\begin{aligned}&-i\omega\tilde{\rho}_{12}^{(3)}(\omega)e^{-i\omega t}+i\omega\tilde{\rho}_{12}^{(3)}(-\omega)e^{i\omega t}-2i\omega\tilde{\rho}_{12}^{(3)}(2\omega)e^{-2i\omega t}+\tilde{\rho}_{12}^{(3)}(-2\omega)e^{2i\omega t}\\ &-3i\omega\tilde{\rho}_{12}^{(3)}(3\omega)e^{-3i\omega t}+\tilde{\rho}_{12}^{(3)}(-3\omega)e^{3i\omega t}\\ =\;&(i\omega_{12}-\Gamma_2)[\tilde{\rho}_{12}^{(3)}(0)+\tilde{\rho}_{12}^{(3)}(\omega)e^{-i\omega t}+\tilde{\rho}_{12}^{(3)}(-\omega)e^{i\omega t}+\tilde{\rho}_{12}^{(3)}(2\omega)e^{-2i\omega t}\\ &+\tilde{\rho}_{12}^{(3)}(-2\omega)e^{2i\omega t}+\tilde{\rho}_{12}^{(3)}(3\omega)e^{-3i\omega t}+\tilde{\rho}_{12}^{(3)}(-3\omega)e^{3i\omega t}]\\ &-i[\tilde{R}^{(1)}(\omega)e^{-i\omega t}+\tilde{R}^{(1)}(-\omega)e^{i\omega t}][\tilde{\rho}_{12}^{(2)}(0)+\tilde{\rho}_{12}^{(2)}(\omega)e^{-i\omega t}\\ &+\tilde{\rho}_{12}^{(2)}(-\omega)e^{i\omega t}+\tilde{\rho}_{12}^{(2)}(2\omega)e^{-2i\omega t}+\tilde{\rho}_{12}^{(2)}(-2\omega)e^{2i\omega t}]\\ &-i[\tilde{R}^{(2)}(\omega)e^{-i\omega t}+\tilde{R}^{(2)}(-\omega)e^{i\omega t}+\tilde{R}^{(2)}(2\omega)e^{-2i\omega t}+\tilde{R}^{(2)}(-2\omega)e^{2i\omega t}]\\ &\times[\tilde{\rho}_{12}^{(1)}(\omega)e^{-i\omega t}+\tilde{\rho}_{12}^{(1)}(-\omega)e^{i\omega t}]+i[\tilde{H}_{12}^{(1)}(\omega)e^{-i\omega t}+\tilde{H}_{12}^{(1)}(-\omega)e^{i\omega t}]\\ &\times[\Delta^{(0)}(0)+\tilde{\Delta}^{(2)}(2\omega)e^{-2i\omega t}+\tilde{\Delta}^{(2)}(-2\omega)e^{2i\omega t}]+i[\tilde{H}_{12}^{(3)}(0)\\ &+\tilde{H}_{12}^{(3)}(\omega)e^{-i\omega t}+\tilde{H}_{12}^{(3)}(-\omega)e^{i\omega t}+\tilde{H}_{12}^{(3)}(2\omega)e^{-2i\omega t}+\tilde{H}_{12}^{(3)}(-2\omega)e^{2i\omega t}\\ &+\tilde{H}_{12}^{(3)}(3\omega)e^{-3i\omega t}+\tilde{\rho}_{12}^{(3)}(-3\omega)e^{3i\omega t}]\Delta^{(0)}. \qquad \text{(B.26)}\end{aligned}$$

Comparing $e^{3i\omega t}$ and $e^{-3i\omega t}$ terms, we get

$$\begin{aligned}\tilde{\rho}_{12}^{(3)}(-3\omega) &= -i[(\tilde{R}^{(1)}(-\omega)\tilde{\rho}_{12}^{(2)}(-2\omega)+\tilde{R}^{(2)}(-2\omega)\tilde{\rho}_{12}^{(1)}(-\omega)\\ &\quad -\tilde{H}_{12}^{(1)}(-\omega)\tilde{\Delta}^{(2)}(-2\omega)-\tilde{H}_{12}^{(3)}(-3\omega)\Delta^{(0)})]\\ &\quad \times\frac{1}{3i\omega-i\omega_{12}+\Gamma_2}\\ \tilde{\rho}_{12}^{(3)}(3\omega) &= -i[(\tilde{R}^{(1)}(\omega)\tilde{\rho}_{12}^{(2)}(2\omega)+\tilde{R}^{(2)}(2\omega)\tilde{\rho}_{12}^{(1)}(\omega)\\ &\quad -\tilde{H}_{12}^{(1)}(\omega)\tilde{\Delta}^{(2)}(2\omega)-\tilde{H}_{12}^{(3)}(3\omega)\}\Delta^{(0)})]\\ &\quad \times\frac{1}{-3i\omega-i\omega_{12}+\Gamma_2}. \qquad \text{(B.27)}\end{aligned}$$

Comparing $e^{-2i\omega t}$ and $e^{2i\omega t}$ terms, we get

$$\tilde{\rho}_{12}^{(3)}(-2\omega) = i[\tilde{R}^{(1)}(-\omega)\tilde{\rho}_{12}^{(2)}(-\omega)+\tilde{R}^{(2)}(-\omega)\tilde{\rho}_{12}^{(1)}(-\omega)$$

$$-\tilde{H}_{12}^{(3)}(-2\omega)\Delta^{(0)}] \times \frac{1}{(2i\omega - i\omega_{12} + \Gamma_2)} \tag{B.28}$$

$$\begin{aligned}\tilde{\rho}_{12}^{(3)}(2\omega) &= i[\tilde{R}^{(1)}(\omega)\tilde{\rho}_{12}^{(2)}(\omega) + \tilde{R}^{(2)}(\omega)\tilde{\rho}_{12}^{(1)}(\omega) \\ &\quad -\tilde{H}_{12}^{(3)}(2\omega)\Delta^{(0)}] \times \frac{1}{(-2i\omega - i\omega_{12} + \Gamma_2)}.\end{aligned} \tag{B.29}$$

Similarly, comparing $e^{i\omega t}$ and $e^{-i\omega t}$, we can get

$$\begin{aligned}\tilde{\rho}_{12}^{(3)}(-\omega) &= [(\tilde{R}^{(1)}(-\omega)\tilde{\rho}_{12}^{(2)}(0) + \tilde{R}^{(1)}(\omega)\tilde{\rho}_{12}^{(1)}(-2\omega) + \tilde{R}^{(2)}(-2\omega)\tilde{\rho}_{12}^{(1)}(\omega)) \\ &\quad -(\tilde{H}_{12}^{(1)}(-\omega)\tilde{\Delta}^{(2)}(0) + \tilde{H}_{12}^{(1)}(\omega)\Delta^{(2)}(-2\omega) + \tilde{H}_{12}^{(3)}(-\omega)\Delta^{(0)})] \\ &\quad \times \frac{1}{(-\omega + \omega_{12} + i\Gamma_2)} \\ \tilde{\rho}_{12}^{(3)}(\omega) &= [(\tilde{R}^{(1)}(\omega)\tilde{\rho}_{12}^{(2)}(0) + \tilde{R}^{(1)}(-\omega)\tilde{\rho}_{12}^{(1)}(2\omega) + \tilde{R}^{(2)}(2\omega)\tilde{\rho}_{12}^{(1)}(-\omega)) \\ &\quad -(\tilde{H}_{12}^{(1)}(\omega)\tilde{\Delta}^{(2)}(0) + \tilde{H}_{12}^{(1)}(-\omega)\Delta^{(2)}(2\omega) + \tilde{H}_{12}^{(3)}(\omega)\Delta^{(0)})] \\ &\quad \times \frac{1}{(\omega + \omega_{12} + i\Gamma_2)}\ .\end{aligned} \tag{B.30}$$

This is the key result of our derivation. It shows that $\tilde{\rho}_{12}^{(3)}$ (which enters in the photoabsorption spectra computed in section 3.4) contains contributions that are <u>not</u> captured by the RWA. In particular, the term $\tilde{R}^{(1)}(\omega)\tilde{\rho}^{(1)}(-2\omega)$ will contribute strongly for asymmetric wells (when $\tilde{R}^{(1)}(\omega)$ is nonzero). This shows the reason for failure of the RWA that we observed in section 3.4.2.

Appendix C

Derivation of the OEP integral equation for a quantum well

The starting point of our derivation of the OEP integral equation is the energy functional (5.5), writing it here again as,

$$E[\{\Phi_{j\sigma}\}] = \sum_{\sigma}\sum_{j}^{N_\sigma}\int d^3r\Phi^*_{j\sigma}(\mathbf{r})(-\nabla^2/2)\Phi_{j\sigma}(\mathbf{r}) + \sum_{\sigma}\int d^3r n_\sigma(\mathbf{r})v_{ext}(\mathbf{r}) + \frac{1}{2}\int d^3r\int d^3r'\frac{n(\mathbf{r})n(\mathbf{r}')}{|\mathbf{r}-\mathbf{r}'|} + E_{\rm x}[\{\Phi_{j\sigma}\}]. \quad \text{(C.1)}$$

Instead of using $E_{\rm xc}[\{\Phi_{j\sigma}\}]$, we take the main advantage of the OEP method, that it allows for the exact treatment of the exchange energy, and derive the OEP integral equation for exchange only. The use of the exact exchange energy has several advantages over the conventional explicitly density dependent xc functionals. Most importantly it ensures the correct asymptotic behavior, reflecting the fact that it is self-interaction free for both the occupied and the unoccupied orbitals. We use the Fock exchange energy expression,

$$E_{\rm x} = -\frac{1}{2}\sum_{\sigma}\sum_{k,l}^{N_\sigma}\int d^3r\int d^3r'\frac{\Phi^*_{k\sigma}(\mathbf{r}')\Phi_{l\sigma}(\mathbf{r}')\Phi^*_{k\sigma}(\mathbf{r})\Phi^*_{l\sigma}(\mathbf{r})}{|\mathbf{r}-\mathbf{r}'|}. \quad \text{(C.2)}$$

For a quantum well, replacing the discrete quantum number k as $(\mathbf{q}_{||}, i)$, the orbitals are

$$\Phi_{k\sigma}(\mathbf{r}) = e^{i\mathbf{q}_{||}\cdot\mathbf{r}_{||}}\varphi_{k\sigma}(z), \quad \text{(C.3)}$$

where $q_{||}$ is the in-plane wave vector and k is the subband index. Then

$$\begin{aligned} E_{\rm x} &= -\frac{1}{2}\sum_{\sigma}\sum_{k,l}^{OCC}\int d^3r\int d^3r'\frac{\varphi^*_{i\sigma}(z')\varphi_{j\sigma}(z')\varphi^*_{i\sigma}(z)\varphi^*_{j\sigma}(z)}{|\mathbf{r}-\mathbf{r}'|} \\ &\times\int\frac{d^2q'_{||}}{(2\pi)^2}\int\frac{d^2q_{||}}{(2\pi)^2}\Theta(\varepsilon_F-\frac{q_{||}^2}{2}-\varepsilon_{i\sigma})\Theta(\varepsilon_F-\frac{q_{||}'^2}{2}-\varepsilon_{j\sigma})e^{(\mathbf{q}_{||}-\mathbf{q}'_{||})(\mathbf{r}_{||}-\mathbf{r}'_{||})}. \end{aligned} \tag{C.4}$$

Let $\rho=(\mathbf{r}_{||}-\mathbf{r}'_{||})$, and carrying out $q_{||}$ integration, one can write one of the $q_{||}$ integrations of (C.4) as

$$\frac{1}{(2\pi)^2}\int_0^\infty q_{||}dq_{||}\Theta(\varepsilon_F-\frac{q_{||}^2}{2}-\varepsilon_{i\sigma})\int_0^{2\pi}d\theta e^{iq_{||}\rho\cos\theta}. \tag{C.5}$$

We have

$$\int_0^{2\pi}d\theta e^{iq_{||}\rho\cos\theta}=2\pi J_0(q\rho), \tag{C.6}$$

where J_0 is a cylindrical Bessel function. Therefore one can solve (C.5) to be

$$\frac{1}{2\pi}\int_0^{k_F^{i\sigma}}dq_{||}J_0(q_{||}\rho), \tag{C.7}$$

where $k_F^{i\sigma}=\sqrt{2(\varepsilon_F-\varepsilon_{i\sigma})}$. Then letting $x=q_{||}\rho$, one can simplify (C.7) to be $\frac{k_F^{i\sigma}}{2\pi\rho}J_1(k_F^{i\sigma})$, where J_1 is a cylindrical Bessel function of order 1. Therefore, (C.4) becomes

$$\begin{aligned} E_{\rm x} &= -\frac{1}{2}\sum_{\sigma}\sum_{k,l}^{OCC}\int d^3r\int d^3r'\frac{\varphi^*_{i\sigma}(z')\varphi_{j\sigma}(z')\varphi^*_{i\sigma}(z)\varphi^*_{j\sigma}(z)}{|\mathbf{r}-\mathbf{r}'|} \\ &\times\frac{k_F^{i\sigma}k_F^{j\sigma}}{4\pi^2\rho^2}J_1(k_F^{i\sigma}\rho)J_1(k_F^{j\sigma}\rho) \qquad\qquad (C.8) \\ &= -\frac{1}{8\pi^2}\sum_{i,j,\sigma}^{OCC}\int dz\int dz'\varphi^*_{i\sigma}(z')\varphi_{j\sigma}(z')\varphi^*_{i\sigma}(z)\varphi^*_{j\sigma}(z) \\ &\times\int d^2r_{||}\int d^2r'_{||}\frac{1}{\rho^2}J_1(k_F^{i\sigma}\rho)J_1(k_F^{j\sigma}\rho)\frac{1}{\sqrt{\rho^2+(z-z')^2}}. \qquad\qquad (C.9) \end{aligned}$$

We can carry out one integral $\int d^2r'_{||}=A$ and write the other one as $\int d^2r_{||}=2\pi\int_0^\infty\rho d\rho$, since the integrand depends only on $|\mathbf{r}_{||}-\mathbf{r}'_{||}|$. Therefore the exact

exchange energy expression for a quantum well is

$$E_{\rm x} = -\sum_{i,j,\sigma} k_F^{i\sigma} k_F^{j\sigma} \int dz \int dz' \varphi_{i\sigma}^*(z)\varphi_{i\sigma}(z')\varphi_{j\sigma}^*(z')\varphi_{j\sigma}(z) F_{ij}^{11}(z,z'), \qquad \text{(C.10)}$$

where

$$F_{ij}^{11}(z,z') = \frac{A}{4\pi}\int_0^\infty \frac{d\rho J_1(k_F^{i\sigma}\rho)J_1(k_F^{j\sigma}\rho)}{\rho\sqrt{\rho^2+(z-z')^2}}. \qquad \text{(C.11)}$$

The next step is to evaluate the terms in (C.1) for a quantum well. First evaluate the kinetic energy term. Let

$$E_{\rm kin} = \sum_\sigma \sum_j^{N_\sigma} \int d^3r \Phi_{j\sigma}^*(\mathbf{r})(-\nabla^2/2)\Phi_{j\sigma}(\mathbf{r}), \qquad \text{(C.12)}$$

then, E_{kin} can be written for a quantum well as

$$E_{\rm kin} = \sum_\sigma \sum_i^{OCC} \int \frac{d^2q_{||}}{(2\pi)^2}\Theta(\varepsilon_F - \frac{q_{||}^2}{2} - \varepsilon_{i\sigma})\varphi_{i\sigma}^*(z)(\frac{q_{||}^2}{2} - \frac{1}{2}\frac{d^2}{dz^2})\varphi_{i\sigma}(z). \qquad \text{(C.13)}$$

This can be evaluated to

$$E_{\rm kin} = \frac{A}{4\pi}\sum_\sigma \sum_i^{OCC} (k_F^{i\sigma})^2 \int \varphi_{i\sigma}^*(z)\left[\frac{1}{4}(k_F^{i\sigma})^2 - \frac{1}{2}\frac{d^2}{dz^2}\right]\varphi_{i\sigma}(z)dz, \qquad \text{(C.14)}$$

noting that

$$\begin{aligned}\int \frac{d^2q_{||}}{(2\pi)^2}\Theta(\varepsilon_F - \frac{q_{||}^2}{2} - \varepsilon_{i\sigma}) &= \frac{2\pi}{(2\pi)^2}\int_0^\infty q_{||}dq_{||}\Theta(\varepsilon_F - \frac{q_{||}^2}{2} - \varepsilon_{i\sigma}) \\ &= \frac{1}{4\pi}(k_F^{i\sigma})^2, \qquad \text{(C.15)}\end{aligned}$$

and

$$\int \frac{d^2q_{||}}{(2\pi)^2}\frac{q_{||}^2}{2}\Theta(\varepsilon_F - \frac{q_{||}^2}{2} - \varepsilon_{i\sigma}) = \frac{1}{4\pi}\frac{1}{4}(k_F^{i\sigma})^4. \qquad \text{(C.16)}$$

Next we will evaluate the external energy term,

$$E_{\rm ext} = \sum_\sigma \int d^3r n_\sigma(\mathbf{r})v_{\rm ext}(\mathbf{r}). \qquad \text{(C.17)}$$

Since the total density is given by

$$n(\mathbf{r}) = \sum_{\sigma} \sum_{i}^{OCC} \int \frac{d^2 q_{||}}{(2\pi)^2} \Theta(\varepsilon_F - \frac{q_{||}^2}{2} - \varepsilon_{i\sigma}) \varphi_{i\sigma}^*(z) \varphi_{i\sigma}(z), \tag{C.18}$$

we have

$$n(z) = \sum_{\sigma} \sum_{i}^{OCC} \frac{1}{4\pi} (k_F^{i\sigma})^2 \varphi_{i\sigma}^*(z) \varphi_{i\sigma}(z). \tag{C.19}$$

Therefore,

$$E_{\text{ext}} = \frac{A}{4\pi} \sum_{\sigma} \sum_{i}^{OCC} (k_F^{i\sigma})^2 \int dz v_{ext} \varphi_{i\sigma}^*(z) \varphi_{i\sigma}(z). \tag{C.20}$$

The Hartree energy is given by

$$E_{\text{H}} = \frac{1}{2} \int d^3 r \int d^3 r' \frac{n(\mathbf{r}) n(\mathbf{r}')}{|\mathbf{r} - \mathbf{r}'|} \tag{C.21}$$

$$= \frac{1}{2} \int d^3 r \int d^3 r' \frac{1}{|r - r'|} \times \sum_{\sigma\sigma'} \sum_{ij}^{OCC} \frac{1}{(4\pi)^2} (k_F^{i\sigma})^2 (k_F^{j\sigma'})^2 \varphi_{i\sigma}^*(z) \varphi_{i\sigma}(z) \varphi_{j\sigma'}^*(z') \varphi_{j\sigma'}(z'). \tag{C.22}$$

This can be evaluated to be,

$$E_{\text{H}} = -\pi A \sum_{\sigma\sigma'} \sum_{ij}^{OCC} \frac{(k_F^{i\sigma})^2 (k_F^{j\sigma'})^2}{(4\pi)^2} \times \int dz \int dz' \varphi_{i\sigma}^*(z) \varphi_{i\sigma}(z) |z - z'| \varphi_{j\sigma'}^*(z') \varphi_{j\sigma'}(z'). \tag{C.23}$$

We have obtained (C.23) by substracting the ∞ contribution which is cancelled out by the ionic background, since

$$\int d^2 r'_{||} \int d^2 r_{||} \frac{1}{|\mathbf{r} - \mathbf{r}'|} = \int d^2 r'_{||} \int d^2 r_{||} \frac{1}{\sqrt{\rho^2 + (z - z')^2}} = 2\pi A \int_0^{\infty} \rho d\rho \frac{1}{\sqrt{\rho^2 + (z - z')^2}} = 2\pi A(\infty - |z - z'|). \tag{C.24}$$

Now we have evaluated all the terms in (C.1), and we can write the total enery as

$$
\begin{aligned}
E &= E_{\rm kin} + E_{\rm ext} + E_{\rm H} + E_{\rm x} \qquad \text{(C.25)} \\
&= \frac{A}{4\pi}\sum_{\sigma}\sum_{i}^{OCC}(k_F^{i\sigma})^2\int \varphi^*_{i\sigma}(z)[\frac{1}{4}(k_F^{i\sigma})^2 - \frac{1}{2}\frac{d^2}{dz^2}]\varphi_{i\sigma}(z)dz \\
&\quad + \frac{A}{4\pi}\sum_{\sigma}\sum_{i}^{OCC}(k_F^{i\sigma)})^2\int dz v_{ext}\varphi^*_{i\sigma}(z)\varphi_{i\sigma}(z) \\
&\quad - \pi A\sum_{\sigma\sigma'}\sum_{ij}^{OCC}\frac{(k_F^{i\sigma)})^2(k_F^{j\sigma')})^2}{(4\pi)^2}\int dz\int dz'\varphi^*_{i\sigma}(z)\varphi_{i\sigma}(z)|z-z'|\varphi^*_{j\sigma'}(z')\varphi_{j\sigma'}(z') \\
&\quad - \sum_{i,j,\sigma}k_F^{i\sigma}k_F^{j\sigma}\int dz\int dz'\phi^*_{i\sigma}(z)\phi_{i\sigma}(z')\phi^*_{j\sigma}(z')\phi_{j\sigma}(z)F^{11}_{ij\sigma}(z,z'). \qquad \text{(C.26)}
\end{aligned}
$$

The OEP equation is obtained by minimization of total energy with respect to the potential. Using the variational principle, this can be written as,

$$
\frac{\delta E}{\delta V_{XX\sigma}} = \sum_{i\sigma'}\int dz'\frac{\delta E}{\delta\varphi_{i\sigma'}(z')}\frac{\delta\varphi_{i\sigma'}(z')}{\delta V_{XX\sigma}} + c.c = 0. \qquad \text{(C.27)}
$$

Now

$$
\frac{\delta\varphi_{i\sigma'}(z')}{\delta V_{XX\sigma}} = -G_{i\sigma}(z',z)\varphi_{i\sigma}(z)\delta_{\sigma\sigma'}. \qquad \text{(C.28)}
$$

This was obtained from lowest order perturbation theory, where the Green function is

$$
G_{i\sigma}(z',z) = \sum_{j\neq i}\frac{\varphi_{j\sigma}(z')\varphi^*_{j\sigma}(z)}{\epsilon_{j\sigma}-\epsilon_{j\sigma}}. \qquad \text{(C.29)}
$$

In order to satisfy Eq. (C.27), we need to find the functional derivatives of E. The functional derivative of kinetic and external energy is

$$
\begin{aligned}
\frac{\delta(E_{\rm kin}+E_{\rm ext})}{\delta\varphi_{i\sigma'}(z')} &= \frac{A}{4\pi}\sum_{\sigma}\sum_{j}^{OCC}(k_F^{j\sigma})^2\int dz\varphi^*_{j\sigma}(z)\left[\frac{1}{4}(k_F^{i\sigma})^2 - \frac{1}{2}\frac{d^2}{dz^2} + v_{\rm ext}(z)\right] \\
&\quad \times\delta(z-z')\delta_{ij}\delta_{\sigma\sigma'} \\
&= \frac{A}{4\pi}(k_F^{i\sigma'})^2\left[\frac{1}{4}(k_F^{i\sigma'})^2 - \frac{1}{2}\frac{d^2}{dz^2} + v_{\rm ext}(z')\right]\varphi^*_{i\sigma'}(z'). \qquad \text{(C.30)}
\end{aligned}
$$

The functional derivative of the Hartree energy is,

$$\begin{aligned}\frac{\delta E_{\rm H}}{\delta\varphi_{i\sigma'}(z')} &= -\pi A\sum_{\sigma\sigma''}\sum_{kj}^{OCC}\frac{(k_F^{k\sigma)})^2(k_F^{j\sigma')})^2}{(4\pi)^2}\int dz\int dz''|z-z''| \\ &\quad\times[\varphi^*_{k\sigma}(z)\delta(z-z')\delta_{ik}\delta_{\sigma\sigma'}\varphi^*_{j\sigma''}(z'')\varphi_{j\sigma''}(z'') \\ &\quad+\varphi^*_{k\sigma}(z)\varphi_{k\sigma}(z)\varphi^*_{j\sigma''}(z'')\delta(z''-z')\delta_{ji}\delta_{\sigma'\sigma''}] \\ &= -\frac{2\pi A}{4\pi}(k_F^{i\sigma'})^2\varphi^*_{i\sigma'}(z')\sum_{\sigma}\sum_{k}^{OCC}\frac{(k_F^{k\sigma})^2}{4\pi}\int\varphi^*_{k\sigma}(z)\varphi_{k\sigma}(z)|z-z'|dz.\end{aligned}$$

Letting

$$v_{\rm H}(z') = -2\pi\sum_{\sigma}\frac{(k_F^{k\sigma})^2}{4\pi}\int\varphi^*_{k\sigma}(z)\varphi_{k\sigma}(z)|z-z'|dz, \tag{C.31}$$

we can write

$$\frac{\delta E_{\rm H}}{\delta\varphi_{i\sigma'}(z')} = \frac{A}{4\pi}(k_F^{i\sigma'})^2 v_H(z')\varphi^*_{i\sigma'}(z'). \tag{C.32}$$

The next task is to find the functional derivative of the exchange energy:

$$\begin{aligned}\frac{\delta E_{\rm x}}{\delta\varphi_{i\sigma'}(z')} &= -\frac{A}{4\pi}\sum_{k,j,\sigma}k_F^{k\sigma}k_F^{j\sigma}\int dz\int dz''\varphi^*_{k\sigma}(z'')\varphi^*_{j\sigma}(z)\varphi_{j\sigma}(z) \\ &\quad\times F^{11}_{ij}(z'',z)\delta_{\sigma\sigma'}[\delta(z-z')\delta_{ik}\varphi_{j\sigma}(z'')+\varphi_{k\sigma}(z)\delta(z''-z')\delta_{ij}] \\ &= -\frac{2A}{4\pi}k_F^{i\sigma'}\sum_{j}^{OCC}k_F^{j\sigma'}\int dz\varphi^*_{i\sigma'}(z)\varphi_{j\sigma'}(z)\varphi^*_{j\sigma'}(z')F_{ij\sigma'}(z,z'). \end{aligned}\tag{C.33}$$

Then one can write

$$\frac{\delta E_{\rm x}}{\delta\varphi_{i\sigma'}(z')} = k_F^{i\sigma'}\varphi^*_{i\sigma'}(z')w_{{\rm x}i\sigma'}(z'), \tag{C.34}$$

defining

$$w_{{\rm x}i\sigma'}(z') = \frac{1}{k_F^{i\sigma'}\varphi^*_{i\sigma'}(z')}\frac{\delta E_{\rm x}}{\delta\varphi_{i\sigma'}(z')}. \tag{C.35}$$

Now let's put all these values in Eq. (C.27) in order to derive the OEP equation. This gives

$$\sum_{i}^{OCC}\int dz' G_{i\sigma}(z',z)\varphi_{i\sigma}(z)$$

$$\times[\frac{A}{4\pi}(k_F^{i\sigma})^2[-\frac{1}{2}\frac{d^2}{dz^2}+v_{\rm ext}(z')+v_{\rm H}(z')+\frac{1}{4}(k_F^{i\sigma})^2]\varphi_{i\sigma}^*(z')$$

$$+k_F^{i\sigma}w_{xi\sigma}(z')\varphi_{i\sigma}^*(z')]+c.c.=0. \tag{C.36}$$

Now,

$$\left[-\frac{1}{2}\frac{d^2}{dz^2}+v_{\rm ext}(z)+v_{\rm H}(z)+\frac{1}{2}(\epsilon_F-\epsilon_{i\sigma})\right]\varphi_{i\sigma}^*(z)=\left[\frac{(\epsilon_{i\sigma}+\epsilon_F)}{2}-V_{XX}(z)\right]. \tag{C.37}$$

Therefore, Eq. (C.36) can be written as

$$\sum_i^{OCC}\int dz' G_{i\sigma}(z',z)\varphi_{i\sigma}(z)\varphi_{i\sigma^*}(z')$$

$$\times\left[\frac{A}{4\pi}(k_F^{i\sigma})^2V_{XX}(z')-k_F^{i\sigma}w_{xi\sigma}(z')\right]+c.c.=0, \tag{C.38}$$

since $\int dz' G_{i\sigma}(z',z)\varphi_{i\sigma}^*(z')=0$. One can then rewrite (C.38) to arrive at the OEP integral equation (5.12),

$$\sum_i^{OCC}(k_F^{i\sigma})^2\int dz'[V_{XX}(z')-u_{X\sigma i}(z')]G_{i\sigma}(z',z)\varphi_{i\sigma}(z)\varphi_{i\sigma}^*(')+c.c.=0, \tag{C.39}$$

where

$$u_{X\sigma i}(z')=\frac{4\pi}{(k_F^{i\sigma})^2}\frac{1}{\varphi_{i\sigma}^*(z')}\frac{\delta E_{\rm x}}{\delta\varphi_{i\sigma'}(z')}. \tag{C.40}$$

Bibliography

[1] J. N. Heyman, K. Craig, B. Galdrikian, M. S. Sherwin, K. Campman, P. F. Hopkins, S. Fafard, and A. C. Gossard, Phys. Rev. Lett. **72**, 2183 (1994).

[2] F. H. Julien, J.-M. Lourtioz, N. Herschkorn, D. Delacourt, J. P. Pocholle, M. Papuchon, R. Planel, and G. Le Roux, Appl. Phys. Lett. **53**, 116 (1988).

[3] K. Craig, B. Galdrikian, J. N. Heyman, A. G. Markelz, J. B. Williams, M. S. Sherwin, K. Campman, P. F. Hopkins, and A. C. Gossard, Phys. Rev. Lett. **76**, 2382 (1996).

[4] E. Dupont, P. B. Corkum, H. C. Liu, M. Buchanan, and Z. R. Wasilewski, Phys. Rev. Lett. **74**, 3596 (1995).

[5] J. N. Heyman, R. Kersting, and K. Unterrainer, Appl. Phys. Lett. **72**, 644 (1998).

[6] P. Bakshi, K. Kempa, A. Scorupsky, C. G. Du, G. Feng, R. Zobl, G. Strasser, C. Rauch, C. Pacher, K. Unterrainer, and E. Gornik, Appl. Phys. Lett. **75**, 1685 (1999).

[7] M. Seto and M. Helm, Appl. Phys. Lett. **60**, 859 (1992).

[8] M. I. Stockman, L. N. Pandey, L. S. Muratov, and T. F. George, Phys. Rev. B **48**, 10966 (1993).

[9] H. O. Wijewardane and C. A. Ullrich, Appl. Phys. Lett. **84**, 3984 (2004).

[10] *Intersubband Transitions in Quantum Wells I*, edited by H. C. Liu and F. Capasso, Semiconductors and Semimetals Vol. 62 (Academic Press, San Diego, 2000).

[11] M. Załużny, Phys. Rev. B **47**, 3995 (1993).

[12] B. Galdrikian and B. Birnir, Phys. Rev. Lett. **76**, 3308 (1996).

[13] A. A. Batista, P. I. Tamborenea, B. Birnir, M. S. Sherwin, and D. S. Citrin, Phys. Rev. B **66**, 195325 (2002).

[14] A. Olaya-Castro, M. Korkusinski, P. Hawrylak, and M. Yu. Ivanov, Phys. Rev. B **68**, 155305 (2003).

[15] J. Li and C. Z. Ning, Phys. Rev. Lett. **91**, 097401 (2003).

[16] E. Runge and E. K. U. Gross, Phys. Rev. Lett. **52**, 997 (1984).

[17] C. A. Ullrich and G. Vignale, Phys. Rev. B **65**, 245102 (2002).

[18] G. Vignale, C. A. Ullrich, and S. Conti, Phys. Rev. B **78**, 4878 (1997).

[19] C. A. Ullrich and G. Vignale, Phys. Rev. B **87**, 037402 (2001).

[20] H. O. Wijewardane and C. A. Ullrich, in *Proceedings of the 27th International Conference on the Physics of Semiconductors*, eds. J. Menendez and C. G. Van de Walle, AIP Conference Proceedings **772**, 1141 (2005).

[21] N. T. Maitra, K. Burke, and C. Woodward, Phys. Rev. Lett. **89**, 023002 (2002).

[22] G. Vignale and W. Kohn, Phys. Rev. Lett. **77**, 2037 (1996).

[23] E. K. U. Gross and W. Kohn, Phys. Rev. Lett. **55**, 2850 (1985).

[24] J. F. Dobson, M. J. Bünner, and E. K. U. Gross, Phys. Rev. Lett. **79**, 1905 (1997).

[25] I. V. Tokatly and O. Pankratov, Phys. Rev. B **67**, 201103(R) (2003); I. V. Tokatly, Phys. Rev. B **71**, 165104 and 165105 (2005).

[26] H. O. Wijewardane and C. A. Ullrich, Phys. Rev. Lett. **95**, 086401 (2005)

[27] C. A. Ullrich, U. J. Gossmann, and E. K. U. Gross, Phys. Rev. Lett. **74**, 872 (1995).

[28] J. D. Talman and W. F. Shadwick, Phys. Rev. A **14**, 36 (1976).

[29] R. T. Sharp and G. K. Horton, Phys. Rev. **90**, 317 (1953).

[30] V. Sahni, J. Gruenebaum, and J. P. Perdew, Phys. Rev. B **26**,4371 (1982).

[31] J. P. Perdew and M. R. Norman, Phys. Rev. B **26**, 545 (1982).

[32] P. Hohenberg and W. Kohn, Phys. Rev. **136**, B864 (1964).

[33] W. Kohn and L. J. Sham, Phys. Rev. **140**, A1133 (1965).

[34] R. M. Dreizler and E. K. U. Gross, *Density Functional Theory* (Springer, Berlin, 1990).

[35] R. G. Parr and W. Yang, *Density-Functional Theory of Atoms and Molecules* (Oxford University Press, New York, 1989).

[36] J. B. Krieger, Y. Li, and G. J. Iafrate, Phys. Rev. A **148**, 470 (1990).

[37] J. B. Krieger, Y. Li, and G. J. Iafrate, Phys. Rev. A **45**, 101 (1992).

[38] E. K. U. Gross and W. Kohn, Adv. Quant. Chem. **21**, 255 (1990).

[39] E. K. U. Gross, J. F. Dobson, and M. Petersilka, in *Density Functional Theory II*, vol. 181 of *Topics in current chemistry*, p. 81 (Springer, Berlin, 1996).

[40] K. Burke and E. K. U. Gross, in *Density functionals: Theory and applications*, ed. D. Joubert (Springer, Berlin, 1998).

[41] R. van Leeuwen, Int. J. Mod. Phys. B **15**, 1969 (2001).

[42] W. Kohn, Rev. Mod. Phys **71**, 1253 (1999).

[43] J. A. Pople, Rev. Mod. Phys **71**, 1267 (1999).

[44] R. van Leeuwen, Phys. Rev. Lett. **82**, 3863 (1999).

[45] L. V. Keldysh, Sov. Phys. JETP **20**, 1018 (1965).

[46] M. A. L. Marques and E. K. U. Gross, Annu. Rev. Phys. Chem. **55**, 427 (2004).

[47] F. Furche and K. Burke, *Time-dependent density-functional theory*, to appear in first edition of annual reviews of computational chemistry (2004).

[48] K. Burke, J. Werschnik, E. K. U. Gross, J. Chem. Phys. **123**, 062206 (2005).

[49] *Time-dependent density functional theory* eds. M. A. L. Marques, C. A. Ullrich, F. Nogueira, A. Rubio, K. Burke, and E. K. U. Gross (Springer, Berlin Heidelberg, 2006).

[50] M. Petersilka, U. J. Gossmann, and E. K. U. Gross, Phys. Rev. Lett. **76**, 1212 (1996).

[51] M. E. Casida, in *Recent advances in density functional methods*, ed. D. P. Chong, p. 155 (World Scientific, Singapore, 1995).

[52] F. Furche and R. Ahlrichs, J. Chem. Phys. **117**, 7433 (2002).

[53] M. A. L. Marques, X. Lopez, D. Varsano, A. Castro, and A. Rubio, Phys. Rev. Lett. **90**, 258101 (2003).

[54] P. J. Stephens, D. M. McCann, E. Butkus, S. Stoncius, J. R. Cheesemann and M. J. Frisch, J. Org. Chem. **69**, 1948 (2004).

[55] M. Seth, T. Ziegler, A. Banerjee, J. Autschbach, S. J. A. van Gisbergen and E. J. Baerends, J. Chem. Phys. **120**, 10942 (2004).

[56] I. Vasiliev, S. Öğüt, and J. R. Chelikowsky, Phys. Rev. B **65**, 115416 (2002)

[57] C. A. Ullrich, S. Erhard, and E. K. U. Gross, in *Super Intense Laser Atom Physics IV*, eds. H. G. Muller and M. V. Fedorov (Kluwer, 1996).

[58] X. Chu and S. I. Chu, Phys. Rev. A, **6302**, 3411 (2001).

[59] H. S. Nguyen, A. D. Bandrauk, and C. A. Ullrich, Phys. Rev. A **69**, 063415 (2004).

[60] A. Pohl, P. -G. Reinhard, and E. Suraud, Phys. Rev. Lett. **84**, 5090 (2000).

[61] M. Petersilka and E. K. U. Gross, Laser Physics **9**, 1 (1999).

[62] D. Bauer and F. Ceccherini, Opt. Express, **8**, 377 (2001).

[63] M. Fuchs, Y. -M. Niquet, X. Gonze, and K. Burke, J. Chem. Phys. **122**, 094116 (2005).

[64] M. H. Mittleman, *Theory of Laser-Atom Interactions*, 2^{nd} edition (Plenum Press, New York, 1993).

[65] C. A. Ullrich and G. Vignale, Phys. Rev. B **58**, 15756 (1998); Phys. Rev. Lett. **87**, 037402 (2001).

[66] J. N. Heyman, K. Unterrainer, K. Craig, B. Galdrikian, M. S. Sherwin, K. Campman, P. F. Hopkins, and A. C. Gossard, Phys. Rev. Lett. **74**, 2682 (1995).

[67] J. B. Williams, M. S. Sherwin, K. D. Maranowski, and A. C. Gossard, Phys. Rev. Lett. **87**, 037401 (2001).

[68] B. Gadrikian, PhD. Thesis, University of California, Santa babara (1994).

[69] A. A. Batista, B. Birnir, M. S. Sherwin, Phys. Rev. B **61**, 15108 (2000).

[70] A. A. Batista, P. I. Tamborenea, B. Birnir, M. S. Sherwin, and D. S. Citrin, Phys. Rev. B **68**, 035307 (2003)

[71] A. K. Dhara and S. K. Ghosh, Phys. Rev. A **35**, R442 (1987).

[72] S. K. Ghosh and A. K. Dhara, Phys. Rev. A **38**, 1149 (1988).

[73] G. Vignale and M. Rasolt, Phys. Rev. Lett. **37**, 10685 (1988).

[74] G. Vignale, Phys. Rev. B **70**, 201102 (2004).

[75] E. K. U. Gross and W. Kohn, Phys. Rev. Lett. **55**, 2850 (1985); **57**, 923(E) (1986).

[76] Z. Qian and G. Vignale, Phys. Rev. B **65**, 235121 (2002).

[77] C. A. Ullrich and I. V. Tokatly, Phys. Rev. B **73**, 235102 (2006).

[78] H. O. Wijewardane and C. A. Ullrich, Phys. Stat. Sol. (c) **3**, 2498 (2006).

[79] S. -K. Ma and K. A. Brueckner, Phys. Rev. **165**, 18 (1968).

[80] D. C. Langreth and M. J. Mehl, Phys. Rev. Lett. **47**, 446 (1981).

[81] J. P. Perdew, Phys. Rev. B **33**, 8822 (1986).

[82] A. D. Becke, Phys. Rev. B **32**, 3876 (1985).

[83] E. Engel, in *A primer in density functional theory*, Eds. C. Fiolhais, F. Nogueira, M. Marques (Springer Berlin Heidelberg 2003).

[84] R. O. Jones and O. Gunnarsson, Rev. Mod. Phys. **61**, 689 (1989).

[85] E. Engel and S. H. Vosko, Phys. Rev. A **47**, 165 (1993).

[86] T. Kotani, Phys. Rev. B **50**, 14816 (1994).

[87] J. P. Perdew, R. G. Parr, M. Levy, and J. L. Balduz, Phys. Rev. Lett. **49**, 1691 (1982).

[88] T. Kreibich, S. Kurth, T. Grabo, and E. K. U. Gross, Adv. Quantum Chem. (1998).

[89] Y. Shigeta, K. Hirao, and S. Hirata, Phys. Rev. A **73**, 010502(R) (2006).

[90] M. Mundt and S. Kümmel, Phys. Rev. A **74**, 022511 (2006).

[91] F. A. Reboredo and C. R. Proetto, Phys. Rev. B **67**, 115325 (2003).

[92] J. C. Slater, Phys. Rev. **81**, 385 (1951).

[93] C. A. Ullrich, Dissertation, University of Würzburg (1995).

[94] M. Mundt and S. Kümmel, Phys. Rev. Lett. **95**, 203004 (2005).

[95] M. Weissbluth, *Atoms and molecules* (Academic Press, San Diego, 1978).

[96] J. P. Perdew and M. Ernzerhof in *Electronic density functional theory*, Eds. J. F. Dobson, G. Vignale, and M. P. Das (Plenum Press, New York, 1998).

[97] J. P. Perdew and A. Zunger, Phys. Rev. B **23**, 5048 (1981).

[98] Z. Penzar and W. Ekardt, Z. Phys. D: At., Mol. Clusters **17**, 69 (1990).

[99] M. Madjet, C. Guet, and W. R. Johnson, Phys. Rev. A **51**, 1327 (1995).

[100] P. Stampfli and K. H. Bennemann, Phys. Rev. A **39**, 1007 (1989).

[101] A. Svane and O. Gunnarsson, Phys. Rev. Lett. **65**, 1148 (1990).

[102] Z. Szotek, W. M. Temmerman, and H. Winter, Phys. Rev. B **47**, 4029 (1993).

[103] C. A. Ullrich, P.-G. Reinhard, and E. Suraud, Phy. Rev. A **62**, 053202 (2000).

[104] A. Gőrling, Phys. Rev. A **55**, 2630 (1997).

[105] *Numerical Recipes in FORTRAN 77*, Second Edition (1992).

[106] R. van Leeuwen, PhD. Thesis, University of Amsterdam (1994).

[107] C. A. Ullrich, J. Chem. Phys. **125**, 234108 (2006).

[108] M. van Fassen, P. L. de Boeij, R. van Leeuwen, J. A. Berger, andd J. G. Snijders, Phys. Rev. Lett. **88**, 186401 (2002).

[109] M. Mundt, S. Kümmel, R. van Leeuwen, and P. -G. Reinhard, Phys. Rev. A **75**, 050501(R) (2007).

[110] R. E. Miles, P. Harrison and D. Lippens (eds), *Terahertz Sources and systems* Vol. 27 (Nato science series II, Kluwer, Dordrecht, 2001).

[111] P. Y. Han, G. C. Cho and X. C. Zhang, Opt. Lett. **25**, 242 (2000).

[112] D. M. Mittleman, R. H. Jacobsen and M. C. Nuss, *IEEE* J. Sel. Top. Quant. Electron. **2**, 679 (1996).

[113] D. M. Mittleman, S. Hunsche, L. Boivin, and M. C. Nuss, Opt. Lett. **22**, 904 (1997).

[114] R. Köhler, A. Tredicucci, F. Beltram, H. E. Beere, E. H. Linfield, A. G. Davies, D. A. Ritchie, R. C. Iotti, and F. Rossi, Nature **417**, 156 (2002).

[115] F. Capasso, C. Gmachl, D. L. Sivco, and A. Y. Cho, *Quantum cascade lasers*, Physics Today **55**, 34 (2002).

[116] H. Haug and S. W. Koch, *Quantum theory of the optical and electronic properties of semiconductors* (World Scientific, Singpore, 1990).

[117] A. V. Kuznetsov, G. D. Sanders and C. J. Stanton, Phys. Rev. B **52**, 12045 (1995).

[118] A. Castro and M. A. L. Marques, *Time-dependent density functional theory*, eds. M. A. L. Marques, C. A. Ullrich, F. Nogueira, A. Rubio, K. Burke, and E. K. U. Gross (Springer, Berlin Heidelberg, 2006).

[119] M. A. L. Marques, A. Castro, G. F. Bertsch and A. Rubio, *Octopus: a first-principles tool for excited electron-ion dynamics*, Comput. Phys. Commun. **151**, 60 (2003).

[120] R. S. Varga, *Matrix iterative analysis* (Prentice-Hall, New Jersey, 1962).

List of Publications

1. *Coherent control of optical bistability*
   H. O. Wijewardane and C. A. Ullrich, Appl. Phys. Lett. **84**, 3984 (2004).

2. *Nonlinear intersubband photoabsorption in asymmetric single quantum wells*
   H. O. Wijewardane and C. A. Ullrich, in *Proceedings of the 27th International Conference on the Physics of Semiconductors*, eds. J. Menendez and C. G. Van de Walle, AIP Conference Proceedings **772**, 1141 (2005).

3. *Time-dependent Kohn-Sham theory with memory*
   H. O. Wijewardane and C. A. Ullrich, Phys. Rev. Lett. **95**, 086401 (2005).

4. *Time-dependent density-functional approaches to ultrafast intersubband dynamics in quantum wells*
   H. O. Wijewardane and C. A. Ullrich, Phys. Stat. Sol. (c) **3**, 2498 (2006).

5. *Exact exchange and retardation in time-dependent density-functional theory: application to real-time intersubband dynamics in quantum wells*
   H. O. Wijewardane and C. A. Ullrich, in preparation (2007).

VITA

Harshani Wijewardane was born to Susil and Dharma Wijewardena on 29^{th} May 1971 in city of Kegalla, Sri Lanka. She graduated with a BSc honors degree from University of Colombo, Sri Lanka in 1997. From February 1998 to December 1998, she worked as an assistant lecturer in the Physics Department, University of Colombo, Sri Lanka. From January 1999 to July 2001, she worked as an educational assistant, The Open University of Sri Lanka, Sri Lanka. In 2002, she began her PhD research under the direction of Prof. Carsten Ullrich at the University of Missouri-Rolla and continued with him joining University of Missouri-Columbia in 2005. She graduated with a PhD in July 2007. She will join Prof. Neepa Maitra at City University of New York, New York as a postdoctoral fellow in August 2007.